



Global DEM Quality Assessment Summary

Author(s):

Kévin GROSS

VisioTerra Task 5 Mission Expert

Axel CORSEaux

VisioTerra Engineer

Approval:

Serge RIAZANOFF

VisioTerra Task 5 Lead

Accepted:

Clément ALBINET

ESA Technical Officer

AMENDMENT RECORD SHEET

The Amendment Record Sheet below records the history and issue status of this document.

ISSUE	DATE	REASON
1.0	02-April 2020	Initial Issue
1.1	26 June 2020	Review of Clément ALBINET (EDAP.REP.005 becomes EDAP.REP.029)
1.2	16 July 2020	Review of Clément ALBINET

TABLE OF CONTENTS

1. INTRODUCTION.....	5
1.1 Reference document.....	5
1.1.1 Quality assessment	5
1.1.2 SRTM-GL1.....	5
1.1.3 ASTER GDEM.....	5
1.1.4 ALOS World 3D	6
1.1.5 ICESat-1	7
1.1.6 Geocoding and orthorectification.....	8
1.2 Attached document	8
1.3 Glossary	9
1.4 Definitions.....	10
2. EXECUTIVE SUMMARY	13
2.1 Product Quality Assessment Matrices	15
2.1.1 SRTM.....	16
2.1.2 ASTER GDEM.....	17
2.1.3 ALOS World 3D	18
3. PRODUCT ASSESSMENT OVERVIEW	19
3.1 SRTM	19
3.1.1 Product Information	19
3.1.2 Product Generation.....	21
3.1.3 Ancillary Information	22
3.1.4 Uncertainty Characterisation	22
3.1.5 Validation	23
3.2 ASTER GDEM.....	24
3.2.1 Product Information	24
3.2.2 Product Generation.....	26
3.2.3 Ancillary Information	27
3.2.4 Uncertainty Characterisation	27
3.2.5 Validation	28
3.3 ALOS World 3D.....	29
3.3.1 Product Information	29
3.3.2 Product Generation.....	30
3.3.3 Ancillary Information	32
3.3.4 Uncertainty Characterisation	32
3.3.5 Validation	33
4. DETAILED ASSESSMENT	34
4.1 DEMs intercomparison.....	34
4.1.1 Absolute height values	34

4.1.1.1	Global differences	34
4.1.1.1.1	SRTM - ASTER GDEM	36
4.1.1.1.2	ASTER GDEM - ALOS World 3D	36
4.1.1.1.3	ALOS World 3D - SRTM	38
4.1.1.2	Artefacts	38
4.1.1.2.1	Artefact 1 – Southern Chile	38
4.1.1.2.2	Artefact 2 - Sahara	39
4.1.1.2.3	Artefact 3 - Border between Russia and Kazakhstan	40
4.1.1.2.4	Artefact 4 - Near Yinchuan, China	41
4.1.1.3	Elevation differences	41
4.1.2	Slope values	43
4.1.2.1	Global slope differences	43
4.1.2.2	Local slope differences	44
4.1.3	Azimuth values	46
4.1.3.1	Global azimuth differences	46
4.1.3.2	Local azimuth differences	48
4.1.3.2.1	Artefact 1 - Caspian Sea	48
4.1.3.3	Azimuth differences	48
4.1.4	Vertical curvature	50
4.2	Elevation assessment from ICESat-1 / GLAS LiDAR	51
4.2.1	Assessment of ICESat-1 / GLAS measurements reliability	51
4.2.1.1	GLAH14 Product	51
4.2.1.2	Sampling of ICESat / GLAS data	52
4.2.1.3	Collocated measurements on the same orbit	52
4.2.1.4	Geographical distribution of ICESat products	53
4.2.2	Assessment of SRTM GL1 from ICESat / GLAS data	53
4.2.2.1	Method and notations	54
4.2.2.1.1	Conversion from TOPEX / Poseidon to WGS84	54
4.2.2.1.2	From ICESat longitude and latitude to the SRTM tile	55
4.2.2.1.3	From EGM96 to WGS84	57
4.2.2.1.4	Computing the height difference	57
4.2.2.1.5	Overall algorithm	57
4.2.2.1.6	Computation of the roughness	58
4.2.2.1.7	Computation of curvatures	60
4.2.2.2	Results	61
4.2.2.2.1	Height differences	61
4.2.2.2.2	Correlation between height errors (dhi) and height values (ICESat)	62
4.2.2.2.3	Correlation between height errors (dhi) and terrain roughness (local standard deviations)	62
4.2.2.2.4	Correlation between height errors (dhi) and terrain curvatures	64
4.2.2.2.5	Analysis of the geographical distributions of elevation errors	65
4.2.3	Assessment of ASTER GDEM from ICESat / GLAS data	69
4.2.3.1	Method and notations	69
4.2.3.2	Results	70
4.2.3.2.1	Height differences	70
4.2.3.2.2	Correlation between height errors (dhi) and height values (ICESat)	71
4.2.3.2.3	Correlation between height errors (dhi) and terrain roughness (local standard deviations)	71
4.2.3.2.4	Correlation between height errors (dhi) and terrain curvatures	72
4.2.3.2.5	Analysis of the geographical distributions of elevation errors	74
4.2.4	Assessment of ALOS World 3D from ICESat / GLAS data	75
4.2.4.1	Method and notations	75
4.2.4.2	Results	76
4.2.4.2.1	Height differences	76
4.2.4.2.2	Correlation between height errors (dhi) and height values (ICESat)	77
4.2.4.2.3	Correlation between height errors (dhi) and terrain roughness (local standard deviations)	78
4.2.4.2.4	Correlation between height errors (dhi) and terrain curvatures	79
4.2.4.2.5	Analysis of the geographical distributions of elevation errors	80
4.3	Use-based assessment – DEMs to orthorectify satellite images	81
4.3.1	Optical image – The parallax effect	81
4.3.2	Radar image – The shortening / dilation / layover effects	82
4.3.3	Optical or radar orthorectification – A dual configuration	83
4.3.4	Algorithm of orthorectification	83
4.3.4.1	Principle and algorithm	83
4.3.4.2	Speeding-up convergence	84
4.3.4.3	Algorithm convergence	84
4.3.4.4	Implementation in VtWeb	84

4.3.5	Examples of radar orthorectification	85
4.3.5.1	Example in Alps	85
4.3.5.2	Example in Himalayas	86
4.3.5.3	Example in Democratic Republic of Congo (DRC)	88
5.	CONCLUSIONS.....	89
5.1	Mission / product assessment overview	89
5.1.1	Clarifying the use of DTM, DSM and DEM	89
5.1.2	Comparing the “FAIR”	90
5.1.3	Features of the three DEMs	90
5.2	Detailed assessment	91
5.2.1	Intercomparison of DEMS	91
5.2.2	Elevation assessment from ICESat-1 / GLAS LiDAR	91
5.2.3	Use-based assessment - Impact on radar orthorectification	92
5.2.3.1	Example of Sentinel-1 IW products orthorectification	92
5.2.3.2	Other orthorectifications	94
5.2.3.3	Other use-based assessments of DEMs	94

1. INTRODUCTION

1.1 Reference document

The following is a list of reference documents with a direct bearing on the content of this Technical Note. Where referenced in the text, these are identified as [RD-n], where 'n' is the number in the list below:

1.1.1 Quality assessment

RD-1. EDAP.REP.001

EDAP Quality Assessment Guidelines

issue 1.3, 16 October 2019

NPL

[../management/20191120_Piro_EDAP.REP.001_1.3 - Mission Quality Assessment Guidelines.pdf](https://management/20191120_Piro_EDAP.REP.001_1.3_-_Mission_Quality_Assessment_Guidelines.pdf)

1.1.2 SRTM-GL1

RD-2. SRTM_User_Guide_V3

The Shuttle Radar Topography Mission (SRTM)

Collection User Guide

October 2015

USGS

https://lpdaac.usgs.gov/documents/179/SRTM_User_Guide_V3.pdf

[../reference_documents/20151000_SRTM_User_Guide_V3.pdf](https://reference_documents/20151000_SRTM_User_Guide_V3.pdf)

RD-3. Quality Assessment

An Assessment of the SRTM Topographic Products

March 2006

E. Rodriguez, C. S. Morris, and J. E. Belz

https://www2.jpl.nasa.gov/srtm/SRTM_D31639.pdf

[../reference_documents/20060300_E_Rodriguez_An_assessment_of_the_SRTM_topographic_products.pdf](https://reference_documents/20060300_E_Rodriguez_An_assessment_of_the_SRTM_topographic_products.pdf)

RD-4. 2005RG000183

The Shuttle Radar Topography Mission

19 May 2007

Tom G. Farr

<https://agupubs.onlinelibrary.wiley.com/doi/full/10.1029/2005RG000183>

[../reference_documents/20070519_Farr_The_shuttle_radar_topography_mission.pdf](https://reference_documents/20070519_Farr_The_shuttle_radar_topography_mission.pdf)

RD-5. Metrology

Metrology, attitude, and orbit determination for

spaceborne interferometric synthetic aperture radar

April 1998

Jet Propulsion Laboratory

https://www2.jpl.nasa.gov/srtm/spie_1998.pdf

[../reference_documents/19980400_Duren_Metrology_attitude_and_orbit_determination_for_spaceborne_interferometric_synthetic_aperture_radar.pdf](https://reference_documents/19980400_Duren_Metrology_attitude_and_orbit_determination_for_spaceborne_interferometric_synthetic_aperture_radar.pdf)

1.1.3 ASTER GDEM

RD-6. README

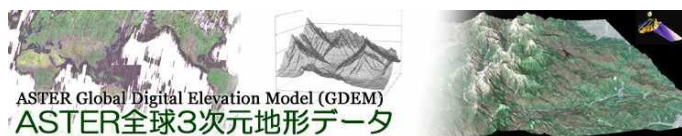
ASTER GDEM 2 README

October 2011

Japan ASTER science team

<https://www.academia.edu/16148894...>

[../reference_documents/20111000_ASTER_GDEM_2_readme.pdf](https://reference_documents/20111000_ASTER_GDEM_2_readme.pdf)



- RD-7. ATBD-AST-08 *Algorithm theoretical basis document for ASTER digital elevation models*
5 February 1999
University of Georgia
<https://eosps.nasa.gov/sites/default/files/atbd/atbd-ast-14.pdf>
[../reference_documents/19990205_Lang_Algorithm_Theoretical_Basis_Document_for_ASTER_Digital_Elevation_Models.pdf](#)
- RD-8. Calibration Plan *Pre-flight and In-Flight Calibration Plan for ASTER*
April 1996
A. Ono and F. Sakuma
<https://journals.ametsoc.org/doi/pdf/10.1175/1520-0426%281996%29013%3C0321%3APAIFCP%3E2.0.CO%3B2>
[../reference_documents/19960400_Ono_Preflight_and_in_flight_calibration_plan_for_ASTER.pdf](#)
- RD-9. Validation Results *ASTER Global Digital Elevation Model Version 2 – Summary of Validation Results*
31 August 2011
ASTER GDEM Validation Team
https://ssl.jspacesystems.or.jp/ersdac/GDEM/ver2Validation/Summary_GDEM2_validation_report_final.pdf
[../reference_documents/20110831_T_Tachikawa_ASTER_Global_Digital_Elevation_Model_Version_2_Summary_of_Validation_Results.pdf](#)
- RD-10. ASTER GDEM flyer *ASTER Global Digital Elevation Model (GDEM) - Overview / Features / Notes / Information*
<https://ssl.jspacesystems.or.jp/ersdac/GDEM/E/>

1.1.4 ALOS World 3D

- RD-11. Product Description *ALOS World 3D-30m (AW3D30) Version 2.2 – Product Description*
April 2019
Japan Aerospace Exploration Agency
https://www.eorc.jaxa.jp/ALOS/en/aw3d30/aw3d30v22_product_e.pdf
[../reference_documents/20190400_ALOS_World_3D_30_m_Product_Description.pdf](#)
- RD-12. GDEM Generation *Precise Global DEM Generation by ALOS PRISM*
2014
Japan Aerospace Exploration Agency
<https://www.isprs-ann-photogramm-remote-sens-spatial-inf-sci.net/II-4/71/2014/isprsannals-II-4-71-2014.pdf>
[../reference_documents/20140000_Tadono_Precise_Global_DEM_Generation_by_ALOS_PRISM.pdf](#)
- RD-13. CalVal ALOS PRISM *Calibration and validation of PRISM onboard ALOS*
January 2004
T. Tadono
https://www.researchgate.net/publication/228729227_Calibration_and_validation_of_PRISM_onboard_ALOS
[../reference_documents/20040100_Tadono_Calibration_and_validation_of_PRISM_onboard_ALOS.pdf](#)



RD-14. Calibration Result

Calibration Result of JAXA standard products
6 September 2011
Japan Aerospace Exploration Agency
https://www.eorc.jaxa.jp/ALOS/en/calval/20110906_en.pdf
[../reference_documents/20110906_JAXA_Calibration_result_of_JAXA_standard_products.pdf](#)

RD-15. AW3D Validation

Validation of 'AW3D' Global DSM generated from ALOS PRISM
2016
Japan Aerospace Exploration Agency
<https://www.isprs-ann-photogramm-remote-sens-spatial-inf-sci.net/III-4/25/2016/isprs-annals-III-4-25-2016.pdf>
[../reference_documents/20160000_Validation_of_AW3D_Global_DSM_Generated_from_ALOS_PRISM.pdf](#)

1.1.5 ICESat-1

RD-16. User Guide



User guide GLAS/ICESat L2 Global Land Surface Altimetry Data
23 October 2014
National Snow and Ice Data Center
https://nsidc.org/data/GLAH14/versions/34?qt-data_set_tabs=3#qt-data_set_tabs
[../reference_documents/20141023_NSIDC_GLAS_ICESat_L2_Global_Land_Surface_Altimetry_Data_\(HDF5\)_Version_34_National_Snow_and_Ice_Data_Center.htm](#)

RD-17. Data Management Plan

Science Data Management Plan
Version 4.0
July 1999
Peggy L. Jester and David W. Hancock III
<https://glas.wff.nasa.gov/wp-content/uploads/sdmp.pdf>
[../reference_documents/19990700_Jester_Science_data_management_plan.pdf](#)

RD-18. Cal/Val Plan

GLAS Altimeter Post-Launch Calibration/Validation Plan
Version 1.0
October 2001
Bob E. Schutz
http://www2.csr.utexas.edu/glas/pdf/plan/validation_plan_v1_oct2001.pdf
[../reference_documents/20011000_Schutz_GLAS_Altimeter_Post_Launch_Calibration_Validation_Plan.pdf](#)

RD-19. Glas_laser_ops_attrib

NSIDC Distributed ICESat GLAS Laser Operations Periods
December 2014
National Snow and Ice Data Center
https://nsidc.org/sites/nsidc.org/files/files/glas_laser_ops_attrib.pdf
[../reference_documents/20141200_NSIDC_glas_laser_ops_attrib.pdf](#)

1.1.6 Geocoding and orthorectification

- RD-20. SPOT Geom. HB *SPOT 123-4-5 Geometry Handbook*
Issue 1, revision 4 - 20/08/2004
Serge RIAZANOFF, GAEL Consultant for CNES /
SPOT IMAGE
<http://www-igm.univ-mlv.fr/~riazano/publications/GAEL-P135-DOC-001-01-04.pdf>

1.2 Attached document

The following is a list of attached documents with a direct bearing on the content of this Technical Note. Where referenced in the text, these are identified as [AD-n], where 'n' is the number in the list below:

- AD-1. HYP-080-VtWeb-v3 *SRTM vs. ASTER GDEM – Heights comparison*
https://visioterra.fr/telechargement/A003_VISIOTERRA_COMMUNICATION/HYP-080-VtWeb-v3_SRTM_ASTER-GDEM_comparison.pdf
https://visioterra.fr/telechargement/A003_VISIOTERRA_COMMUNICATION/hyperlinks_VtWeb/HYP-080-VtWeb-v3_SRTM_ASTER-GDEM_comparison.pdf
- AD-2. HYP-082-VtWeb *SRTM vs. ASTER GDEM – Local statistics comparison*
https://visioterra.fr/telechargement/A003_VISIOTERRA_COMMUNICATION/HYP-082-VtWeb_SRTM_ASTER-GDEM_local_statistics_comparison.pdf
https://visioterra.fr/telechargement/A003_VISIOTERRA_COMMUNICATION/hyperlinks_VtWeb/HYP-082-VtWeb_SRTM_ASTER-GDEM_local_statistics_comparison.pdf
- AD-3. VT-P317-KML-001-E *ICESat-1 / SRTM height errors*
issue 1 rev. 0,
VisioTerra
https://visioterra.fr/telechargement/P317_ESA_EDAP/VT-P317-KML-001-E-01-00_ICESat1_SRTM_height_errors.kml
https://visioterra.fr/telechargement/P317_ESA_EDAP/VT-P317-KML-001-E-01-00_ICESat1_SRTM_height_errors.kml
- AD-4. VT-P317-KML-002-E *ICESat-1 / ASTER GDEM height errors*
issue 1 rev. 0,
VisioTerra
https://visioterra.fr/telechargement/P317_ESA_EDAP/VT-P317-KML-002-E-01-00_ICESat1_ASTER_GDEM_height_errors.kml
https://visioterra.fr/telechargement/P317_ESA_EDAP/VT-P317-KML-002-E-01-00_ICESat1_ASTER_GDEM_height_errors.kml
- AD-5. VT-P317-KML-003-E *ICESat-1 / ALOS World 3D height errors*
issue 1 rev. 0,
VisioTerra
https://visioterra.fr/telechargement/P317_ESA_EDAP/VT-P317-KML-003-E-01-00_ICESat1_ALOS_World_3D_height_errors.kml
https://visioterra.fr/telechargement/P317_ESA_EDAP/VT-P317-KML-003-E-01-00_ICESat1_ALOS_World_3D_height_errors.kml

AD-6. VT-P317-KML-004-E *ICESat-1 / SRTM high height errors*
 issue 1 rev. 0,
 VisioTerra
https://visioterra.fr/telechargement/P317_ESA_EDAP/VT-P317-KML-004-E-01-00_ICESat1_SRTM_high_height_errors.kml
[VT-P317-KML-004-E-01-00_ICESat1_SRTM_high_height_errors.kml](https://visioterra.fr/telechargement/P317_ESA_EDAP/VT-P317-KML-004-E-01-00_ICESat1_SRTM_high_height_errors.kml)

1.3 Glossary

The following acronyms and abbreviations have been used in this Report.

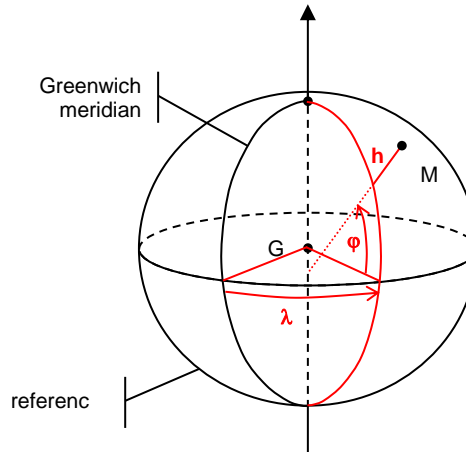
ALOS	Advanced Land Observing Satellite
ASTER	Advanced Spaceborne Thermal Emission and Reflection Radiometer
ATBD	Algorithm Theoretical Basis Document
AVNIR-2	Advanced Visible and Near Infrared Radiometer type 2
AW3D	ALOS World 3D
AW3D30	ALOS World 3D – 30 m
CRS	Coordinates Reference System
DEM	Digital Elevation Model
DSM	Digital Surface Model
DTM	Digital Terrain Model
EGM96	Earth Gravity Model 1996
EGM2008	Earth Gravity Model 2008
EPSG	European Petroleum Survey Group
GCP	Ground Control Point
GDEM	Global Digital Elevation Model
GeoTIFF	Geocoded TIFF
GL1	Global 1" arc
GLAS	Geoscience Laser Altimeter System
GPS	Global Positioning System
GSD	Ground Sampling Distance
HDF5	Hierarchical Data Format version 5
ICESat	Ice, Cloud and land Elevation Satellite
JAXA	Japan Aerospace Exploration Agency
LIDAR	Light Detection And Ranging
LP DAAC	Land Processes Distributed Active Archive Center
KML	Keyhole Markup Language
METI	Ministry of Economy, Trade, and Industry (Japan)
NASA	National Aeronautics and Space Administration (USA)
NGA	National Geospatial-Intelligence Agency (USA, former NIMA)
NSIDC	National Snow and Ice Data Center
PALSAR	Phased Array L-band Synthetic Aperture Radar
PRISM	Panchromatic Remote-sensing Instrument for Stereo Mapping
RMSE	Root Mean Square Error
SIR-C	Shuttle Imaging Radar-C
SRTM	Shuttle Radar Topography Mission
SRTM-GL1	Shuttle Radar Topography Mission Global 1 arc second
STS-99	Space Transportation System 99 (Endeavour)
TIFF	Tagged Image File Format
USGS	United States Geological Survey
VRS	Vertical Reference System
WGS84	World Geodetic System 1984

1.4 Definitions

The following definitions have been used in this Report.

coordinates
reference
system (CRS)

geographic

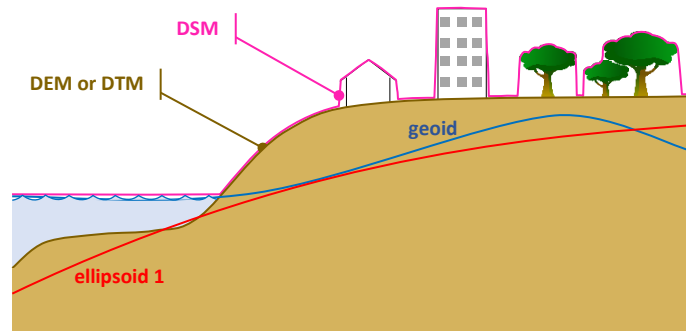


DTM
or
DEM
or
DSM

The “Digital Terrain Model” is also called “Digital Elevation Model” (DEM) or sometimes “Altimetry model”. A DEM is a raster data made of a georeferenced grid in which each cell gives an altitude with regard to a geoid (most frequent case) or a height above an ellipsoid.

In maritime parts, the altitudes or elevations may give the sea level (altitude equal to 0 metres above a geoid) or may give the ocean floor (negative values also called bathymetry).

The “Digital Surface Model” (DSM) gives altitudes or heights above overground: building roofs, top of canopy, sea level...



KML

The KML (Keyhole Markup Language) is a XML grammar describing the objects (points, lines, images, polygons) handled by Google Earth.

KML is based on the version 3.0 of the GML (Geographic Markup Language).

hyperlook

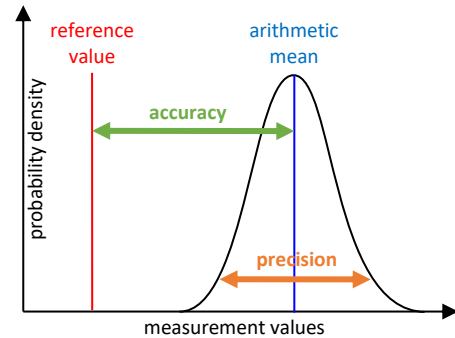
Rich URL containing the server address / product identifier / processing parameters / geometry of view) that readers may activate to achieve the same views in their usual Web browser (Internet Explorer, Firefox, Chrome, Safari...).

Metrology

accuracy vs. precision

Accuracy measures the closeness of agreement between a measured quantity value and a true quantity value. Distance between the arithmetic mean and the reference value is called the bias.

The precision measures the closeness of agreement between indications or measured quantity values obtained by replicate measurements on the same or similar objects under specified conditions.



See https://www.bipm.org/utis/common/documents/jcgm/JCGM_200_2012.pdf

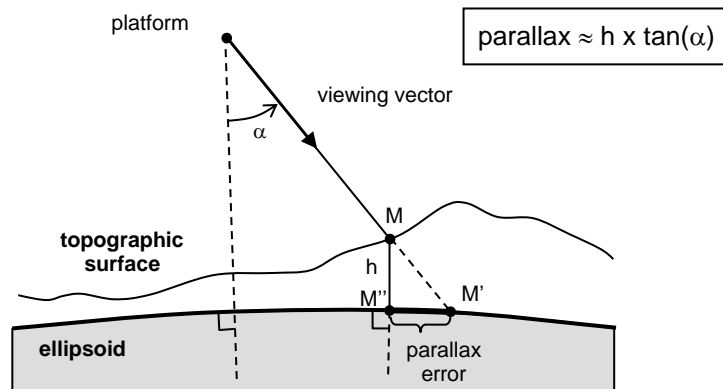
orthorectified

An image is orthorectified if its internal deformations due to the relief and the viewing geometry have been corrected. The orthorectified image does not exhibit parallax defects for the optical instrument or the shortening / dilation / layover defects caused by the radar instrument.

parallax

The parallax error is observed on a reference surface (generally an ellipsoid) when the viewing vector of an optical instrument is not perpendicular to this surface.

For a given viewing angle α , the parallax error (M' , M'') has a magnitude growing with the elevation h of the imaged point M above the reference surface.



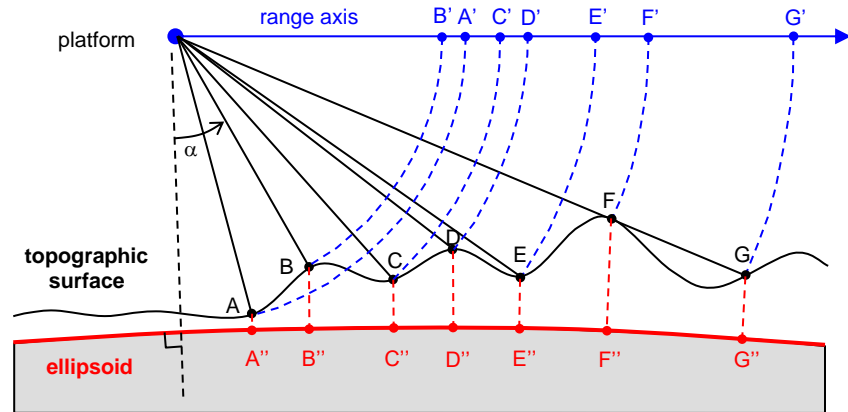
radar

For radar acquisition, positioning along the across-track axis (*slant range*) depends on the signal travel time.

geometry defects :

-shortening
-dilatation
-layover
-shadow

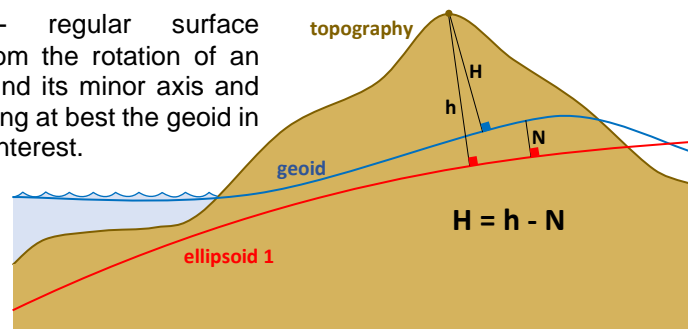
Depending on the viewing angle α and on the terrain relief, such a positioning technique may produce deformations illustrated by the figure like -shortening of the exposed faces (CD or EF), -layover (AB), -dilatation of the opposite faces (DE) up to -shadow (FG).



vertical reference system

There are three types of reference surface:

- topography - being the site of the interface between the solid phase and the gaseous and liquid phases of terrestrial matter;
- geoid - equipotential surface of the acceleration field of gravity (gravity + centrifugal force); the geoid is close to the mean surface of the sea;
- ellipsoid - regular surface resulting from the rotation of an ellipse around its minor axis and approximating at best the geoid in an area of interest.



The heights H with respect to the geoid (also called "altitude") are reference heights for the study of physical phenomena such as runoff. The altitude 0 metre corresponds to the mean sea level.

The heights h with respect to the ellipsoid (also called "elevation") are used for terrestrial modelling and in particular for orthorectification with respect to a reference ellipsoid (often WGS84).

2. EXECUTIVE SUMMARY

This document assesses the quality of three global DEMs widely used around the world: SRTM, ASTER GDEM and ALOS World 3D. In addition to a classic method of controlling heights using reference altimetry data (here the LiDAR ICESat-1), innovative methods are used to compare DEMs with each other, their heights but also derivative measurements such as slopes, azimuths or curvatures. Finally, a section is dedicated to the comparison of the uses of DEMs and more specifically to the impact of the characteristics of DEMs on the quality of orthorectification on a same scene (here a Sentinel-1 IW scene).

The evaluation of each DEM is carried out using a template designed for the evaluation of missions carrying out multi-date acquisitions. It follows an interpretation not always adapted to the analysis of a single product having often undergone several editions. These tensions are particularly noticeable in the maturity matrices and in the "mission assessment overview".

The evaluation of the three DEMs could have motivated the publication of three separate documents. It was however chosen to treat the three DEMs in a single document for several reasons:

- The explanation of the methods, the description of the ICESat-1 reference mission or the motivation of the choices would have been duplicated three times, making maintenance difficult for future editions of three documents in parallel.
- The intercomparison of DEMs provides interesting results. This intercomparison motivates the description of the three DEMs together in a single document.
- The document is organized by separating whenever necessary the description, analysis and results of each of the three DEMs.

For each DEM, numerous documents are available relating to product design, their control, their versions, their uses, etc. These documents were used to design maturity matrixes that reflect the maturity of the documentation, the compliance with the best practices in term of Calibration/Validation, and the quality of the data with regards to a reference dataset and in-situ data.

The VisioTerra VtWeb tool has been adapted to allow viewing and comparison of DEMs. It is thus possible to evaluate at any scale the differences between two DEMs and to immediately locate their anomalies. On a small scale, it is easy to spot the footprints of the acquisition segments used for optical photogrammetry and a little less those of the shuttle of the SRTM radar interferometry mission. On large scale, large structures, such as a 300 m raised drainage basin in SRTM or an under-elevated tile in ALOS World 3D. For each of the three DEMs, we find singularities in different places that we do not observe in the other two. All these defects reveal the difficulties inherent in radar or optical acquisition on (often uniform) surfaces of ice, snow, desert, open water...

A more conventional study is carried out by calculating the difference between the elevations of the LiDAR instrument (GLAS) on board the ICESat-1 satellite and the elevations interpolated at the same points from each DEM. According to the quality masks of the DEMs, this statistical study concerns up to 92 million points distributed over the entire surface of the globe. This numerical study shows that the DEM "ALOS World 3D" is the best one both in terms of quadratic mean error (RMSE) of 4.5 m and an arithmetic mean (bias) of 0.05 m. Second place is held by SRTM with roughly the same RMSE of 4.7 m but a larger bias of 0.59 m. Finally, ASTER GDEM obtains the worst results with a huge RMSE of 27.8 m and a large bias of 2.3 m.

The originality of the study also concerns the evaluation of the quality for the use of DEMs. Here, we estimate the quality of orthorectification by comparing two spacemaps of a same Sentinel-1 radar product but orthorectified by two different DEMs. Examples of altimetric differences between SRTM and ASTER GDEM produce amazing deformations in the Alps

or in the Himalayas. The singularities identified by comparing the DEMs with each other produce large differences between the orthorectified products. The study shows that an error of only one (1) meter can produce a planimetric error up to 1.80 m.

2.1 Product Quality Assessment Matrices

The entire document and in particular these first two sections "Executive Summary" and "Product Assessment Overview" have been drafted according to the standards set out in document RD-1.

As noted above, the term "mission" originally used in the EDAP guidelines does not apply strictly here and has been replaced by the term "product". Thus, the meaning of some of the terms appearing in the product quality evaluation matrixes has been reformulated:

- **Product generation**

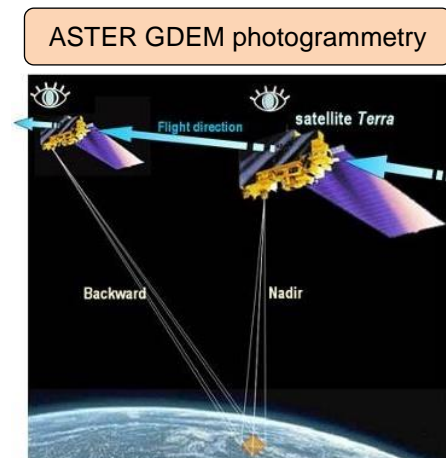
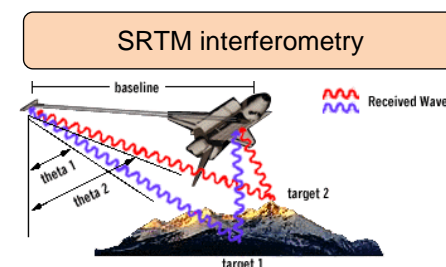
- Sensor Calibration & Characterisation Pre-Flight – DEMs are restituted after time-limited missions (case of interferometry of SRTM) or after having aggregated series of stereoscopic views (case of photogrammetric stereorestitution of ASTER GDEM or ALOS World 3D). In both cases, the characteristics of the sensors shall be tested / calibrated / characterised before the launch.

For the interferometry mechanism of SRTM, the knowledge of the precise distance (around 60 m) between the two antennas (onboard and outboard), the impact of vibrations, thermal dilations... shall be assessed and a correction model shall be given before the launch. In the particular case of SRTM, interferometric measurements have been performed in two bands from both SRTM-C (the main instrument provided by NASA) and SRTM-X (an ancillary instrument provided by DLR). These two instruments have been certainly inter-calibrated even if no public documentation has been provided about this issue (see section 1.1.2).

For the photogrammetric stereorestitution of ASTER GDEM or ALOS World 3D, one shall assess the parallax that depends on a precise knowledge of the instrument viewing angles for each one of the CCD of the two stereoscopic cameras. These angles are measured in laboratory before the launch.

- Sensor Calibration & Characterisation Post-Launch – Interferometric and photogrammetric products are not managed in the same way during the post-launch phase. Interferometry data are acquired in a limited period of time of the acquisition mission (10 days for SRTM). While the stereorestitution may be progressively produced / refined by using an unlimited number of stereoscopic views acquired during a much larger period of time that often depend on the number of cloud-free scenes or parts of scenes.

For the photogrammetric stereorestitution of ASTER GDEM or ALOS World 3D, one major source of errors is the difficulty to find homologous points in the disparity analysis; i.e. when trying to find the point of image 2 matching the one in image 1. This difficulty is linked to the lack of local radiometry variations in uniform areas like deserts, inlands, snow or ice extents.



2.1.1 SRTM

Product Information	Product Generation	Ancillary Information	Uncertainty Characterisation	Validation
Product Details	Sensor Calibration & Characterisation Pre-Flight	Product Flags	Uncertainty Characterisation Method	Reference Data Representativeness
Availability & Accessibility	Sensor Calibration & Characterisation Post-Launch	Ancillary Data	Uncertainty Sources Included	Reference Data Quality
Product Format	Retrieval Algorithm Method		Uncertainty Values Provided	Validation Method
User Documentation	Retrieval Algorithm Tuning		Geolocation Uncertainty	Validation Results
Metrological Traceability Documentation	Additional Processing			

Key

Not Assessed

Not Assessable

Basic

Intermediate

Good

Excellent


 Information Not Public

Figure 1 – SRTM Product Quality Evaluation Matrix.

2.1.2 ASTER GDEM

Product Information	Product Generation	Ancillary Information	Uncertainty Characterisation	Validation
Product Details	Sensor Calibration & Characterisation Pre-Flight	Product Flags	Uncertainty Characterisation Method	Reference Data Representativeness
Availability & Accessibility	Sensor Calibration & Characterisation Post-Launch	Ancillary Data	Uncertainty Sources Included	Reference Data Quality
Product Format	Retrieval Algorithm Method		Uncertainty Values Provided	Validation Method
User Documentation	Retrieval Algorithm Tuning		Geolocation Uncertainty	Validation Results
Metrological Traceability Documentation	Additional Processing			

Key

Not Assessed

Not Assessable

Basic

Intermediate

Good

Excellent


 Information Not Public

Figure 2 – ASTER GDEM Product Quality Evaluation Matrix.

2.1.3 ALOS World 3D

Product Information	Product Generation	Ancillary Information	Uncertainty Characterisation	Validation
Product Details	Sensor Calibration & Characterisation Pre-Flight	Product Flags	Uncertainty Characterisation Method	Reference Data Representativeness
Availability & Accessibility	Sensor Calibration & Characterisation Post-Launch	Ancillary Data	Uncertainty Sources Included	Reference Data Quality
Product Format	Retrieval Algorithm Method		Uncertainty Values Provided	Validation Method
User Documentation	Retrieval Algorithm Tuning		Geolocation Uncertainty	Validation Results
Metrological Traceability Documentation	Additional Processing			

Key

Not Assessed

Not Assessable

Basic

Intermediate

Good

Excellent


 Information Not Public

Figure 3 – ALOS World 3D Product Quality Evaluation Matrix.

3. PRODUCT ASSESSMENT OVERVIEW

3.1 SRTM

3.1.1 Product Information

Product Details	
Product Name	<i>SRTM-GL1</i>
Sensor Name	<i>SRTM instrument</i>
Sensor Type	<i>SIR-C – Shuttle Imaging Radar-C</i>
Mission Type	<i>STS-99 Endeavour</i>
Mission Orbit	<i>Low Earth orbit, 57.0 degrees of inclination</i>
Product Version Number	<i>3.0</i>
Product ID	<i>SRTM-GL1 v003</i>
Processing level of product	<i>Level 3 (multi date and multi sensor synthesis)</i>
Measured Quantity Name	<i>Elevation</i>
Measured Quantity Units	<i>metres</i>
Stated Measurement Quality	<i>RD-3 - section 1.6 “Performance Summary and SRTM Error Products”</i>
Spatial Resolution	<i>1 arc second</i>
Spatial Coverage	<i>180 W to 180 E, 60 N to 56 S</i>
Temporal Resolution	<i>Not Applicable</i>
Temporal Coverage	<i>11 February 2000 to 22 February 2000</i>
Point of Contact	<i>NASA / NGA</i>
Product locator (DOI/URL)	https://lpdaac.usgs.gov/products/SRTM-GL1v003/
Conditions for access and use	<i>Free</i>
Limitations on public access	<i>No limitation</i>
Product Abstract	<p><i>The Land Processes Distributed Active Archive Center (LP DAAC) is responsible for the archive and distribution of the NASA Making Earth System Data Records for Use in Research Environments (MEaSUREs) version SRTM, which includes the global 1 arc second (~30 metres along equator) product.</i></p> <p><i>NASA Shuttle Radar Topography Mission (SRTM) datasets result from a collaborative effort by the National Aeronautics and Space Administration (NASA) and the National Geospatial-Intelligence Agency (NGA - previously known as the National Imagery and Mapping Agency, or NIMA), as well as the participation of the German and Italian space agencies. The purpose of SRTM was to generate a near-global digital elevation model (DEM) of the Earth using radar interferometry. SRTM was a primary component of the payload on the Space Shuttle Endeavour during its STS-99 mission. Endeavour launched February 11, 2000 and flew for 11 days.</i></p>

	<p>Each SRTM-GL1 data tile contains a mosaic and blending of elevations generated by averaging all "data takes" that fall within that tile. These elevation files use the extension ".HGT", meaning height (such as N37W105.SRTM-GL1.HGT). The primary goal of creating the version 3 data was to eliminate voids that were present in earlier versions of SRTM data. In areas with limited data, existing topographical data were used to supplement the SRTM data to fill the voids. The source of each elevation pixel is identified in the corresponding SRTM-GL1N product (such as N37W105.SRTM-GL1N.NUM).</p> <p>SRTM collected data in swaths, which extend from ~30 degrees off-nadir to ~58 degrees off-nadir from an altitude of 233 kilometres (km). These swaths are ~225 km wide, and consisted of all land between 60° N and 56° S latitude. This accounts for about 80% of Earth's total landmass.</p>
--	---

To discriminate between the four FAIR principles and to assess a global notation more traceable, four notations have been given over 4 (Findable), 3 (Accessible), 3 (Interoperable) and 4 (Reusable) leading to a total notation over 14.

Availability & Accessibility	
Compliant with FAIR principles	<p>Findable: Mostly yes (3/4)</p> <p>Accessible: Yes (3/3)</p> <p>Interoperable: Intermediate (1.5/3)</p> <p>Reusable: Mostly yes (3/4)</p> <p style="text-align: right;">Global: 10.5/14</p>
Data Management Plan	One shot data
Availability Status	Available for download

Product Format	
Product File Format	HGT (HeiGhT)
Metadata Conventions	v1.0
Analysis Ready Data?	No, the data contains the height value above EGM96 in a raw format not always readable by standard GIS.

User Documentation		
Document	Reference	QA4ECV Compliant
Product User Guide	RD-2	Not Assessed
ATBD	RD-4	Not Assessed

Metrological Traceability Documentation	
Document Reference	RD-5
Traceability Chain / Uncertainty Tree Diagram Available	Yes (Figure 4: SRTM Height Error Budget)

3.1.2 Product Generation

Sensor Calibration & Characterisation – Pre-Flight	
Summary	<i>This section and in particular the section 3.2 of RD-4 describe the characteristics of the SRTM system and C Radar subsystem that has been used to process the SRTM GL1 product.</i>
References	<i>RD-4 - under section 3 “SRTM SYSTEM”</i>

Sensor Calibration & Characterisation – Post-Launch	
Summary	<i>Geometric and phase calibration of the interferometer was an essential part of processing the data. Since many components of the system, the baseline and receiver phase characteristics in particular, varied over time, these quantities could not be calibrated per se. Therefore, the calibration strategy employed was to determine those quantities that were stable over the 10 days of the mission and estimate them statically and then dynamically estimate those that varied with time.</i>
References	<i>RD-4- under section 5.1.5 “Calibration Efforts”.</i>

Retrieval Algorithm Method	
Summary	<i>The section describes the methodology of retrieving the height value based on an interferometric pair.</i>
References	<i>RD-4 - under section 5.1.4 “Topographic Processing of Radar Data”.</i>

Retrieval Algorithm Tuning	
Summary	<i>The section describes how the various version of SRTM (from 1 to 3) have been processed and what are the differences between them.</i>
References	<i>RD-2 – under section 2.1.1 “Versioning”.</i>

Additional Processing	
<i>Additional Processing 1 – Gap filling</i>	
Description	<i>One of the major defects of the first versions of the SRTM product was the presence of many voids leading to gaps in the height coverage. Different strategies have been used to fill these gaps (interpolations, use of low resolution SRTM30, or use of external values) that are documented.</i>
Reference	<i>RD-2 – under section 2.1.1 “Versioning”.</i>

3.1.3 Ancillary Information

Product Flags	
Product Flag Documentation	RD-2
Comprehensiveness of Flags	Flag values are available at a pixel level in an external file.

Ancillary Data	
Ancillary Data Documentation	RD-2
Comprehensiveness of Data	Flag values also describe the origin of the pixel (SRTM or other DEM filled) and the number of interferometric pairs used.
Uncertainty Quantified	Not found

3.1.4 Uncertainty Characterisation

Uncertainty Characterisation Method	
Summary	Section 1.5 of the reference document covers the SRTM error model, with respect to the observations written in the previous sections of the reference document
Reference	RD-3 – under section 1.5 “SRTM Error Model”

Uncertainty Sources Included	
Summary	Section 1.3 of the reference document covers the SRTM error sources (the entire list is available in Appendix A of the reference document)
Reference	RD-3 - under 1.3 SRTM Error Sources

Uncertainty Values Provided	
Summary	Figures 4.5 to 4.9 of the reference document provide maps of height error on several continents for the SRTM mission.
Reference	RD-3 - Figures 4.5, 4.6, 4.7, 4.8, 4.9 (height error maps)
Analysis Ready Data?	Yes

Geolocation Uncertainty	
Summary	<p>In contrast to the previous sections, the estimation of geolocation accuracy requires the identification of specific geometric features in either the SRTM topography or in the image. In the following sections, both techniques are used, sometimes jointly to obtain estimates of the geolocation accuracy of SRTM.</p> <p>In the first section, radar corner reflectors, which can be identified in the image (both in the range-Doppler and ground planes) are used to estimate the system delay errors, which cause a geolocation error in the look direction of the radar.</p>

	<i>In the second section, kinematic GPS track topography and road detection are combined to estimate the residual planimetric errors after timing errors are corrected. The final geolocation results are reported in Table 1.3, which shows that the geolocation requirements are amply met by the SRTM data.</i>
Reference	<i>RD-3 - under Chapter 5: "Geolocation errors"</i>

3.1.5 Validation

Validation Activity #1	
Independently Assessed?	Yes
Reference Data Representativeness	
Summary	<i>The quality assessment of SRTM-GL1 is processed using all the terrain acquisitions of the GLAS instrument (GLAH14 product). The number of compared heights may vary from one DEM study to another, as bad quality data is filtered both on the DEM products and ICESat products.</i>
Reference	<i>see section 4.2.2.2 of this document (in tab "Statistics of the (ICESat - SRTM) comparison")</i>
Reference Data Quality & Suitability	
Summary	<i>GLAS acquisitions are analysed on the same orbit on multiple periods to ensure the consistency of the retrieved heights. A particularly flat area has been chosen for this assessment: Bonneville Salt Flats. The results of this study highlight the accuracy and constancy of GLAS acquisitions.</i>
Reference	<i>see section 4.2.1 of this document</i>
Validation Method	
Summary	<i>SRTM-GL1 heights are compared to ICESat acquisitions to assess their accuracy. ICESat's data is filtered using the provided quality flags. At each ICESat footprint location, an interpolated height is processed from SRTM-GL1. Both ICESat and SRTM-GL1 heights are converted from their original vertical reference system to the WGS84 ellipsoid, from which every SRTM-GL1 interpolated height is subtracted to the corresponding ICESat footprint.</i>
Reference	<i>see section 4.2.2.1 of this document</i>
Validation Results	
Summary	<i>The results show an average difference between the height value in SRTM and ICESat of 0.590 metres with a standard deviation of 4.704 metres. No correlation has been found between the distribution of the error and characteristics extracted from SRTM.</i>
Reference	<i>see section 4.2.2.2 of this document</i>

3.2 ASTER GDEM

3.2.1 Product Information

Product Details	
Product Name	ASTER GDEM
Sensor Name	ASTER (Advanced Spaceborne Thermal Emission and Reflection Radiometer)
Sensor Type	Optical
Mission Type	Terra satellite
Mission Orbit	Sun synchronous
Product Version Number	V2.0
Product ID	ASTGTMV002
Processing level of product	N/A
Measured Quantity Name	Elevation
Measured Quantity Units	metres
Stated Measurement Quality	N/A
Spatial Resolution	1 arc second
Spatial Coverage	180 W to 180 E, 83 N to 83 S
Temporal Resolution	Multi-Year
Temporal Coverage	18 December 1999 to 28 February 2011
Point of Contact	NASA / METI
Product locator (DOI/URL)	https://lpdaac.usgs.gov/products/astgtmv002/
Conditions for access and use	Free
Limitations on public access	N/A
Product Abstract	<p>The ASTER Global Digital Elevation Model (ASTGTM) was developed jointly by the U.S. National Aeronautics and Space Administration (NASA) and Japan's Ministry of Economy, Trade, and Industry (METI).</p> <p>ASTER is capable of collecting in-track stereo using nadir-looking and aft-looking near infrared cameras. Since 2001, these stereo pairs have been used to produce single-scene (60 kilometres by 60 kilometres) digital elevation models (DEM) having vertical root mean square error (RMSE) accuracies generally between 10 and 25 metres.</p> <p>The methodology used by Japan's Sensor Information Laboratory Corporation (SILC) to produce the ASTER GDEM involves automated processing of the entire ASTER Level 1A archive. Stereo-correlation is used to produce over one million individual scene-based ASTER DEMs, to which cloud masking is applied to remove cloudy pixels. All cloud-screened DEMs are stacked and residual bad values and outliers are removed. Selected data are averaged to create final pixel values, and residual anomalies are corrected before partitioning the data into 1 degree by 1 degree tiles.</p>

Availability & Accessibility	
Compliant with FAIR principles	<i>Findable: Mostly yes (3/4)</i> <i>Accessible: Yes (3/3)</i> <i>Interoperable: Mostly yes (2/3)</i> <i>Reusable: Mostly yes (3/4)</i> <i>Global: 11/14</i>
Data Management Plan	N/A
Availability Status	Available for download

Product Format	
Product File Format	GeoTIFF
Metadata Conventions	v1
Analysis Ready Data?	Mostly yes, the height values are provided in GeoTIFF format over EGM96.

User Documentation		
<i>Document</i>	<i>Reference</i>	<i>QA4ECV Compliant</i>
Product User Guide	README file available in each tile archive file	Not Assessed
ATBD	RD-7	Not Assessed

Metrological Traceability Documentation	
Document Reference	N/A
Traceability Chain / Uncertainty Tree Diagram Available	N/A

3.2.2 Product Generation

Sensor Calibration & Characterisation – Pre-Flight	
Summary	<i>Section 2 of the referenced document describes the pre-flight calibration and characterization of the ASTER instrument (radiometric calibration and spectral bands characterization).</i>
References	<i>RD-8 - section 2. Pre-flight calibration/characterization methodology</i>

Sensor Calibration & Characterisation – Post-Launch	
Summary	<i>Section 5 of the referenced document describes the post-launch calibration and characterization of the ASTER instrument (instrument-based and target-based calibrations).</i>
References	<i>RD-8 - section 5. In-orbit radiometric calibration/characterization methodology</i>

Retrieval Algorithm Method	
Summary	<i>A digital stereo correlation approach will be used to calculate parallax differences and derive DEMs from ASTER Level 1 stereo pairs. The mathematical concept of one approach to stereo correlation is described in Appendix 6-2; other mathematical treatments of equivalent procedures are provided by Ackermann (1984), Ehlers and Welch (1987), and Rao et al. (1996).</i>
References	<i>RD-7</i>

Retrieval Algorithm Tuning	
Summary	<i>Because of inadequate pointing and ephemeris information for use with 15 m ASTER pixels, absolute DEMs must be referenced to a map coordinate system using ground control points (GCPs).</i>
References	<i>RD-7 - (Figure 3.0-2)</i>

Additional Processing	
Additional Processing 1	
Description	<i>N/A As no information have been found concerning the additional processing steps of ASTER GDEM products, the "Additional Processing" part of this section could not be assessed.</i>
Reference	<i>N/A</i>

3.2.3 Ancillary Information

Product Flags	
Product Flag Documentation	N/A <i>As no product flags have been found concerning ASTER GDEM version 2, the "Product Flags" part of this section could not be assessed.</i>
Comprehensiveness of Flags	N/A

Ancillary Data	
Ancillary Data Documentation	<i>Readme file contained in each tile archive file (RD-6)</i>
Comprehensiveness of Data	<i>The flag values describe the origin of the height on a pixel basis or the number of stereoscopic views used to compute the height value.</i>
Uncertainty Quantified	N/A

3.2.4 Uncertainty Characterisation

Uncertainty Characterisation Method	
Summary	<i>The method is described in the section Methods & Reference Elevation Data Sets on page 3.</i>
Reference	RD-9

Uncertainty Sources Included	
Summary	<i>The reference elevation dataset used is described in the section Methods & Reference Elevation Data Sets on page 3.</i>
Reference	RD-9

Uncertainty Values Provided	
Summary	<i>The section presents the result of the vertical assessment using various elevation references.</i>
Reference	RD-9 - under Vertical error section
Analysis Ready Data?	No

Geolocation Uncertainty	
Summary	<i>The section presents the results of the horizontal error by comparing to two others DEMs</i>
Reference	RD-9 - under Horizontal error section

3.2.5 Validation

Validation Activity #1	
Independently Assessed?	Yes
Reference Data Representativeness	
Summary	<i>The quality assessment of ASTER GDEM is processed using all the terrain acquisitions of the GLAS instrument (GLAH14 product). The number of compared heights may vary from one DEM study to another, as bad quality data is filtered both on the DEM products and ICESat products.</i>
Reference	<i>see section 4.2.3.2 of this document (in tab "Statistics of the (ICESat - ASTER GDEM) comparison")</i>
Reference Data Quality & Suitability	
Summary	<i>GLAS acquisitions are analysed on the same orbit on multiple periods to ensure the consistency of the retrieved heights. A particularly flat area has been chosen for this assessment: Bonneville Salt Flats. The results of this study highlight the accuracy and constancy of GLAS acquisitions.</i>
Reference	<i>see section 4.2.1 of this document</i>
Validation Method	
Summary	<i>ASTER GDEM heights are compared to ICESat acquisitions to assess their accuracy. ICESat's data is filtered using the provided quality flags. At each ICESat footprint location, an interpolated height is processed from ASTER GDEM. Both ICESat and ASTER GDEM heights are converted from their original vertical reference system to the WGS84 ellipsoid, from which every ASTER GDEM interpolated height is subtracted to the corresponding ICESat footprint.</i>
Reference	<i>see section 4.2.3.1 of this document</i>
Validation Results	
Summary	<i>The results show an average difference between the height values in ASTER GDEM and ICESat of 2.315 metres and a standard deviation of 27.667 metres.</i>
Reference	<i>see section 4.2.3.2 of this document</i>

3.3 ALOS World 3D

3.3.1 Product Information

Product Details	
Product Name	<i>ALOS World 3D</i>
Sensor Name	<i>ALOS (Advanced Land Observing Satellite)</i>
Sensor Type	<i>PRISM (Panchromatic Remote-sensing Instrument for Stereo Mapping)</i>
Mission Type	<i>Satellite</i>
Mission Orbit	<i>Sun Synchronous</i>
Product Version Number	<i>V2.2</i>
Product ID	<i>AW3D30</i>
Processing level of product	<i>Level 3</i>
Measured Quantity Name	<i>Elevation</i>
Measured Quantity Units	<i>Metres</i>
Stated Measurement Quality	<i>N/A</i>
Spatial Resolution	<i>1 arc second</i>
Spatial Coverage	<i>180 W to 180 E, 83 N to 83 S</i>
Temporal Resolution	<i>Multi-Year</i>
Temporal Coverage	<i>24 January 2006 to 12 May 2011</i>
Point of Contact	<i>JAXA</i>
Product locator (DOI/URL)	https://www.eorc.jaxa.jp/ALOS/en/aw3d30/index.htm
Conditions for access and use	<i>Free</i>
Limitations on public access	<i>N/A</i>
Product Abstract	<p><i>This data set is a global digital surface model (DSM) with horizontal resolution of approximately 30 metres (1 arc second) by the Panchromatic Remote-sensing Instrument for Stereo Mapping (PRISM) on board the Advanced Land Observing Satellite "ALOS". Any of the commercial and non-commercial purposes can be used free of charge under the conditions of the "5. Terms of Use" below.</i></p> <p><i>In May 2015, "ALOS World 3D-30m (AW3D30)", free 30 metres resolution version of "ALOS World 3D (AW3D)", was released. An area of no-data or low-quality, from 60 degrees north to 60 degrees south, was filled in with version 1.1 released in March 2017 and 2.1 released in April 2018.</i></p> <p><i>Version 2.2 released in April 2019 is an improved version of the northern region over 60 degrees north. In this version, along with the complement of no-data or low-quality area, updating of coastline was also performed.</i></p> <p><i>We hope that this dataset will be widely used in scientific research, education, and new services that use geospatial information.</i></p>

Availability & Accessibility	
Compliant with FAIR principles	<i>Findable: Yes (4/4)</i> <i>Accessible: Yes (3/3)</i> <i>Interoperable: Intermediate (1.5/3)</i> <i>Reusable: Yes (4/4)</i> <i>Global: 12.5/14</i>
Data Management Plan	N/A
Availability Status	Available for download

Product Format	
Product File Format	GeoTIFF
Metadata Conventions	v1
Analysis Ready Data?	Mostly yes, the height values are provided in GeoTIFF format over EGM96.

User Documentation		
Document	Reference	QA4ECV Compliant
Product User Guide	RD-11	Not Assessed
ATBD	RD-12	Not Assessed

Metrological Traceability Documentation	
Document Reference	N/A As no metrological traceability documentation have been found for ALOS World 3D, the "Metrological Traceability Documentation" part of this section could not be assessed.
Traceability Chain / Uncertainty Tree Diagram Available	N/A

3.3.2 Product Generation

Sensor Calibration & Characterisation – Pre-Flight	
Summary	This paper introduces the updated plans for sensor calibration and product validation of the Panchromatic Remote-sensing Instrument for Stereo Mapping (PRISM), which is to fly on the Advanced Land Observing Satellite (ALOS) satellite that will be launched this Japanese fiscal year. PRISM is used to derive digital elevation models (DEMs) with very high spatial resolution, which is also one of the objectives of the ALOS mission. To achieve this objective, PRISM consists of three panchromatic radiometers for forward-, nadir-, and backward-looking in the along-track direction, and acquires the images in the same orbit and at almost the same time. The geometric calibration is important in generating a highly accurate DEM with high spatial resolution by using PRISM's triplet images. Highly accurate ground control

	<i>points (GCP) are necessary to calibrate the geometric accuracy and validate the generated DEM. Collecting GCP worldwide is difficult and hard work in spite of its importance. In this paper, we describe the current plans for calibrating and validating PRISM aboard the ALOS, and in particular, our strategies for preparing GCP with evaluation items for geometric calibration, including expected problem effects regarding geometric accuracy.</i>
References	RD-13

Sensor Calibration & Characterisation – Post-Launch

Summary	<i>High resolution satellite imageries demonstrate the effective performance when they are used on the Geographical Information System (GIS). Three instruments onboard ALOS were to observe the Earth surface in detail, and their geometric and radiometric accuracies are important not only for showing the instruments performance themselves, but also for utilizing the images and products in several applications. ALOS was operated from January 24, 2006 to May 12, 2011, and the products were continuously calibrated and validated by JAXA for all through the time. The following calibration results show the accuracies of the standard products for PRISM, AVNIR-2 and PALSAR.</i>
References	RD-14

Retrieval Algorithm Method

Summary	<i>The Japan Aerospace Exploration Agency (JAXA) generated the global digital elevation/surface model (DEM/DSM) and orthorectified image (ORI) using the archived data of the Panchromatic Remote-sensing Instrument for Stereo Mapping (PRISM) onboard the Advanced Land Observing Satellite (ALOS, nicknamed "Daichi"), which was operated from 2006 to 2011. PRISM consisted of three panchromatic radiometers that acquired along-track stereo images. It had a spatial resolution of 2.5 m in the nadir-looking radiometer and achieved global coverage, making it a suitable potential candidate for precise global DSM and ORI generation. In the past 10 years or so, JAXA has conducted the calibration of the system corrected standard products of PRISM in order to improve absolute accuracies as well as to validate the high-level products such as DSM and ORI. In this paper, we introduce an overview of the global DEM/DSM dataset generation project, including a summary of ALOS and PRISM, in addition to the global data archive status. It is also necessary to consider data processing strategies, since the processing capabilities of the level 1 standard product and the high-level products must be developed in terms of both hardware and software to achieve the project aims. The automatic DSM/ORI processing software and its test processing results are also described.</i>
References	RD-13

Retrieval Algorithm Tuning

Summary	<i>N/A As no further information has been found concerning ALOS World 3D's product generation, the "Retrieval Algorithm Tuning" part of this section could not be assessed.</i>
References	N/A

Additional Processing	
Additional Processing 1	
Description	N/A <i>As no further information has been found concerning ALOS World 3D's product generation, the "Additional Processing" part of this section could not be assessed.</i>
Reference	N/A

3.3.3 Ancillary Information

Product Flags	
Product Flag Documentation	RD-11 - section 2.1
Comprehensiveness of Flags	<i>The mask file describes on a pixel level the valid/invalid pixel value and other information such as the sea mask and origin of the pixel (if other DEMs are used).</i>

Ancillary Data	
Ancillary Data Documentation	RD-11 - section 2.1
Comprehensiveness of Data	<i>The "Staking number file" describes on a pixel level the number of scenes used to compute the height value.</i>
Uncertainty Quantified	No

3.3.4 Uncertainty Characterisation

Uncertainty Characterisation Method	
Summary	<i>Not described in the document of validation.</i>
Reference	N/A

Uncertainty Sources Included	
Summary	<i>The perspective global absolute accuracy of the processed tiles is being routinely monitored by comparison with existing global height reference i.e., ICESat data, while the detailed relative accuracy is independently evaluated at validation sites of GCPs and LiDAR/DEM in valid data areas.</i>
Reference	RD-15 - under section 3.1, 3.2

Uncertainty Values Provided	
Summary	<i>The result is summed up in various tables depending on the sources used.</i>

Reference	RD-15 -table 3 / table 4
Analysis Ready Data?	No

Geolocation Uncertainty	
Summary	N/A <i>As no information has been found about the geolocation error of ALOS World 3D, the "Geolocation Uncertainty" part of this section could not be assessed.</i>
Reference	N/A

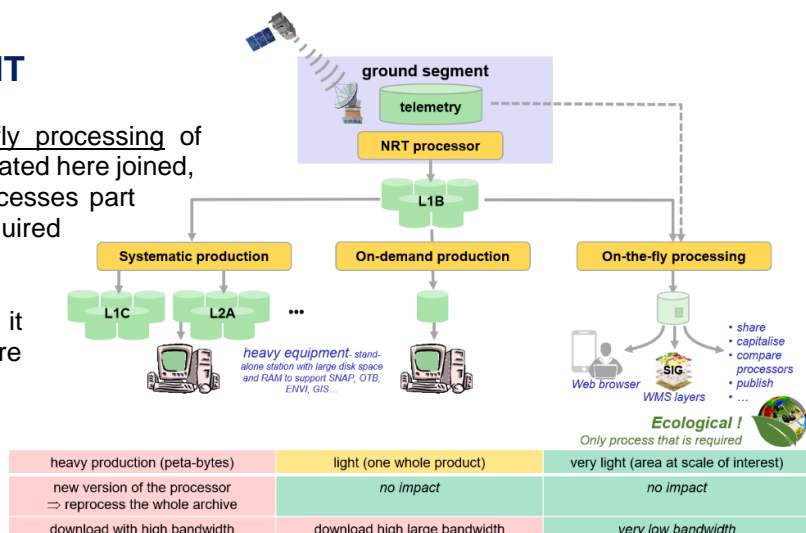
3.3.5 Validation

Validation Activity #1	
Independently Assessed?	Yes
Reference Data Representativeness	
Summary	<i>The quality assessment of ALOS World 3D is processed using all the terrain acquisitions of the GLAS instrument (GLAH14 product). The number of compared heights may vary from one DEM study to another, as bad quality data is filtered both on the DEM products and ICESat products.</i>
Reference	<i>see section 4.2.4.2 of this document (in tab "Statistics of the (ICESat – ALOS World 3D) comparison")</i>
Reference Data Quality & Suitability	
Summary	<i>GLAS acquisitions are analysed on the same orbit on multiple periods to ensure the consistency of the retrieved heights. A particularly flat area has been chosen for this assessment: Bonneville Salt Flats. The results of this study highlight the accuracy and constancy of GLAS acquisitions.</i>
Reference	<i>see section 4.2.1 of this document</i>
Validation Method	
Summary	<i>ALOS World 3D heights are compared to ICESat acquisitions to assess their accuracy. ICESat's data are filtered using the provided quality flags. At each ICESat footprint location, an interpolated height is processed from ALOS World 3D. Both ICESat and ALOS World 3D heights are converted from their original vertical reference system to the WGS84 ellipsoid, from which every ALOS World 3D interpolated height is subtracted to the corresponding ICESat footprint.</i>
Reference	<i>see section 4.2.4.1 of this document</i>
Validation Results	
Summary	<i>The results show an average difference between height values in ALOS World 3D and ICESat of 0.050 metres and a standard deviation of 4.516 metres.</i>
Reference	<i>see section 4.2.4.2 of this document</i>

4. DETAILED ASSESSMENT

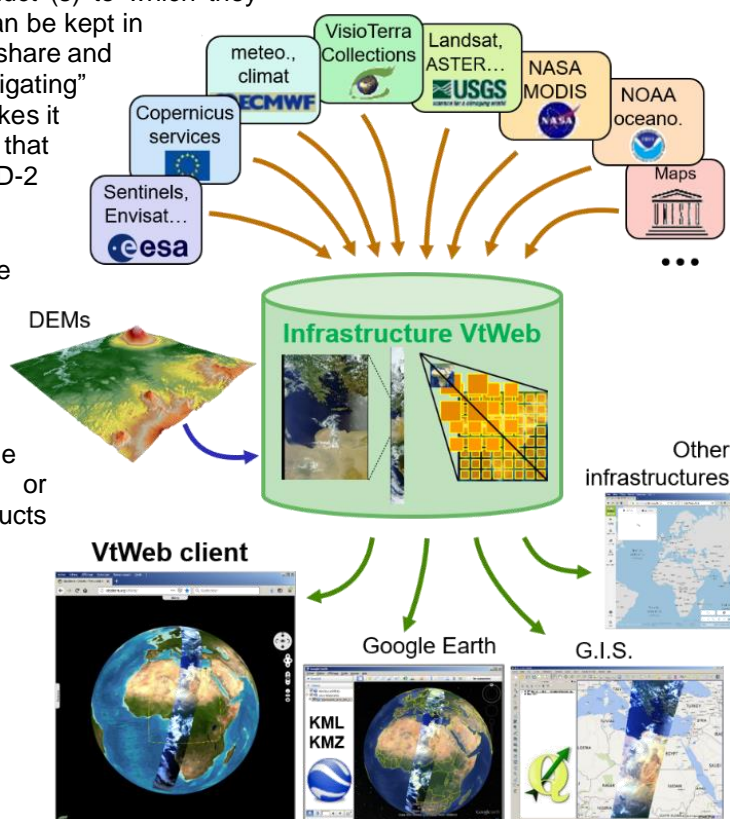
VisioTerra promotes the on-the-fly processing of data required by the user. As illustrated here joined, this “ecological process” only processes part of the products and on the required scale.

This processing strategy makes it possible to interactively configure the functions and to tune the rendering parameters according to the range of values and/or the features of the landscape.



These processing parameters, the product (s) to which they apply as well as the viewing geometry can be kept in a hyperlook, a rich URL that the user can share and that other users will replay by “navigating” interactively in the data. This process makes it possible to design galleries of use cases that can be kept, for example, in AD-1 or AD-2 hyperlooks documents.

These new possibilities require the maintenance of a server called “Data Processing Relay (DPR)” capable here of -viewing DEMs with different restitution styles (for example different shading directions), -calculating on-the-fly derived measurements (for example slope, azimuth, curvatures), or even -orthorectifying on-the-fly products previously prepared, i.e. downloaded from ESA servers (or other data providers) and organized in quadrees without modifying their geometry neither their radiometry



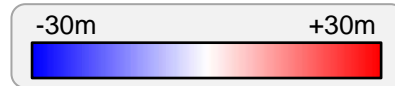
4.1 DEMs intercomparison

4.1.1 Absolute height values

4.1.1.1 Global differences

The following figures (Figure 4, Figure 5, and Figure 6) display the difference in metres between the different DEMs. The altitude of the first DEM is deducted from the altitude of the second DEM. The blue areas represent the higher areas for the second DEM, the red areas represent the higher areas for the first DEM and the white areas correspond to identical altitude. Differences have been stretched in the range [-30m ; +30m]

The three DEMs to be compared are SRTM, ASTER GDEM and ALOS World 3D (AW3D30).



[2D view](#)

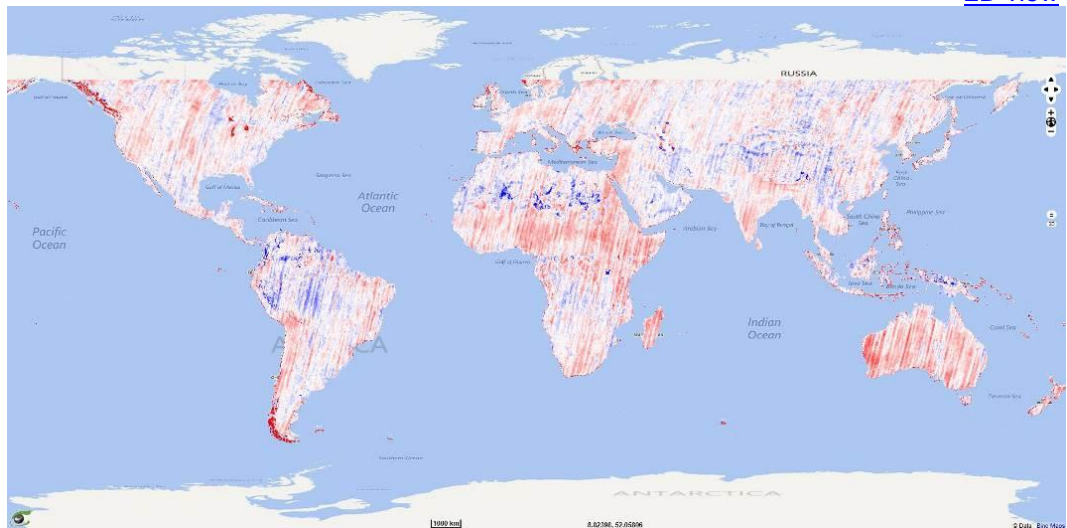


Figure 4 – Differences between SRTM and ASTER GDEM.

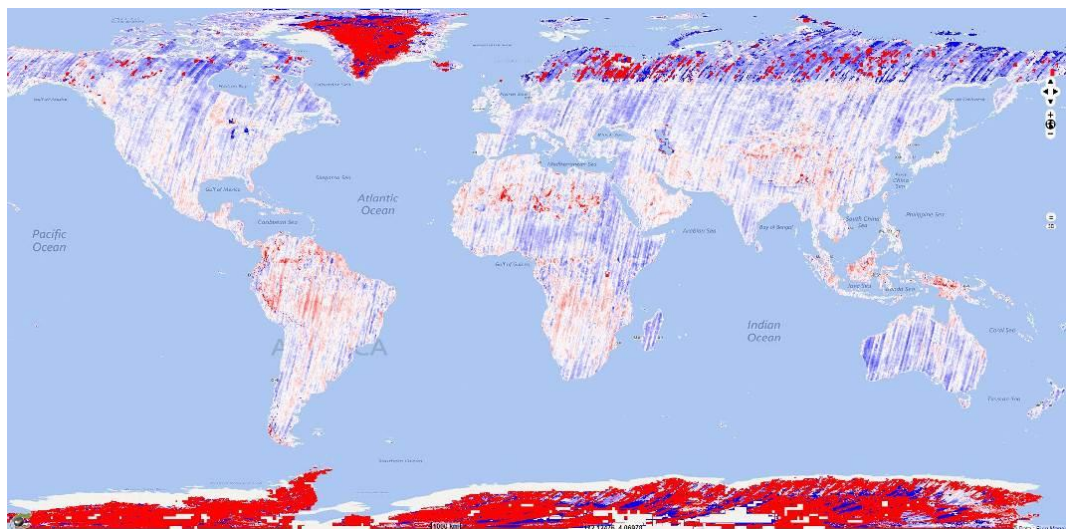


Figure 5 – Differences between ASTER GDEM and ALOS World 3D.

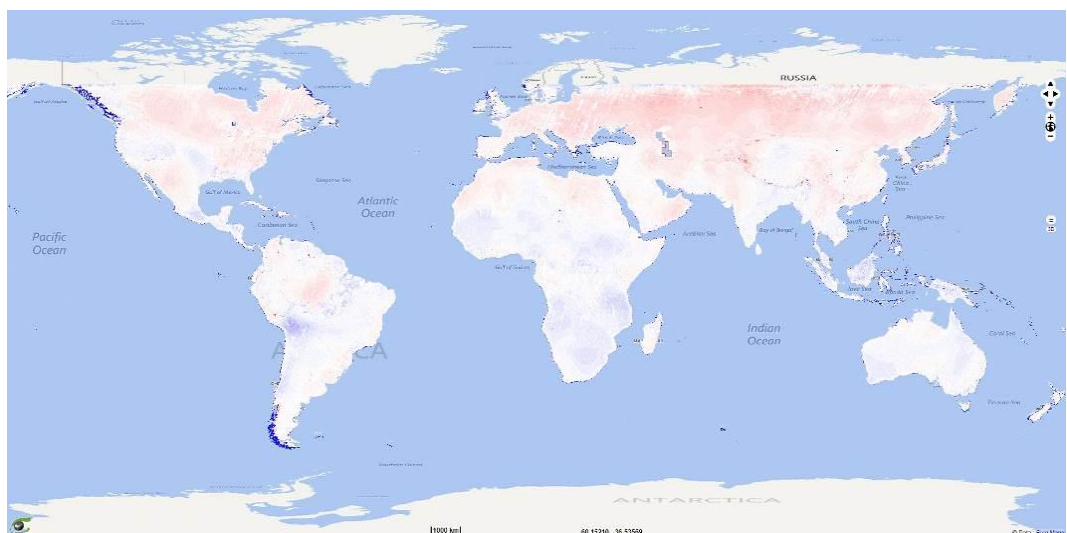


Figure 6 – Differences between ALOS World 3D and SRTM.

4.1.1.1.1 SRTM - ASTER GDEM

Figure 4 highlights some differences between the SRTM and the ASTER GDEM DEM. No data were acquired on the pole (-60° N and $+56^{\circ}$ S) for the SRTM DEM so no comparison can be made. The dominant red in this figure indicates that the elevation data acquired by SRTM are higher than that of ASTER GDEM. Both are sensitive to the top of canopy. The elevation data of ASTER GDEM are higher in the areas of Amazonia, Himalaya and the Sahara Desert.

The highly visible swaths common to the first two figures (Figure 4 and Figure 5) are those of ASTER GDEM, recognizable by their inclination. See below the coverage maps of the two DEMs.

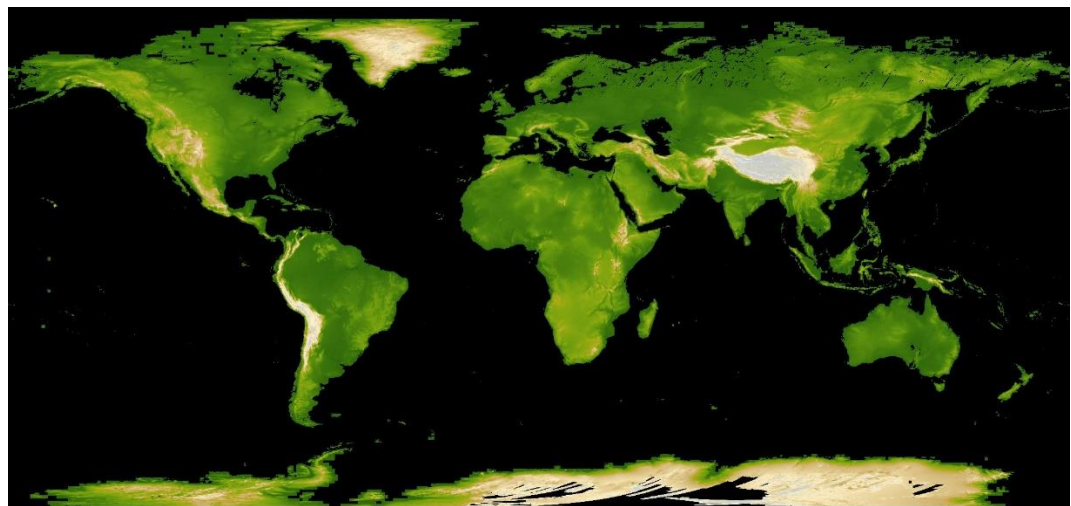
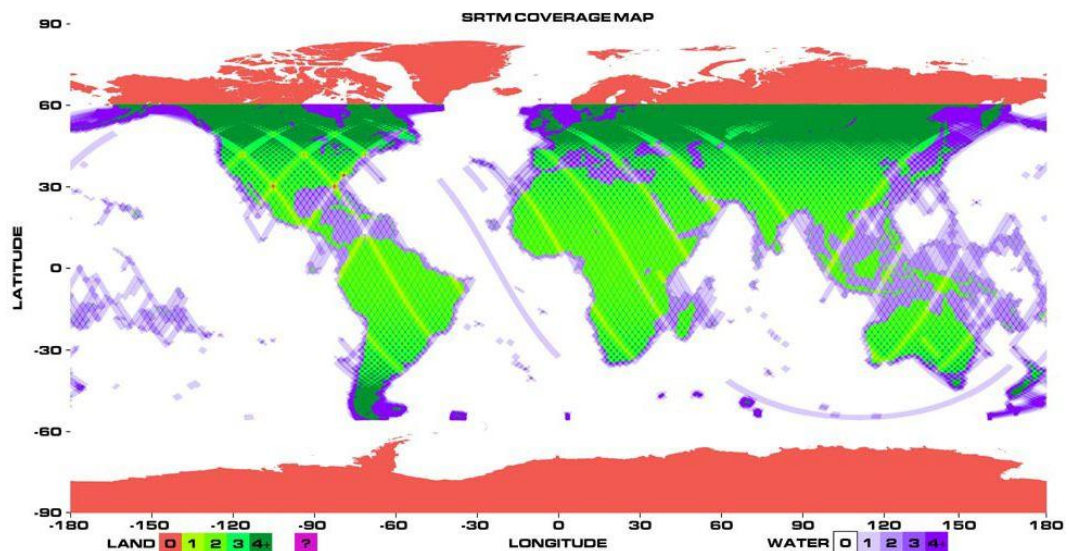


Figure 7 – Coverage maps of SRTM ([top](#)) and ASTER GDEM ([bottom](#)) as seen in VtWeb.

4.1.1.1.2 ASTER GDEM - ALOS World 3D

The Figure 5 discloses differences between ASTER GDEM and ALOS World 3D (AW3D30). The blue areas (Europe, North Asia, North America, Australia...) on this figure reveal that the surfaces acquired by AW3D30 are higher than those of ASTER GDEM. The swaths of ASTER GDEM are visible (see explanation for Figure 7).

Differences are inaccurate at $\pm 60^\circ$ latitude in northeast Russia, Finland and Antarctica due to lack of data caused by clouds, snow and ice on both DEMs. The following figures show their coverage. White in AW3D30 coverage map (right) is place without tiles, black is no data.

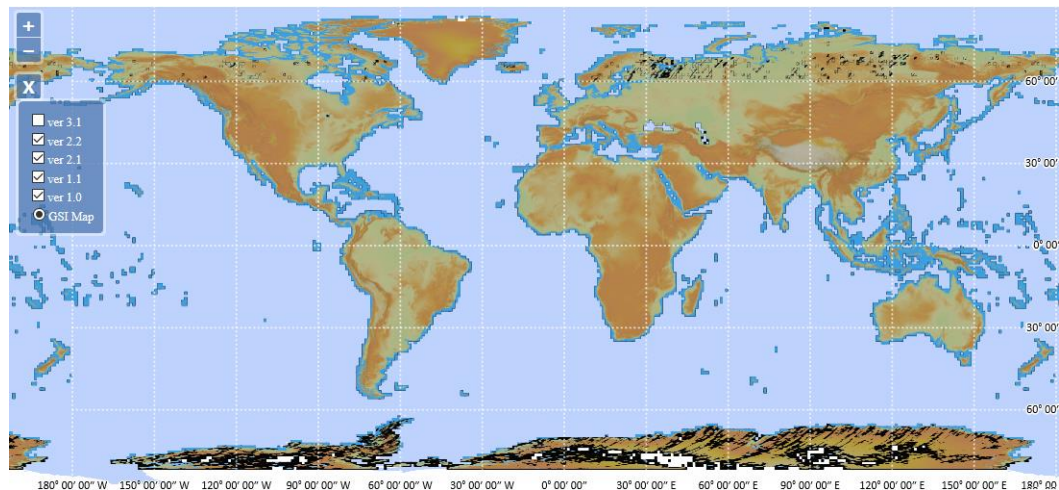
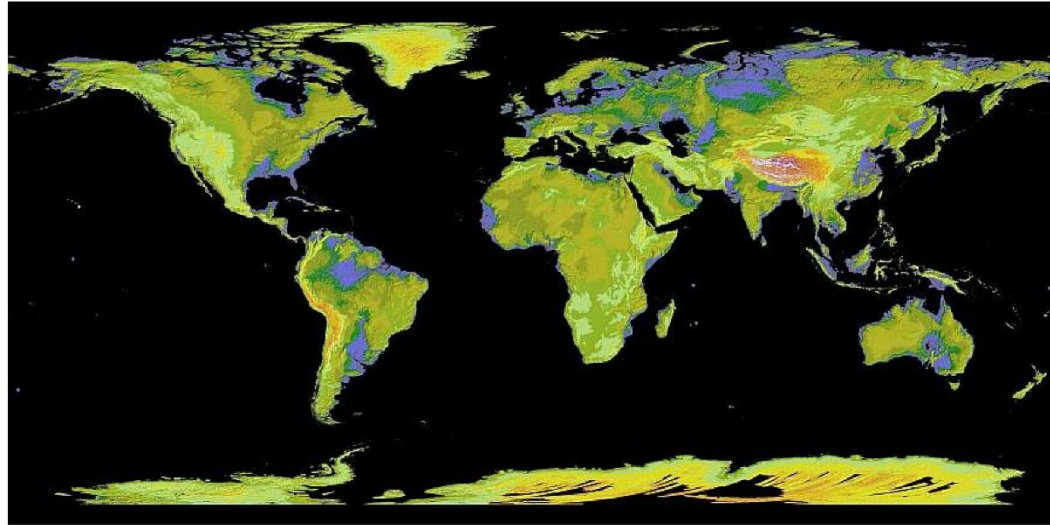


Figure 8 – Coverage maps of ASTER GDEM ([top](#)) and ALOS World 3D ([bottom](#)).

Moreover, the Figure 9 shows that the number of acquisitions on the poles is less than 3.

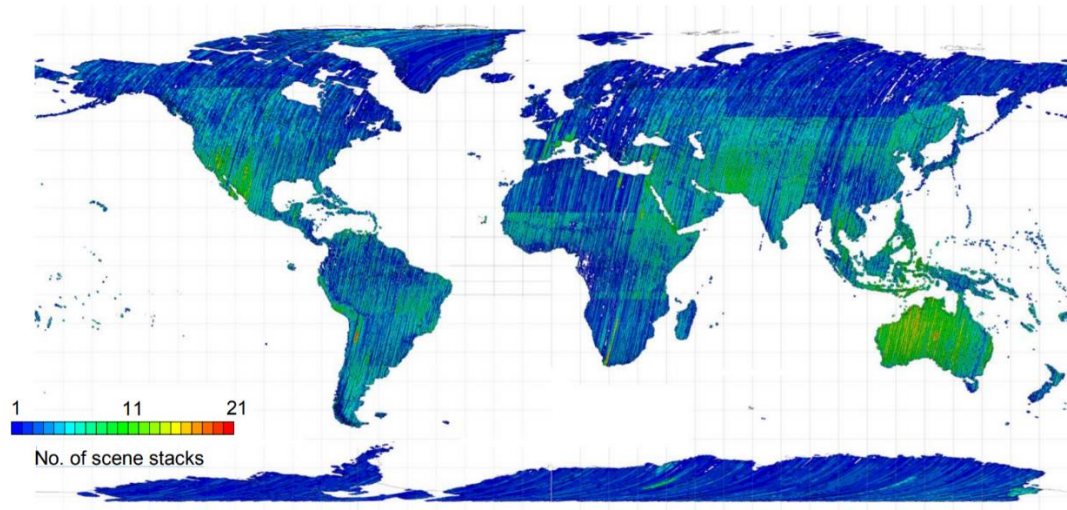


Figure 9 – ALOS World 3D number of scenes (RD-12).

4.1.1.1.3 ALOS World 3D - SRTM

The Figure 6 shows that these DEMs are quite similar. The northern hemisphere is red while the southern hemisphere is rather blue. This means that AW3D30 recorded elevations higher than SRTM in the north and lower than SRTM in the south.

4.1.1.2 Artefacts

Sampling the differences between -1000 metres (blue) and +1000 metres (red) reveals artefacts that may be due to clouds, snow, ice or acquisition errors.

4.1.1.2.1 Artefact 1 – Southern Chile

The difference between SRTM and ASTER GDEM highlights artefacts over southern Chile. Blue and red areas can be observed.

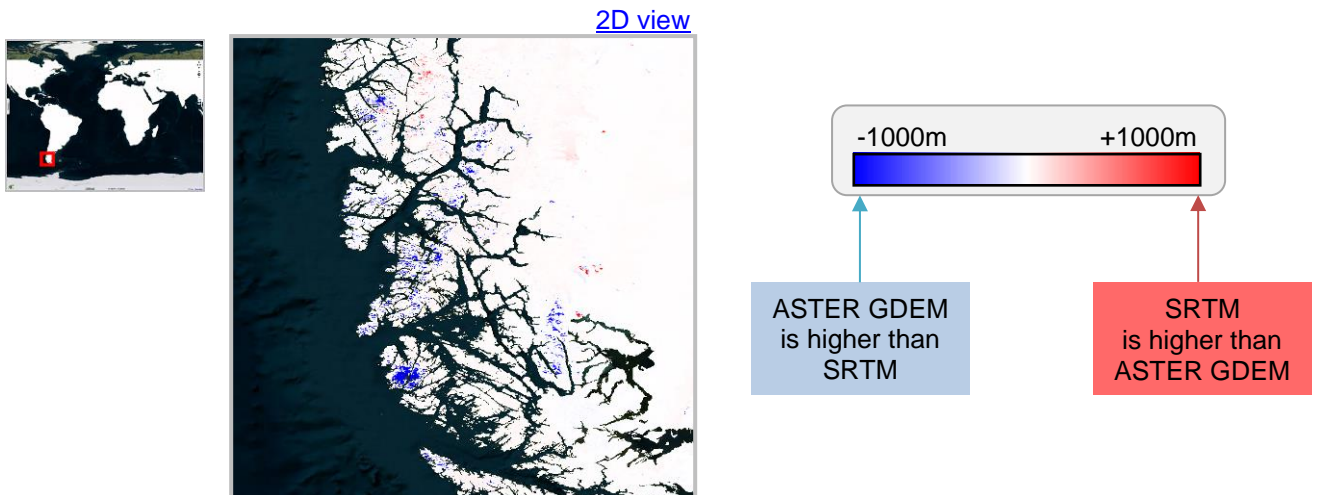


Figure 10 – Artefacts over southern Chile.

4.1.1.2.2 Artefact 2 - Sahara

Several artefacts can be noticed over the Sahara on differences between SRTM and ASTER GDEM.

By comparing Landsat and Landsat-7 satellite images acquired in 1999 and ENVISAT MERIS images acquired between 2011 and 2012, no differences are noticeable.

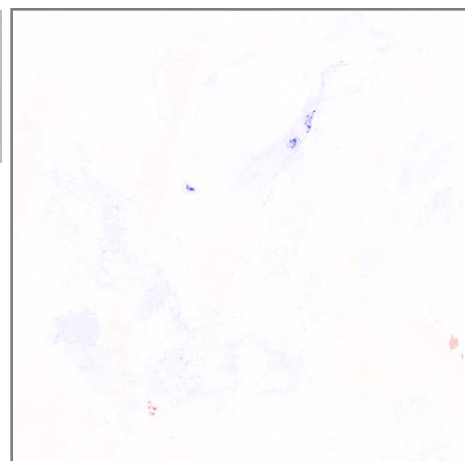


Figure 11 – Artefacts over Sahara

Artefact 2a:

<https://visioterra.org/VtWeb/hyperlook/0acc848c100e4f7fb9cab62fd0afa6c5>

Differences located in a drainage sub-network show that SRTM values are about 300 metres higher than the ones from ASTER GDEM. Comparing SRTM and ALOS World 3D shows similar results. This artefact seems to come from SRTM.

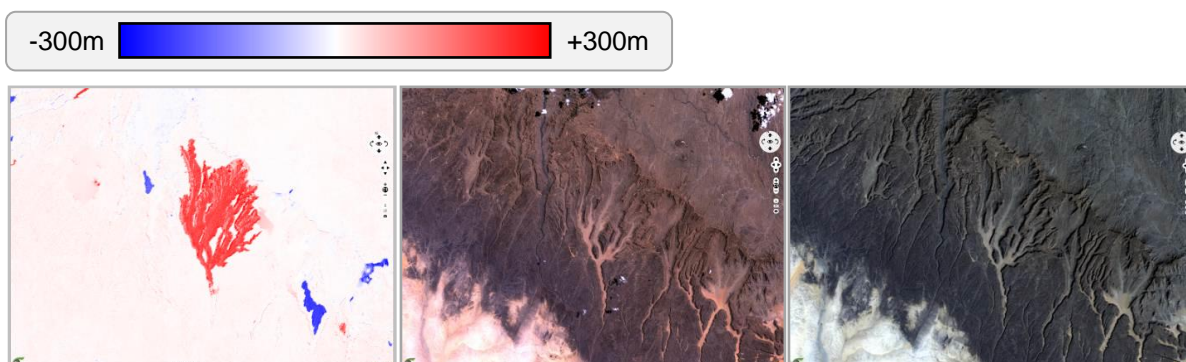


Figure 12 – Artefact 2a (left), Landsat-7 acquired on 12/07/1999 (centre) and 26/01/2011 (right).

Artefact 2b:

<https://visioterra.org/VtWeb/hyperlook/2182e5286276422f9ca31ad016576a00>

This artefact (2b) and the next one (2c) show high differences between SRTM and ASTER GDEM. The strong blue colour in the two difference images shows that ASTER GDEM is higher than SRTM of about 1 000 metres. This could be due to some remaining clouds in the data used for the photo-restitution of ASTER GDEM.

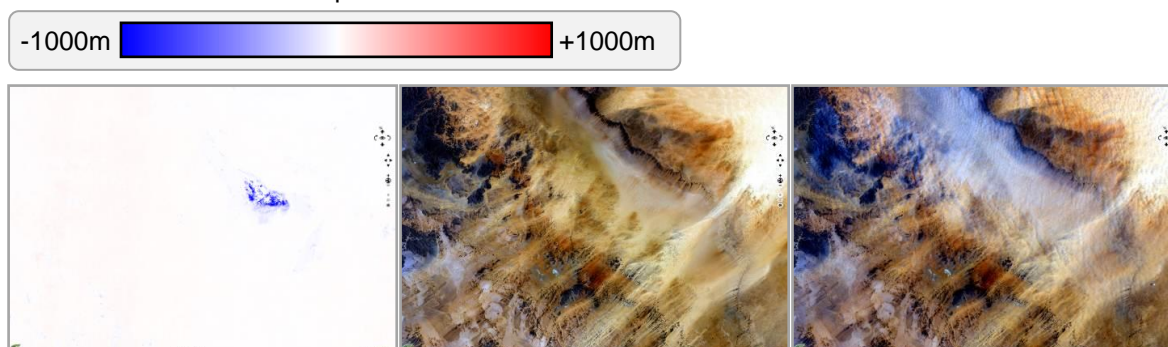


Figure 13 – Artefact 2b (left), Landsat-5 acquired on 01/08/1999 (centre) and 18/08/2011 (right).

Artefact 2c:

<https://visioterra.org/VtWeb/hyperlook/399db61ca4b045ccbf243b0b20e4e04>

The other source of error in optical photogrammetry is the lack of details (anchor points) for matching homologous points. Thus, in all homogeneous areas such as deserts, aquatic surfaces or snow or ice surfaces, the photo-restitution calculates disparity maps with very low confidence values.

In a desert context, the movement of sands, dunes, the covering of rocks by moving sands are another source of error. This is particularly the case in this area of southwest Libya on the border with Chad where wind corridors are visible.

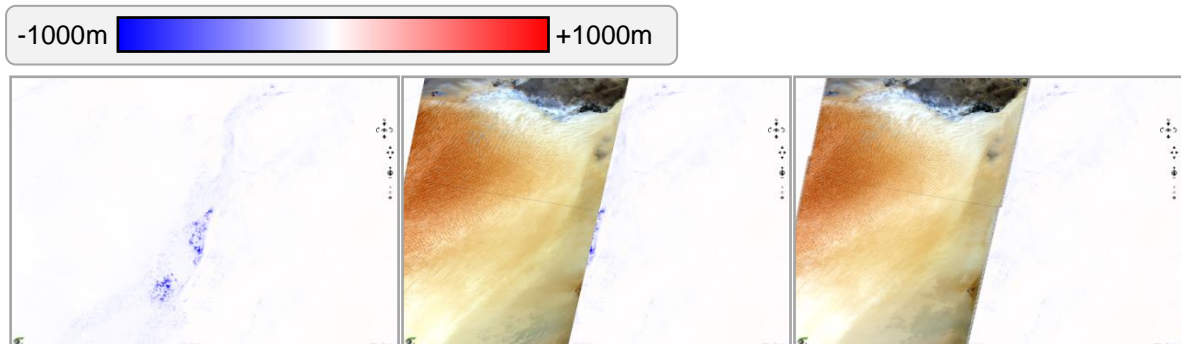


Figure 14 – Artefact 2c (left), Landsat-5 acquired on 25/07/1999 (centre) and 10/07/2011 (right).

4.1.1.2.3 Artefact 3 - Border between Russia and Kazakhstan

Red rectangles can be observed on both sides of the border between Russia and Kazakhstan in the image of difference between AW3D30 and SRTM DEMs. Nevertheless, by comparing Landsat-7 satellite images acquired before the launch of the SRTM mission and Landsat-5 satellite images acquired during the last year of AW3D30 acquisition, no difference appears (see Figure 15 below).

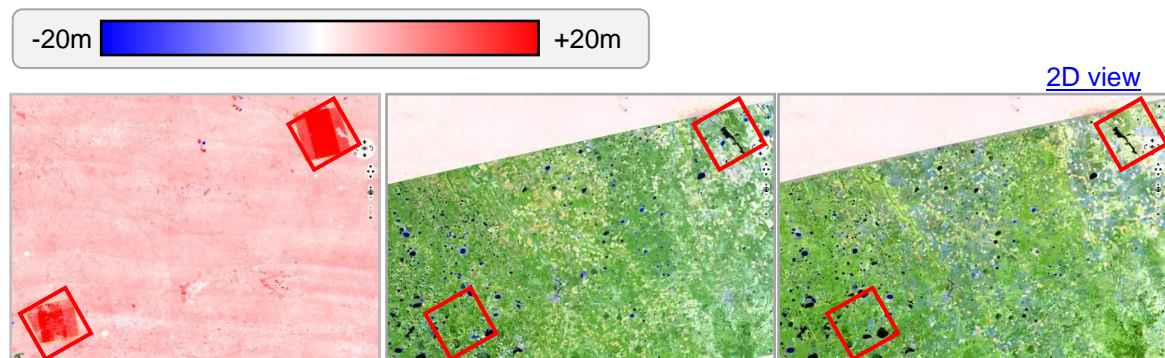


Figure 15 – Artefacts 3- Comparison image: AW3D30 and SRTM DEM difference (left), Landsat -7 acquired on 2nd of July 1999 (centre) and Landsat-5 acquired on 12th of August 2011 (right).

4.1.1.2.4 Artefact 4 - Near Yinchuan, China

A rectangular artefact appears on DEM ALOS near Yinchuan in China. This zone is thus higher on ASTER (Figure 16 - centre) and SRTM (Figure 16 - right).

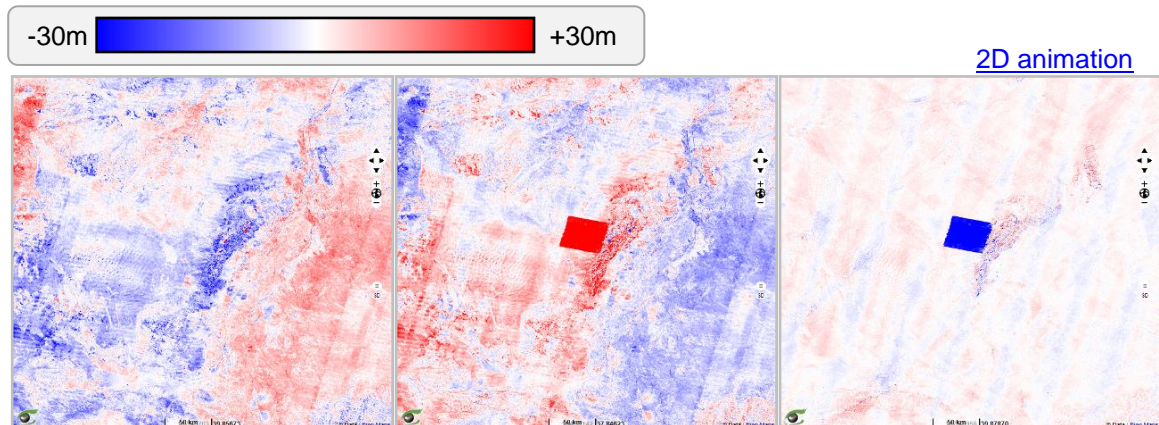


Figure 16 – Artefact 4 - Appearance of an artefact on AW3D30 near Yinchuan, China.

4.1.1.3 Elevation differences

One can notice differences between the three DEMs over lakes, seas... Below a difference emphasized over the Caspian Sea. The lake of data over the sea (white or black squares) is due to the fact that tiles covering entirely water bodies are not distributed.

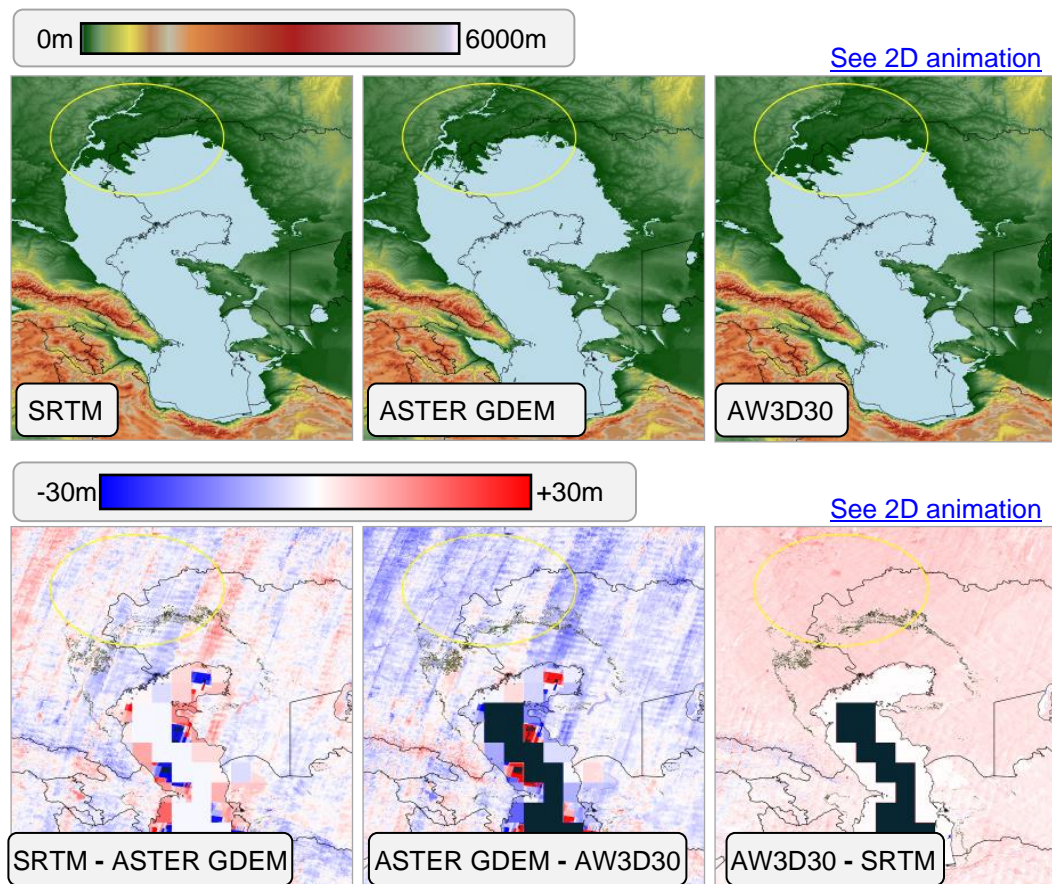


Figure 17 – Difference between DEMs over Caspian Sea.

Greenland appears to be higher in ASTER GDEM than in AW3D30 (see Figure 18). Comparing with CryoSat altimetry data (see <https://visioterra.net/VtCryoSat/>), it can be seen that the elevation of Greenland is quite uniform in its centre. It is therefore concluded that the elevations of ASTER GDEM should be less accurate than those of SRTM or ALOS World 3D.

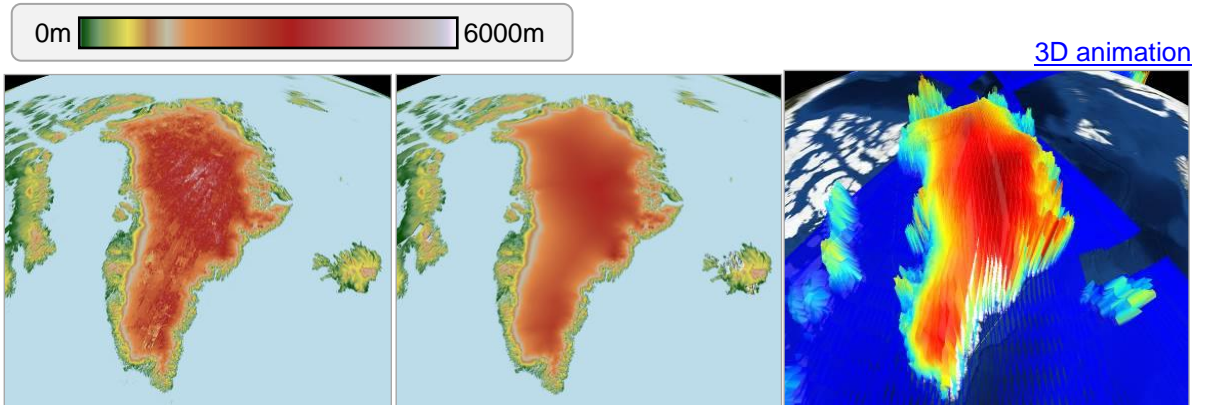


Figure 18 – Elevation of Greenland by ASTER GDEM (left) ALOS World 3D (centre) and CryoSat (right).

4.1.2 Slope values

4.1.2.1 Global slope differences

The main notable global differences on the 3 figures below are at $\pm 60^\circ$ latitude. These differences are due to the acquisition methods of the three missions. SRTM has not acquired any data on the poles (hence the blue areas in Figure 19), ASTER GDEM lacks data on the poles (see Figure 8) and ALOS World 3D has a higher coverage than the other two DEMs (see the blue areas in Figure 20 and the red areas in Figure 21).

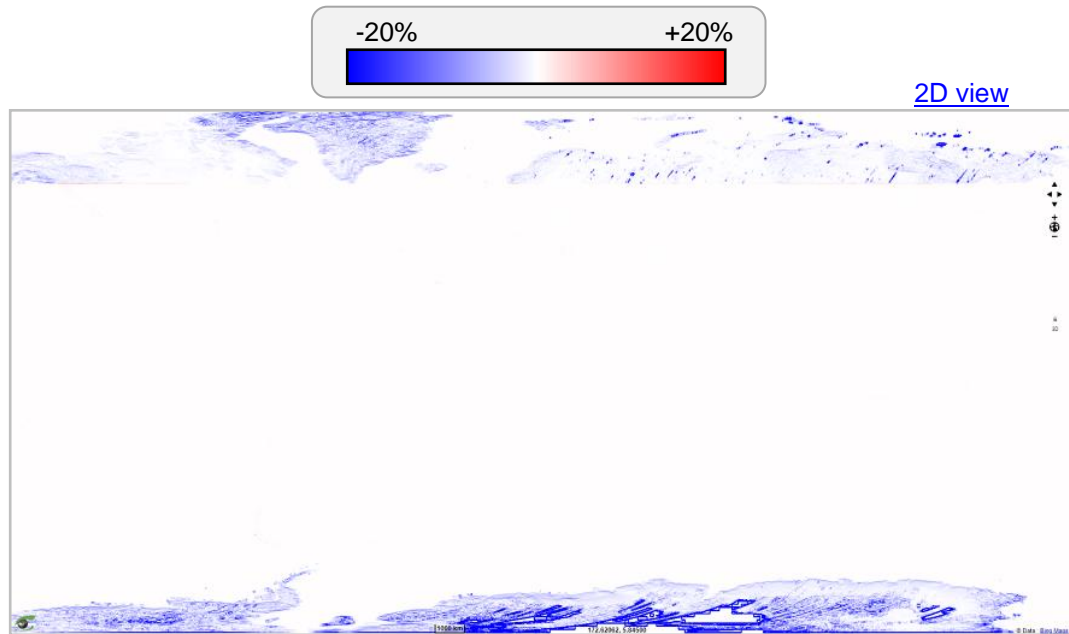


Figure 19 – Slope differences between SRTM and ASTER GDEM DEM.

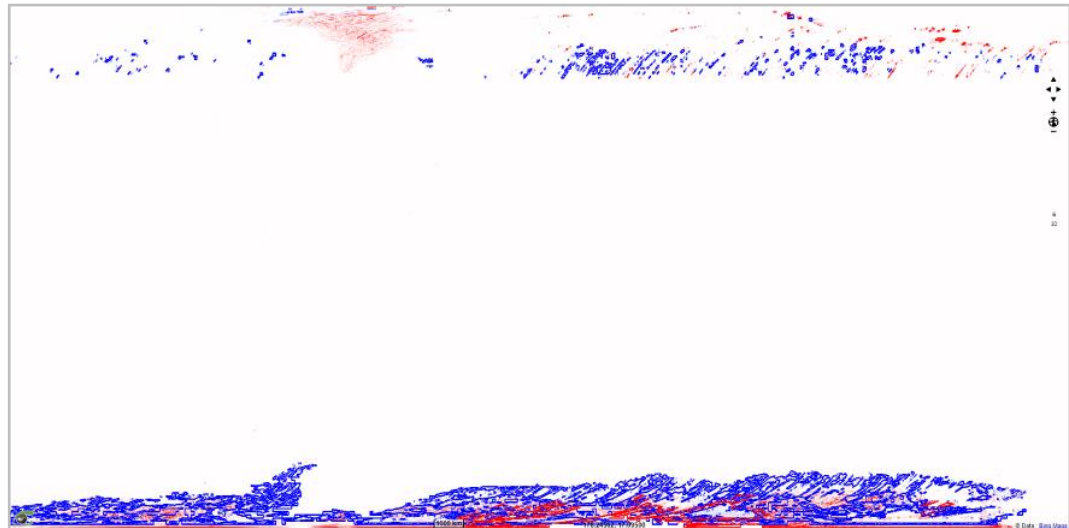


Figure 20 – Slope differences between ASTER GDEM and ALOS World 3D DEM.

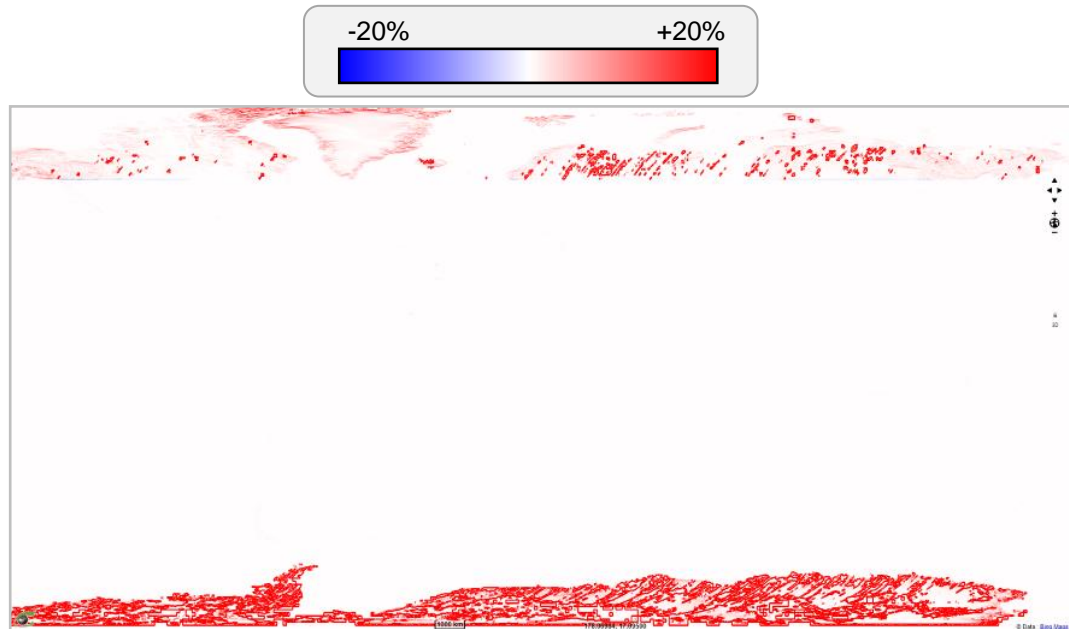


Figure 21 – Slope differences between ALOS World 3D and SRTM.

4.1.2.2 Local slope differences

The first three following images show the slope computation of SRTM, ASTER GDEM and AW3D30. The colour map shows the slope between 0% and 100% (i.e. 0° to 45° of elevation above the horizontal plan). The last three images show the difference in slopes between the DEMs two by two. These images are located in *Vallée du Rhône*, South of *Montélimar* in France. The structures showing the largest difference of slopes between the different DEMs are located along the water streams: *Rhône* and *Canal de Donzère-Mondragon*.

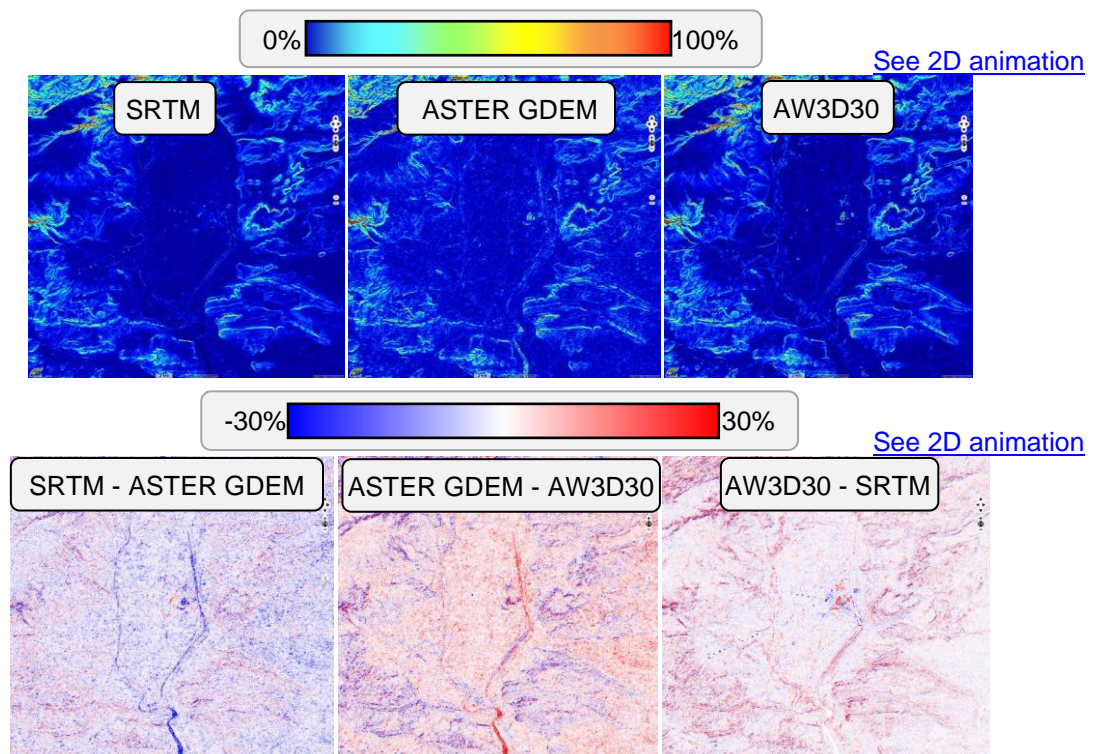


Figure 22 – Slope computation of DEMs and their differences.

Figure 23 shows the coefficient of variation within a slicing statistics window of 5x5 pixels. The coefficient of variation is the ratio between the local standard deviation and the local mean. This highlights the Millau Viaduct (France), built between October 2001 and December 2004. It does not appear in SRTM and ASTER GDEM (the acquisition of this area may have been completed before 2004 for ASTER GDEM) but it appears on AW3D30.

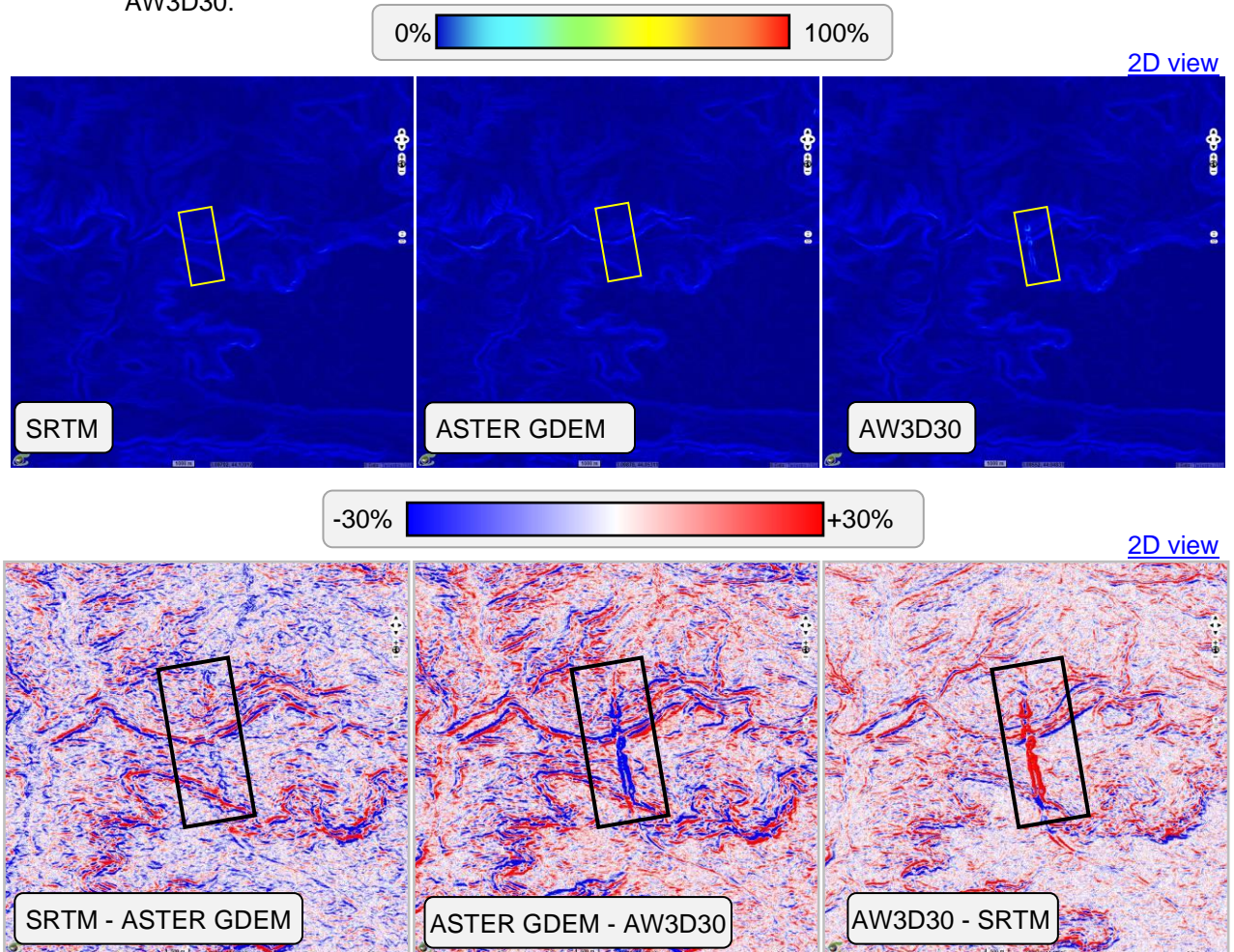


Figure 23 – Coefficient of variation 5x5 pixels over Millau Viaduct (France). STRM (left), ASTER GDEM (centre), AW3D30 (right).

Figure below shows the slope computation for each DEM has been set as elevation. The electrical pylons seem to be more prominent in SRTM than in the other two DEMs. This effect is simply due to the strong backscattering of radar signal over metal targets.

At the opposite, the Tricastin nuclear site appears higher in ASTER GDEM and AW3D30 than in SRTM.

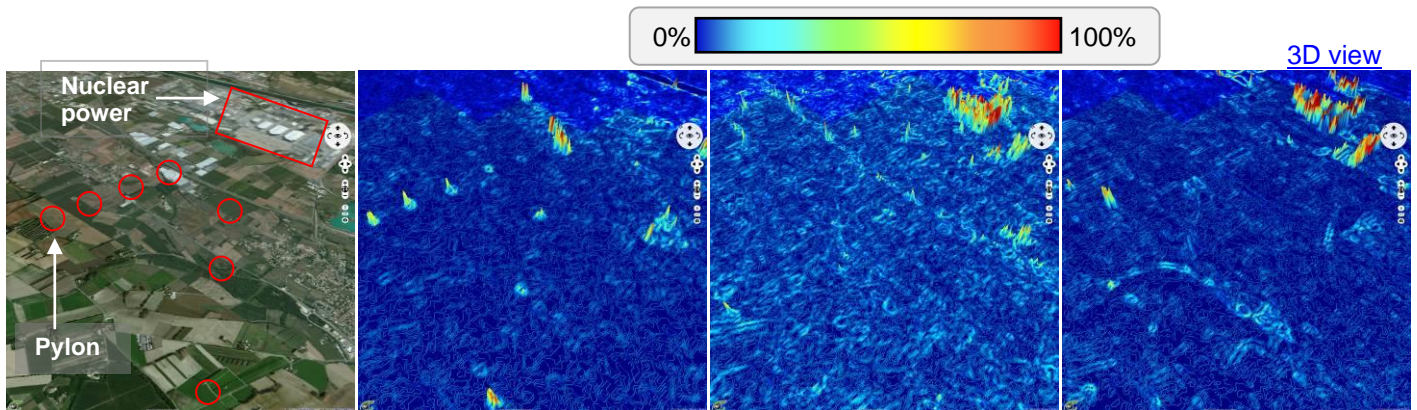


Figure 24 – Slope computation over Vallée du Rhône (France) set as elevation for each DEM: Bing map view (left), SRTM (left centre), ASTER GDEM (right centre) and AW3D30 (right).

4.1.3 Azimuth values

4.1.3.1 Global azimuth differences

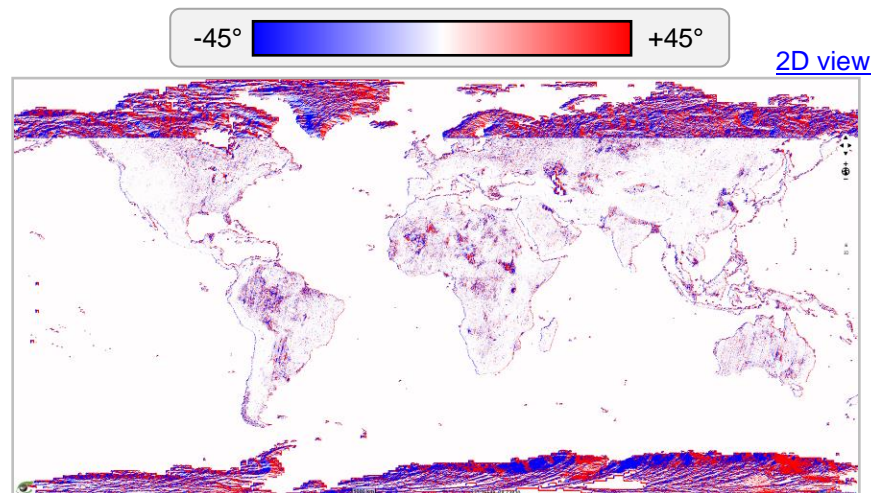


Figure 25 – Azimuth differences between SRTM and ASTER GDEM.

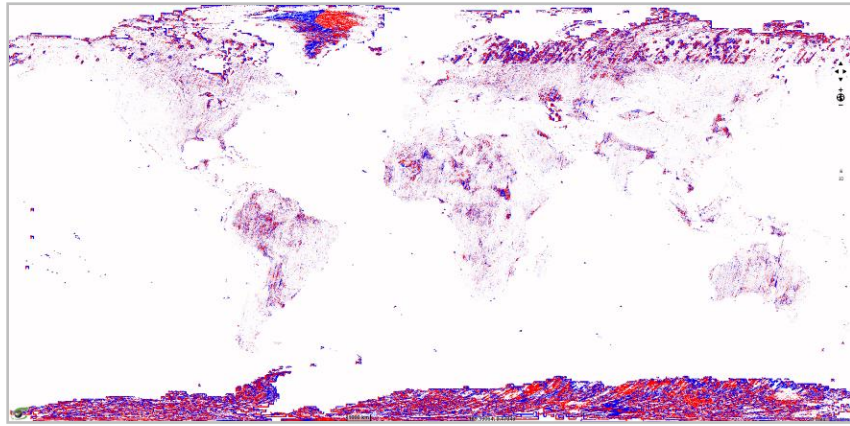


Figure 26 – Azimuth differences between ASTER GDEM and ALOS World 3D.

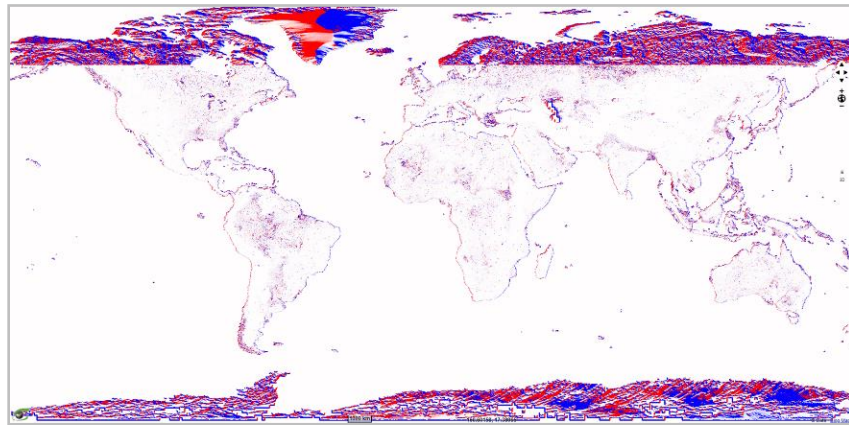


Figure 27 – Azimuth differences between ALOS World 3D and SRTM.

The high frequency variations at $\pm 60^\circ$ latitude are due to the fact that SRTM has not acquired data on the poles (Figure 25 and Figure 27). The other areas that appear in purple are flat areas.

4.1.3.2 Local azimuth differences

4.1.3.2.1 Artefact 1 - Caspian Sea

Artefacts appear on AW3D30 over the Caspian Sea but by comparing Landsat satellite images from 1999 and 2011, nothing seems to have changed.

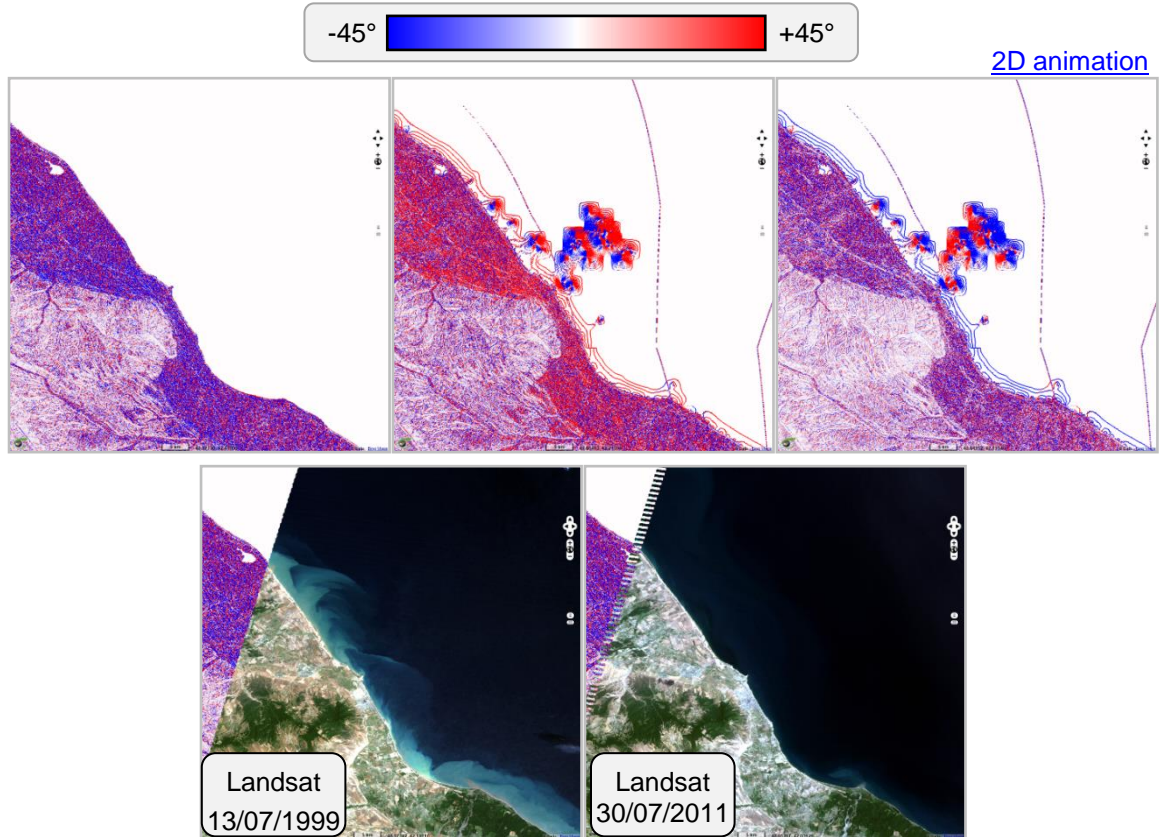


Figure 28 – Artefact 1 - Appearance of artefacts on AW3D30 over Caspian Sea.

4.1.3.3 Azimuth differences

The following images show the slope azimuth computation from SRTM, ASTER GDEM and AW3D30 and the differences between them.

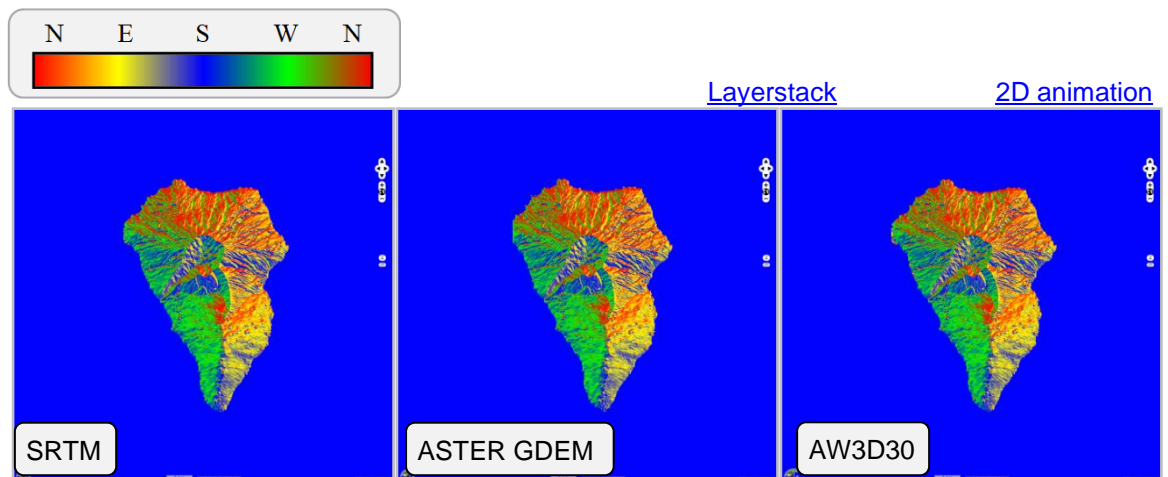


Figure 29 – Slope azimuth over La Palma.

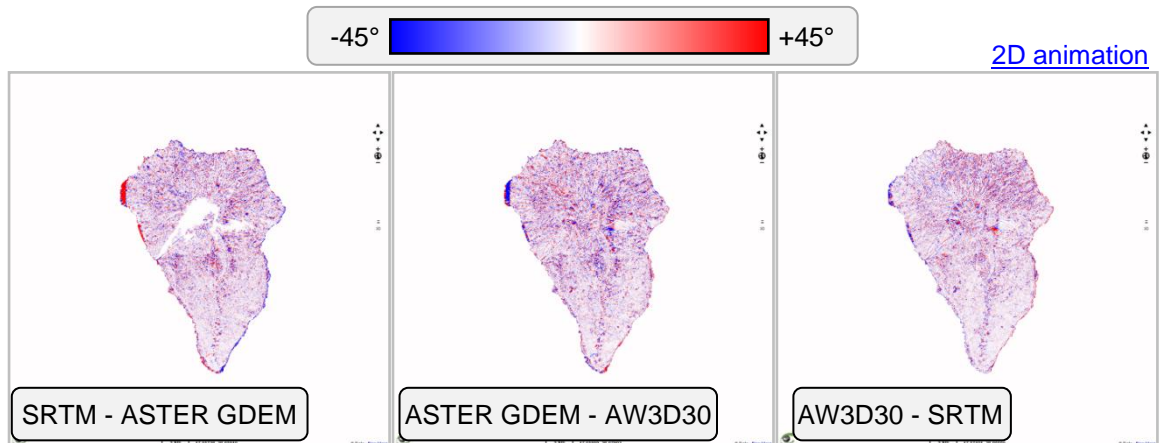


Figure 30 – Slope azimuth differences over La Palma.

The white area in the centre of La Palma in the difference image between SRTM and ASTER GDEM here above can be due to the filling algorithm in one of the DEM based on the other one.

Other azimuth differences can be observed over quite flat areas, such as the Namibia-Angola border (see Figure 31).

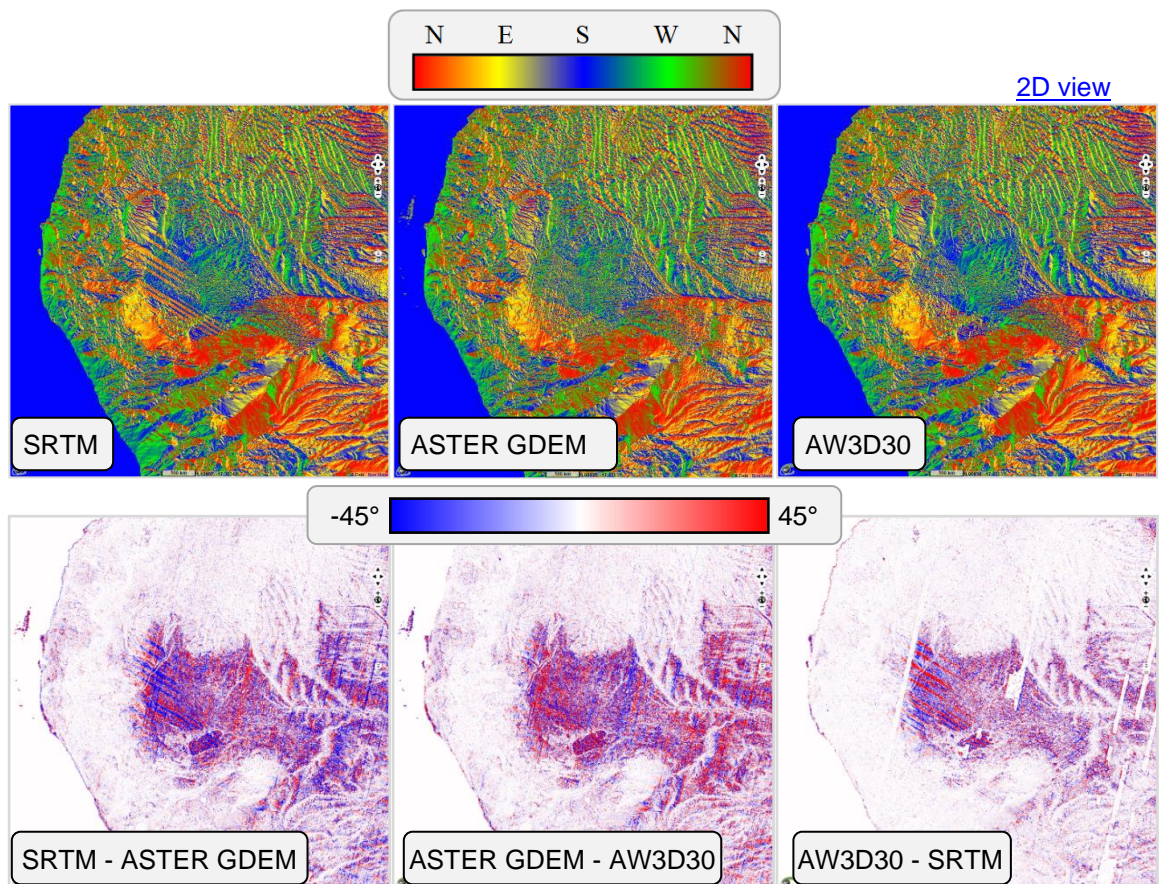


Figure 31 – Slope azimuth computation (top) and difference (bottom) over Angola and Namibia border.

4.1.4 Vertical curvature

Images shown in the next figures display the vertical curvature (see computation in section 4.2.2.1.7) computed from SRTM (left) and ASTER GDEM (middle) and the difference between them (right). The vertical curvature highlights the mountain ridges in red, the valleys in green and the flat areas in blue.

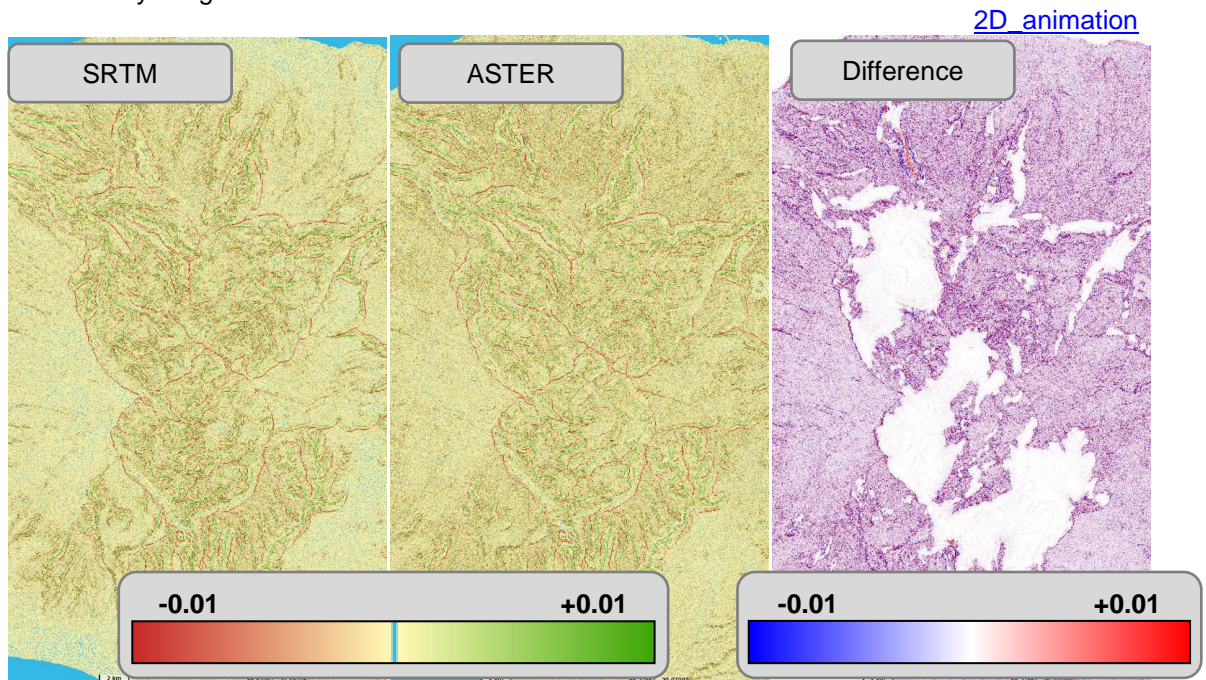


Figure 32 – Vertical curvature and difference over the three cirques (La Réunion).

The previous figure is centred over the three “Cirques” of La Réunion. Their edges are clearly visible with the red line. Notwithstanding the high-frequency variation in the difference image, there are some parts that show little difference.

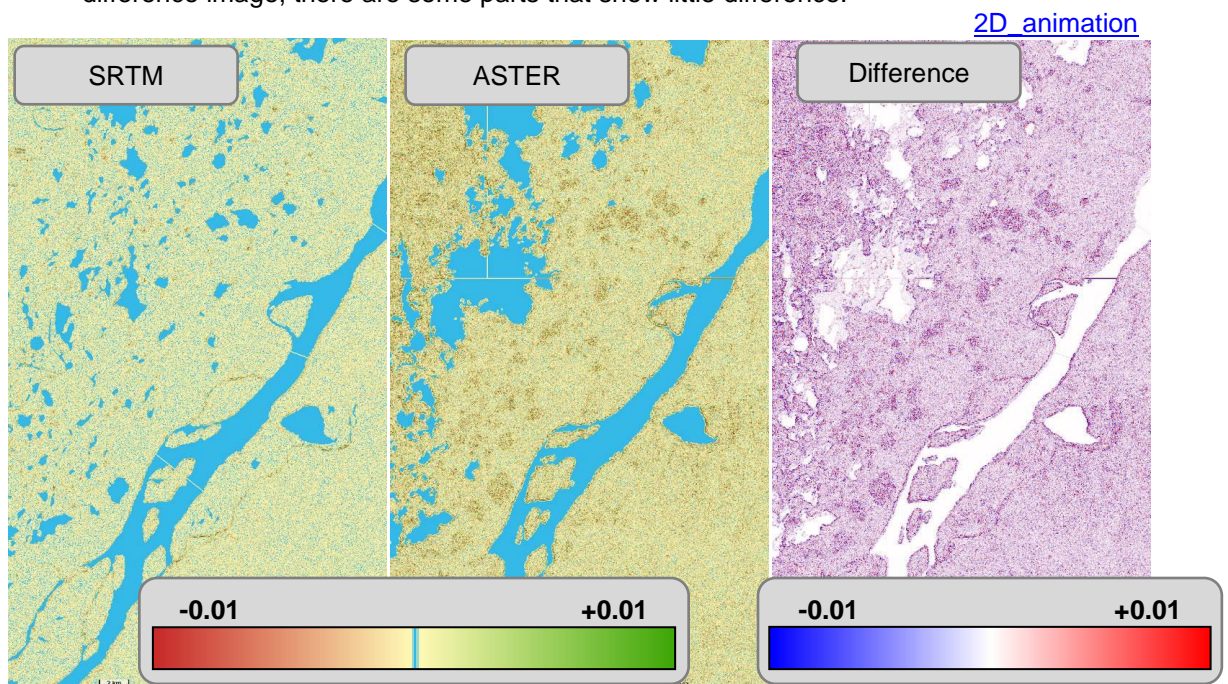


Figure 33 – Vertical curvature and difference over Le Rio Paraná.

In Figure 33, we can see the Rio Paraná River in Argentina. In the SRTM vertical curvature, one may notice lines crossing the river. These lines may correspond to the steps where the river height decrease of 1 metre. The straight lines in ASTER GDEM (horizontal or vertical) highlight the limit of the optical data used in input.

4.2 Elevation assessment from ICESat-1 / GLAS LiDAR

This section 4.2 presents the quantitative evaluation of the vertical accuracy of SRTM, ASTER GDEM or ALOS World 3D data using reference data from the ICESat / GLAS LiDAR.

Unlike the previous section 4.1, the evaluation here is quantitative by comparing each valid elevation given in LiDAR products to its homologous point to be interpolated from the DEM to be verified.

4.2.1 Assessment of ICESat-1 / GLAS measurements reliability

4.2.1.1 GLAH14 Product

Land altimetry data is available in the GLAH14 product. Each product contains variables concerning location, elevation and quality of the data (in both 1 Hz and 40 Hz frequencies). For the purpose of this assessment, only 40 Hz data are used.

Each GLAH14 product used is filtered using these quality flags:

- `elev_use_flg` indicating whether the elevations on the record should be used (0 = true, 1 = false)
- `sat_corr_flg` indicating if a saturation correction needs to be applied (between 0 and 4, values meaning is detailed below)
- `elv_cloud_flg` indicating probable cloud contamination (0 = false, 1 = true)

The following table summarizes the meaning of each `sat_corr_flg` value (<https://nsidc.org/icesat/saturation-correction>):

Value	Meaning
0	Not saturated or no signal (no correction needed)
1	Inconsequential
2	Applicable
3	Not computable
4	Not applicable

Elevations having a `sat_corr_flg` value over 2 are excluded, as they can't be corrected. Saturation correction is added to the elevation values where `sat_corr_flg` equals 1 or 2. Potentially cloud contaminated elevations are removed from all the measures (where `elv_cloud_flg` equals 1).

The variable `d_satElevCorr` contains the saturation correction applied to elevations. Another correction, `d_ElevBiasCorr`, is applied to the data: this correction was determined by the GSFC on post flight analysis.

4.2.1.2 Sampling of ICESat / GLAS data

This section defines the equations used in the sampling of ICESat data. The following equation is used to process linear interpolation:

$$h_i = h_1 + (h_2 - h_1) * \frac{(l_1 - L_i)}{(l_2 - l_1)} \quad (\text{eq. 1})$$

Where:

- L_i is the longitude of the height to be compared to a reference
- h_i is the interpolated height at L_i
- l_1 is the highest longitude $< L_i$ from the reference acquisition points
- l_2 is the lowest longitude $> L_i$ from the reference acquisition points
- h_1 is the height of the point of longitude l_1
- h_2 is the height of the point of longitude l_2

4.2.1.3 Collocated measurements on the same orbit

Multiple measurements are analysed on the same orbit to assess the ICESat's instrument reliability. A particularly flat area is chosen for this assessment: Bonneville Salt Flats.

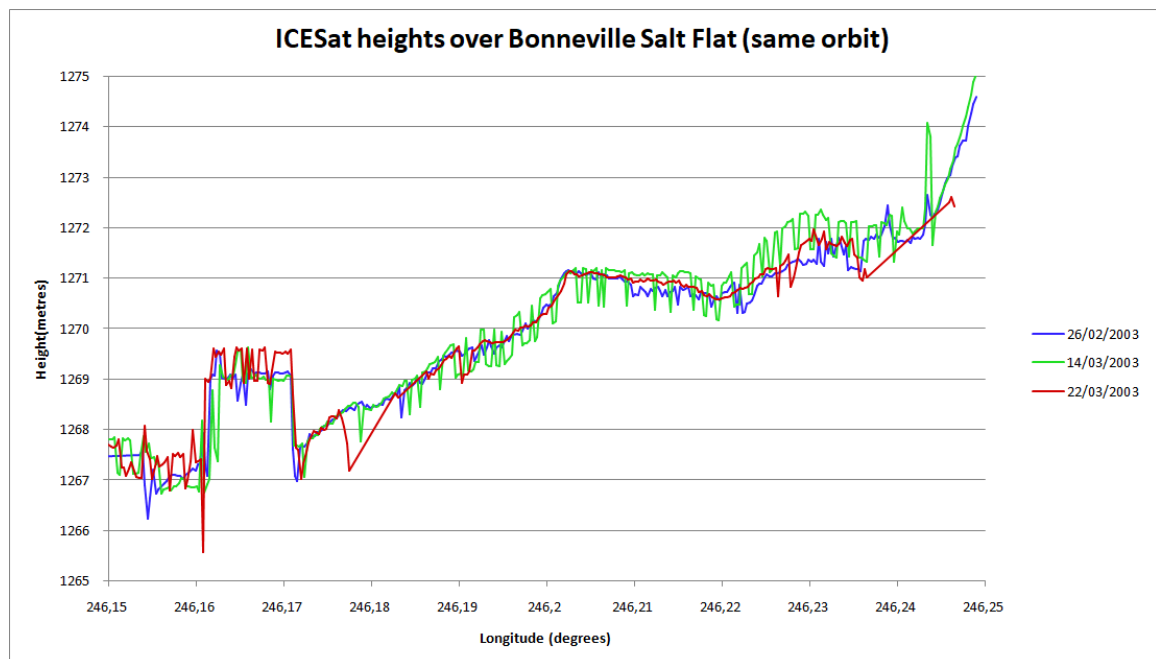


Figure 34 – ICESat heights over Bonneville Salt Flat (same orbit, different acquisition period).

Note: In ICESat products, longitude is expressed between 0.0 and 360.0 degrees, starting from the Prime Meridian.

Heights acquired by ICESat on 26/02/2003, 14/03/2003 and 22/03/2003 share the same orbit. The preceding curves visually highlight the similarity between those 3 different acquisitions. The first acquisition of this study (26/02/2003) is used as a reference from which the other acquisitions (14/03/2003 and 22/03/2003) are compared.

From one acquisition to another, longitude may vary. Comparing the reference acquisition to the other acquisitions is processed using linear interpolation. Each interpolated

reference height is compared to the point of same longitude from another acquisition using this equation:

$$e_i = h_i - H_i \quad (\text{eq. 2})$$

Where:

- e_i is the calculated height error between the two acquisitions.
- h_i is the interpolated height from the reference acquisition.
- H_i is the height to be compared to the reference height.

Here are the statistics of this study:

Acquisition date	Number of differences	Algebraic mean	Root Mean Square
14/03/2003	323	-0.137m	0.621m
22/03/2003	263	0.546m	1.019m

Figure 35 – Differences between successive measurements along homologues tracks.

The overall statistics show the reliability of the GLAS instrument, which is assessed to have a maximal root mean square of 1.019m in that area.

4.2.1.4 Geographical distribution of ICESat products

The assessments performed in this document are based on the **642 products** of ICESat mission. Most of the products contain one day acquisition over 14 revolutions. These products are distributed all over the world as shown in the following figures.

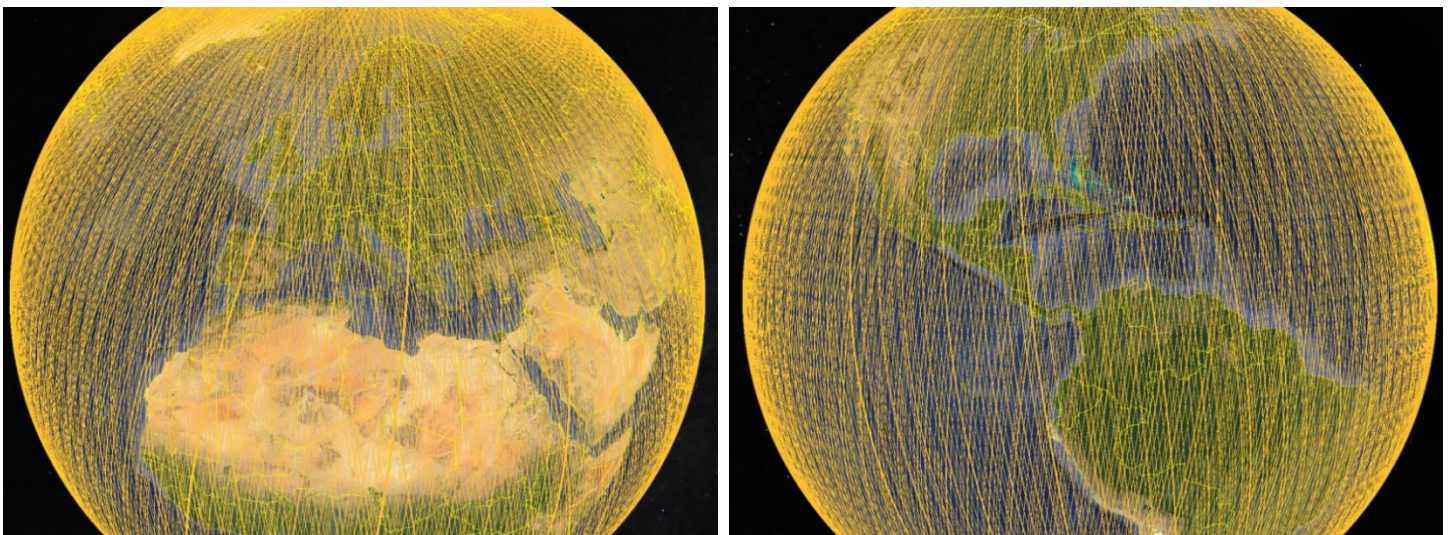


Figure 36 – Distribution of 642 ICESat products.

4.2.2 Assessment of SRTM GL1 from ICESat / GLAS data

This section 4.2.2 presents the quantitative evaluation of the vertical accuracy of SRTM data using reference data from the ICESat / GLAS LiDAR. The method and the notations of the next subsection 4.2.2.1 are detailed here after. The same methods will apply for the evaluation of ASTER GDEM (section 4.2.3) and ALOS World 3D (section 4.2.4) and will not be repeated.

4.2.2.1 Method and notations

Scope of the numerical analysis is to assess:

- the **distribution of the height differences** (dh_i) and
- a possible **correlation** between the magnitude of these height errors and
 - the height itself – one could think that the higher the DEM is, the more the height difference dh_i would be,
 - the local variance – one could think the higher the variance is, the more the height difference dh_i would be,
 - the local curvature – one could think that the more the curvature is, the more the height difference dh_i would be.

4.2.2.1.1 Conversion from TOPEX / Poseidon to WGS84

ICESat elevations are relative to the TOPEX/Poseidon ellipsoid and shall be converted to the WGS84 ellipsoid using the following formula (see <https://www.mdpi.com/2072-4292/10/2/297/htm>):

$$\Delta h = \frac{a'(1 - e'^2)}{\sqrt{1 - e'^2 \sin^2 \phi}} - \frac{a(1 - e^2)}{\sqrt{1 - e^2 \sin^2 \phi}} \quad (\text{eq. 3})$$

Where:

- a is the semi-major axis of the WGS84 ellipsoid,
- e is the eccentricity of the WGS84 ellipsoid,
- a' is the semi-major axis of the TOPEX/Poseidon ellipsoid,
- e' is the eccentricity of the TOPEX/Poseidon ellipsoid,
- ϕ is the latitude of the elevation (relative to the TOPEX/Poseidon ellipsoid),
- Δh is the difference in elevation between the TOPEX/Poseidon and WGS84 ellipsoids.

This formula gives the difference in elevation between the WGS84 and TOPEX/Poseidon ellipsoids. This difference has to be subtracted from the TOPEX/Poseidon referenced elevations, as the TOPEX/Poseidon ellipsoid is smaller than WGS84. The following table summarizes the differences between the WGS84 and TOPEX/Poseidon ellipsoids:

	TOPEX/Poseidon	WGS84
Equatorial radius (a)	6 378 136.3 metres	6 378 137.0 metres
Polar radius (b)	6 356 751.600 563 metres	6 356 752.314 245 metres
Reciprocal flattening (1/f)	298.25700000	298.25722356
Eccentricity (e)	0.081819221456	0.081819190843

Figure 37 – Difference between TOPEX/Poseidon and WGS84 ellipsoids.
(<https://nsidc.org/data/icesat/faq.html#alt7>)

The differences in latitudes between these two ellipsoids are small (up to ± 1.5 cm), as illustrated by the following graph:

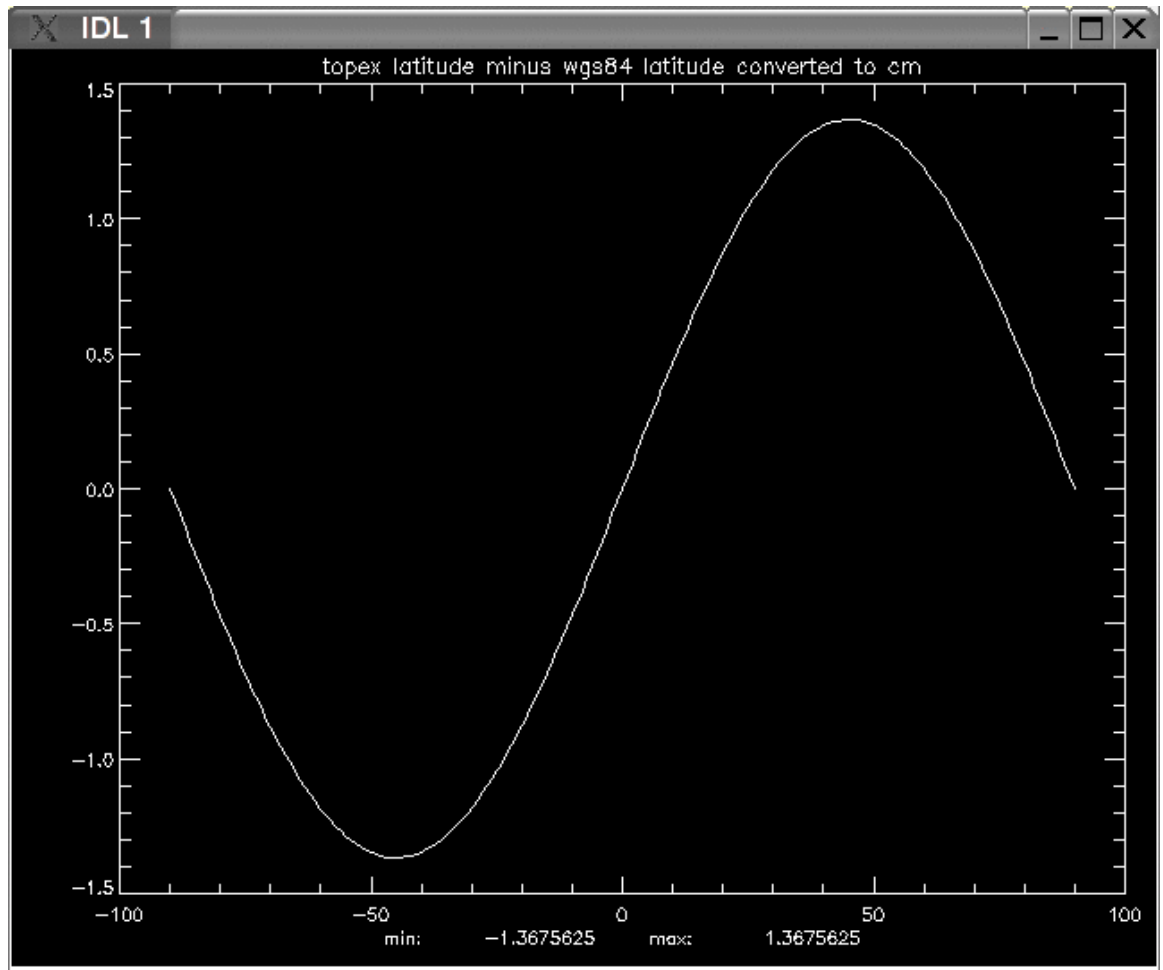


Figure 38 – Latitude difference between WGS84 and TOPEX/Poseidon ellipsoids (in centimetres).

(<ftp://sidacs.colorado.edu/pub/DATASETS/icesat/tools/idl/ellipsoid/>)

Latitudes can be considered as equal from TOPEX/Poseidon to WGS84, as the maximum difference in latitude between the two ellipsoids is far below the horizontal accuracy of ICESat. On average, horizontal accuracy ranges from 0.0 to 4.63 metres, with a minimal standard deviation of 2.22 metres.

4.2.2.1.2 From ICESat longitude and latitude to the SRTM tile

The longitude and latitude ranges of each product are the following:

- ICESat longitude $\in [0^\circ, 360^\circ]$ latitude $\in [-90^\circ, +90^\circ]$
- SRTM-GL1 longitude $\in [-180^\circ, +180^\circ]$, latitude $\in [-56^\circ, +60^\circ]$

To match SRTM-GL1 with ICESat longitudes, 360° are subtracted from all ICESat longitudes values greater than 180° . ICESat's elevations being filtered by latitudes, all the footprints not included in SRTM-GL1 latitude range are removed.

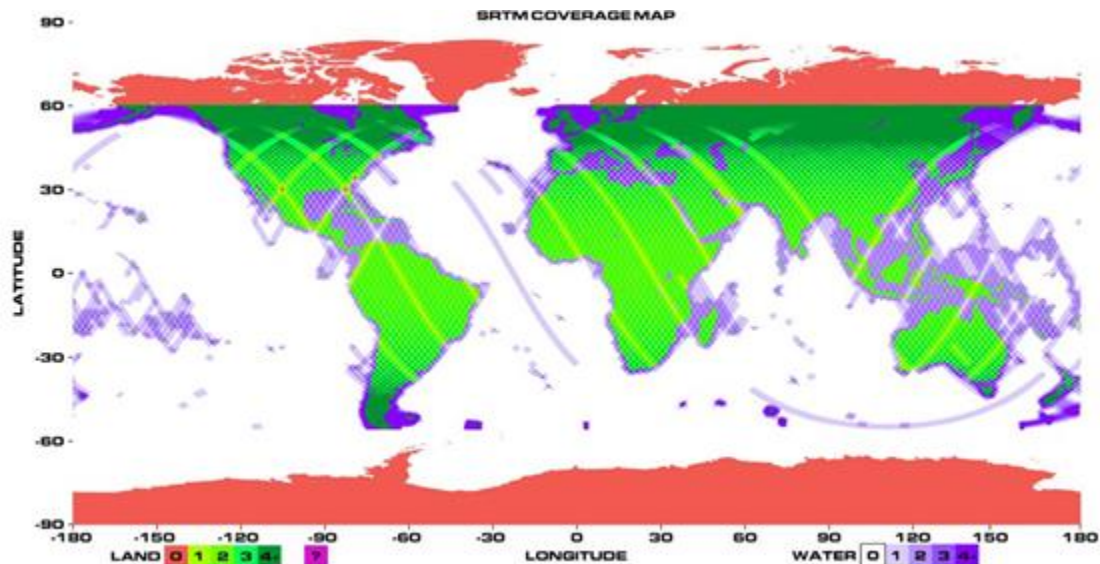


Figure 39 – SRTM coverage map.
(<https://www2.jpl.nasa.gov/srtm/coverage.html>)

To compare ICESat to SRTM-GL1 elevations, a corresponding SRTM-GL1 tile is found for each ICESat footprint, and the exact cell of the SRTM-GL1 grid containing it. The SRTM-GL1 tile name pattern is the following:

c11CLLL.hgt

Where:

- c corresponds to the latitude's cardinal (S for South or N for North)
- l is the latitude in degrees ranging from 00 to 90
- C corresponds to the longitude's cardinal (E for East or W for West)
- L is the longitude in degrees ranging from 000 to 180

Example: For ICESat_longitude = -96.051 and ICESat_latitude = 42.472, the corresponding SRTM-GL1 tile is entitled "**N42W97**".

A SRTM-GL1 tile is composed of 3601 columns by 3601 rows. The bottom left value of the file corresponds to the smallest longitude and latitude. The following equation gives the position of the corresponding sample in the file:

$$p = |C - C \times y| \times L + |L \times x| \quad (\text{eq. 4})$$

Where:

- p is the position of the sample
- L is the line size in bytes
- C is the column size
- x corresponds to ICESat longitude's digits
- y corresponds to ICESat latitude's digits

As the pixel size of SRTM-GL1 is 1" arc (i.e. 30 metres along equator), each ICESat measure is always located between four SRTM-GL1 height measures. Interpolating

ICESat's footprints on the SRTM-GL1 grid is necessary. Bilinear interpolation is used on the SRTM-GL1 grid to obtain elevations at each ICESat footprint location.

4.2.2.1.3 From EGM96 to WGS84

The EGM96 geoid is the vertical reference system of SRTM-GL1, longitudes and latitudes referring to the WGS4 ellipsoid. As a result, only elevations need to be converted from EGM96 to the WGS84 ellipsoid, which is done considering EGM96's geoid undulations. EGM96 is distributed by the [NGA/NASA](#) as a grid (with respect to the WGS84 ellipsoid). At each ICESat/SRTM-GL1 comparison location, bilinear interpolation is used on the EGM96 undulation grid to retrieve heights relative to the WGS84 ellipsoid.

In this case, EGM96 undulation values are added to the interpolated SRTM GL1 heights, retrieving SRTM GL1 heights relative to WGS84.

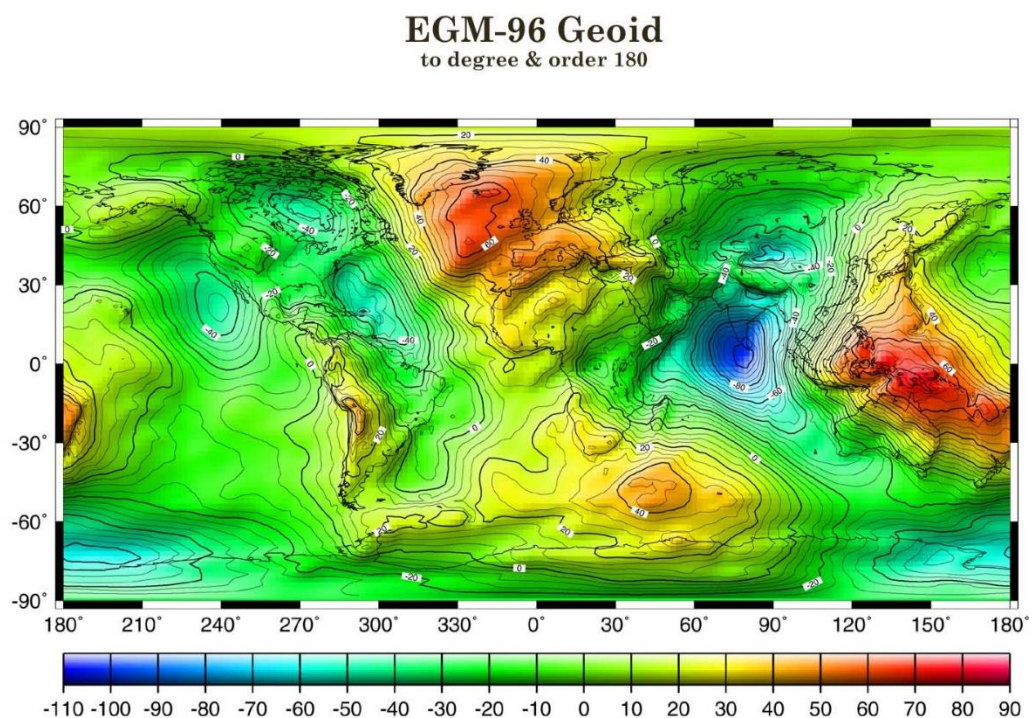


Figure 40 – EGM96 map with reference to WGS84.
(<http://www.geocities.ws/geodsci/egm96geoid.jpg>)

4.2.2.1.4 Computing the height difference

Height difference between SRTM-GL1 and ICESat is finally calculated:

$$\Delta h = h_{ICESat} - h_{SRTM} \quad (\text{eq. 5})$$

Where:

- Δh is the height difference between SRTM-GL1 and ICESat,
- h_{ICESat} is the ICESat height (with respect to the WGS84 ellipsoid),
- h_{SRTM} is the SRTM-GL1 height (with respect to the WGS84 ellipsoid).

4.2.2.1.5 Overall algorithm

The following diagram summarizes all the steps of the ICESat/SRTM-GL1 height comparison:

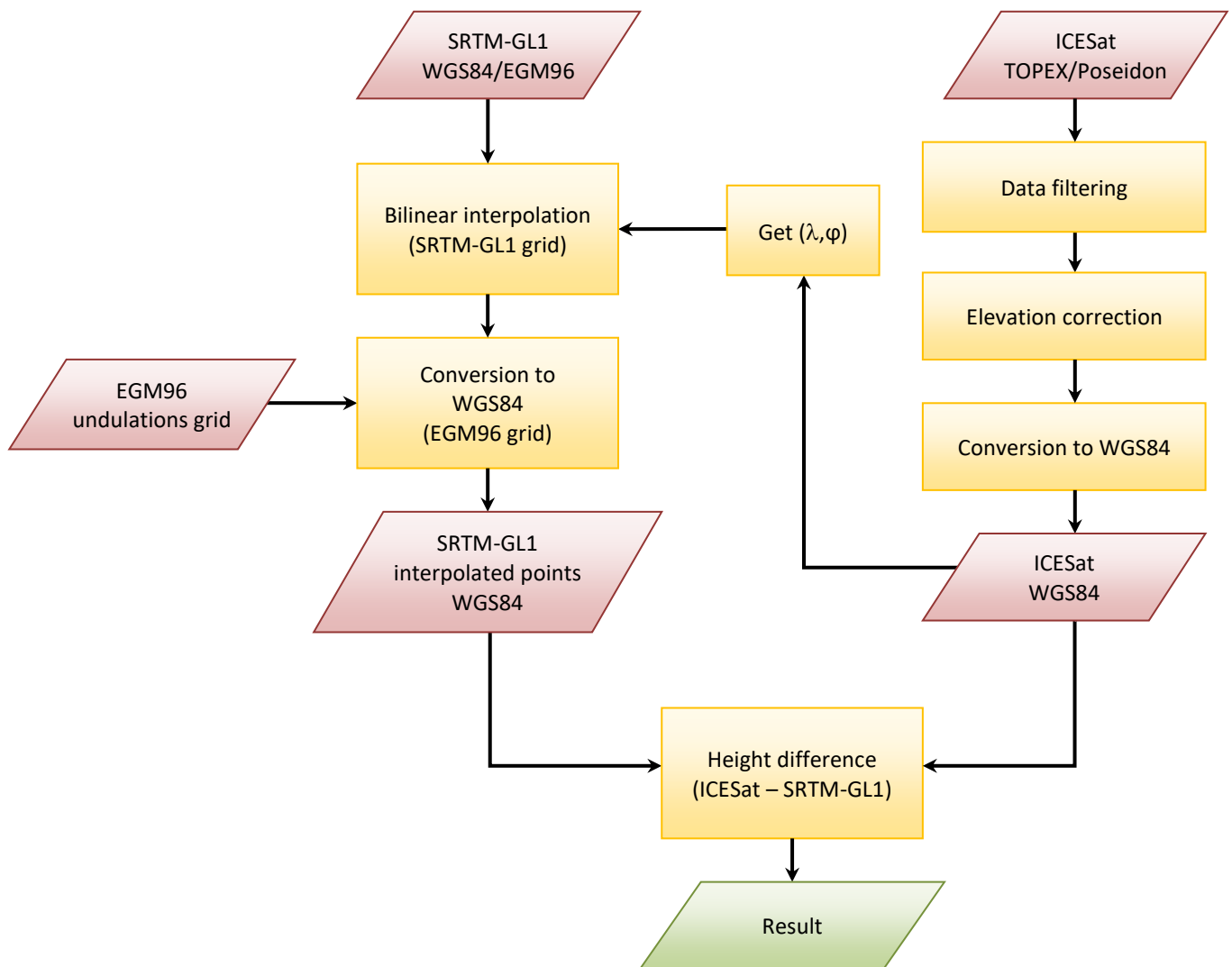


Figure 41 – Summary of the SRTM-GL1 assessment method.

4.2.2.1.6 Computation of the roughness

SRTM-GL1's height values are analysed at different scales, establishing a terrain roughness variable. Roughness is studied by calculating the variance of SRTM-GL1 heights surrounding each ICESat footprint (in a squared area).

As SRTM-GL1's data is given as a projected grid of height values, high latitudes suffer from the deformation of the geographic projection. To eliminate potential deformations of the study area, an orthographic projection is established at each ICESat measurement location (given WGS84 ellipsoid's major axis as radius). From this projection, squares of 3x3 points are defined, centred on the measurement location.

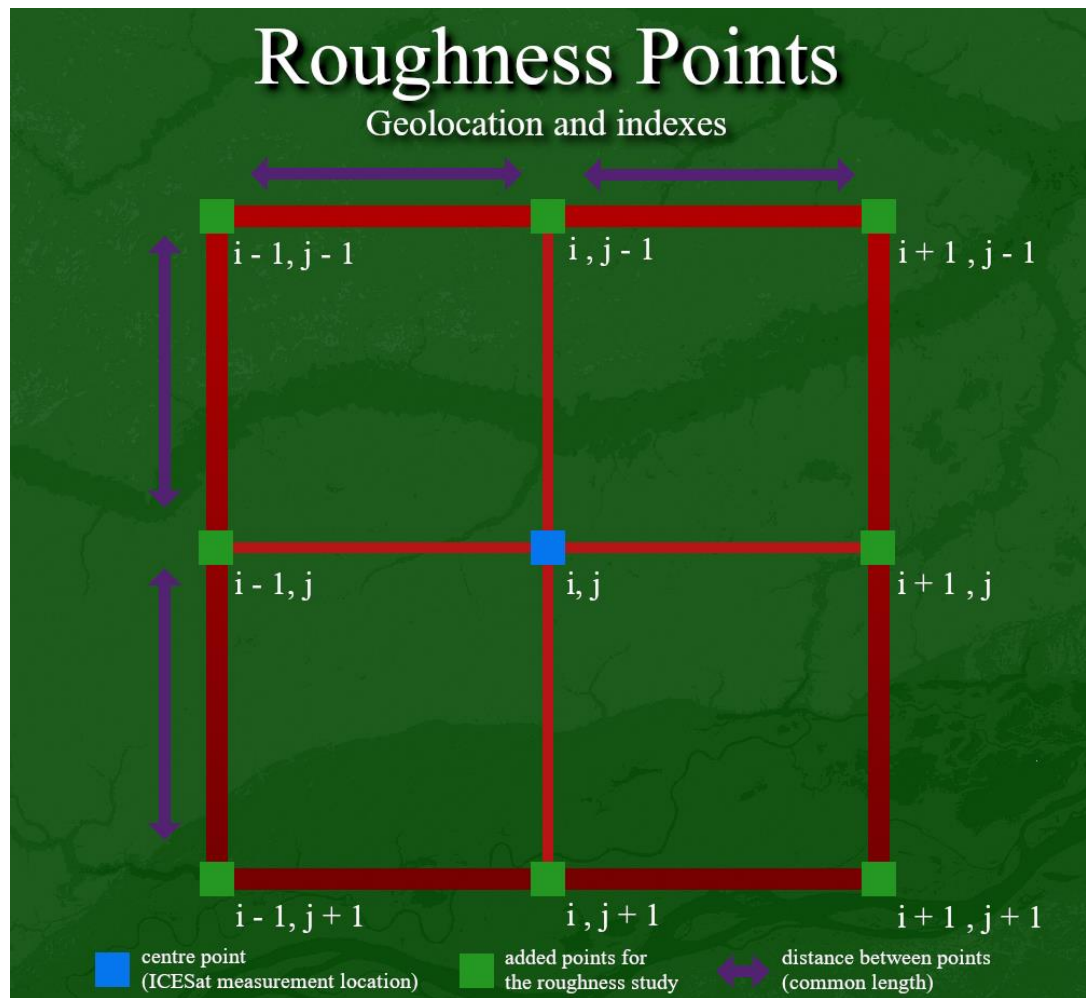


Figure 42 – Spatial repartition of points considered for each roughness calculation.

Each point of the squared area is finally converted from the orthographic projection coordinates (easting and northing in metres) to geographic coordinates (longitude and latitude). SRTM-GL1's heights are retrieved at each point location using bilinear interpolation.

Standard deviation is calculated from the 3x3 points square, estimating terrain's roughness according to the SRTM-GL1 DEM heights:

$$R_s(i, j) = \sqrt{\frac{1}{s^2} \times \sum_{k=-\frac{s}{2}}^{\frac{s}{2}} \sum_{l=-\frac{s}{2}}^{\frac{s}{2}} h_{SRTMGL1}(i+k, j+l)^2 - \left(\frac{1}{s^2} \times \sum_{k=-\frac{s}{2}}^{\frac{s}{2}} \sum_{l=-\frac{s}{2}}^{\frac{s}{2}} h_{SRTMGL1}(i+k, j+l) \right)^2} \quad (\text{eq. 6})$$

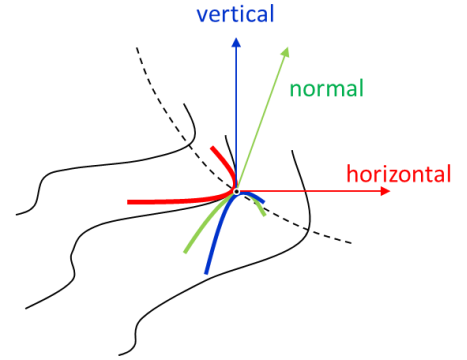
Where:

- $R_s(i, j)$ is the local standard deviation to be computed.
- s is the size of the statistical window (s^2 being the number of samples),
- $h_{SRTM-GL1}(i, j)$ is the height retrieved from the point of coordinates of the square (from nearest neighbour interpolation on the SRTM-GL1 grid).

4.2.2.1.7 Computation of curvatures

As shown in the attached figure, one may compute three kinds of curvatures depending on the plan along which the curve is inserted.

Horizontal, vertical and tangential curvatures are processed on the 3x3 SRTM-GL1 heights squares. The equations used to process curvatures are the following (respectively horizontal, vertical and tangential curvature):



$$Kh = \frac{dXX \times dY^2 - 2 \times dXY \times dX \times dY + dYY \times dX^2}{p \times \sqrt{p}} \quad (\text{eq. 7})$$

$$Kv = \frac{dXX \times dX^2 - 2 \times dXY \times dX \times dY + dYY \times dY^2}{p \times q \times \sqrt{q}} \quad (\text{eq. 8})$$

$$Kt = \frac{dXX \times dY^2 - 2 \times dXY \times dX \times dY + dYY \times dX^2}{p \times \sqrt{q}} \quad (\text{eq. 9})$$

All the variables used in these equations are calculated from SRTM-GL1's heights:

$$dX = \frac{-[h_{i+1,j} - h_{i-1,j}]}{2 \times GSD_x} \quad (\text{eq. 10})$$

$$dY = \frac{-[h_{i,j+1} - h_{i,j-1}]}{2 \times GSD_y} \quad (\text{eq. 11})$$

$$dXX = \frac{h_{i+1,j} - 2 \times h_{i,j} + h_{i-1,j}}{GSD_x^2} \quad (\text{eq. 12})$$

$$dYY = \frac{h_{i,j+1} - 2 \times h_{i,j} + h_{i,j-1}}{GSD_y^2} \quad (\text{eq. 13})$$

$$dXY = \frac{(h_{i+1,j+1} - h_{i+1,j-1}) - (h_{i-1,j+1} - h_{i-1,j-1})}{4 \times GSD_x \times GSD_y} \quad (\text{eq. 14})$$

$$p = dX^2 + dY^2 \quad (\text{eq. 15})$$

$$q = p + 1 \quad (\text{eq. 16})$$

Where:

$h(i,j)$ is the height of indexes i and j according to SRTM-GL1.

GSD_x is the ground sampling distance (distance between two points of the square along the equator)

GSD_Y is the ground sampling distance (distance between two points of the square across the equator)

4.2.2.2 Results

4.2.2.2.1 Height differences

Here are the results of this study. All the statistics refer to the differences between ICESat and SRTM-GL1 heights (ICESat - SRTM):

Number of ICESat products	642
Number of compared heights	60 160 803
Mean (metres)	0.590 m
RMSE (metres)	4.741 m
Standard deviation (metres)	4.704 m
Median (metres)	0.618m

Figure 43 – Statistics of the (ICESat - SRTM) comparison.

Arithmetic mean (0.590 m) gives the systematic bias between ICESat and SRTM heights. Root Mean Square Error or RMSE (4.741 m) is the quadratic mean of the errors including the bias. Standard deviation (4.704 m) gives the distribution of the errors around the mean out of the bias. The median error m is the one for which 50% of the pixels have an error less than m and 50% have an error greater than m.

The following histogram shows the distribution of SRTM-GL1's error:

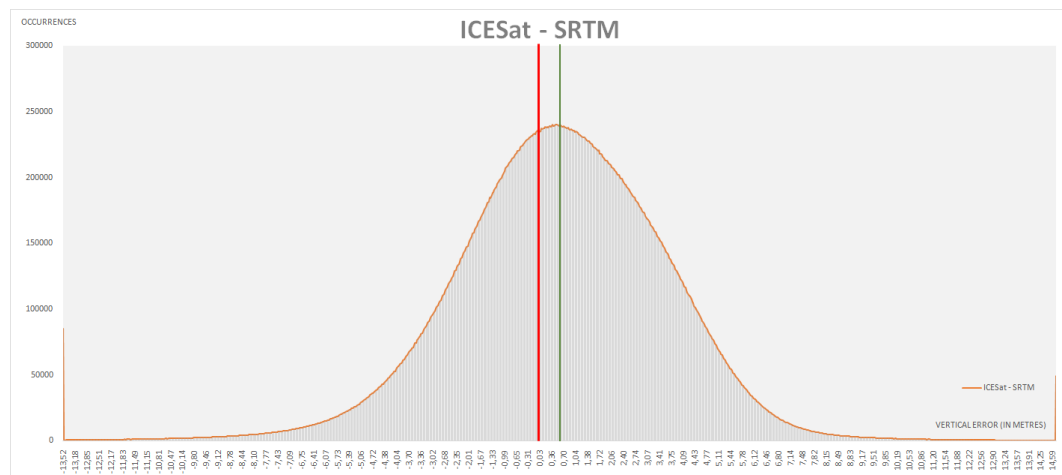


Figure 44 – Histogram of height difference between ICESat and SRTM-GL1.

This histogram looks like the Normal distribution (Gaussian) with a clear positive bias on the right of the 0 axis (red).

4.2.2.2.2 Correlation between height errors (dhi) and height values (ICESat)

After conversion from TOPEX/Poseidon ellipsoid to WGS84 ellipsoid, the distribution of the ICESat heights is given by the statistics and histogram below. The dashed vertical axis represents the heights.

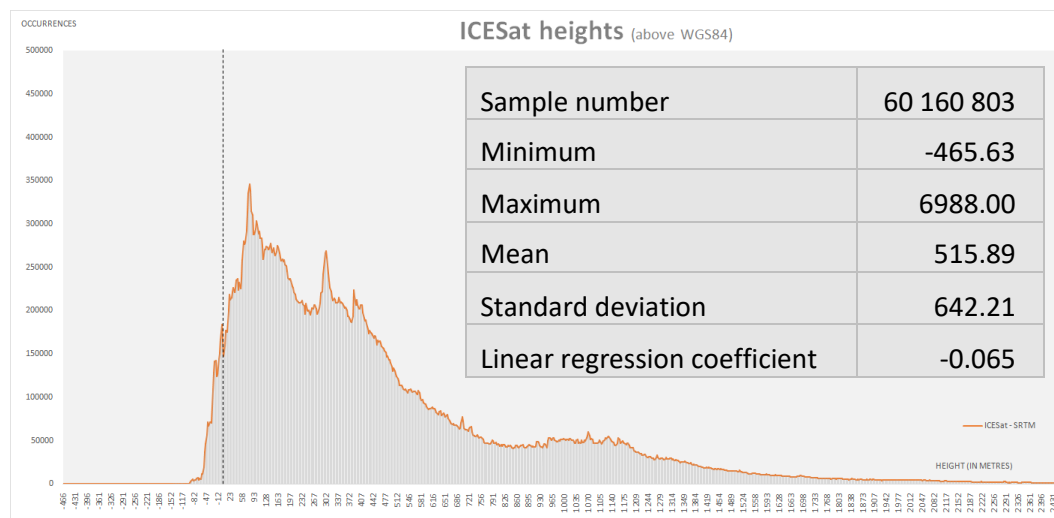


Figure 45 – Distribution of ICESat heights above WGS84.

Heights do not follow a Normal Distribution Law. This could explain the low value of the linear correlation coefficient ($r = -0,065$).

This low value is confirmed by computing the two-dimensional histogram with the heights ICESat (hICESat) on the ordinates axis and the observed errors (dhi) on the abscissa axis.

We observe a dispersion of the errors whatever the height and no straight line or even curve of regression appears in the attached figure.

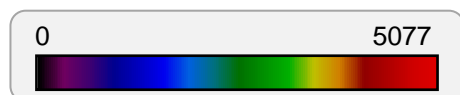
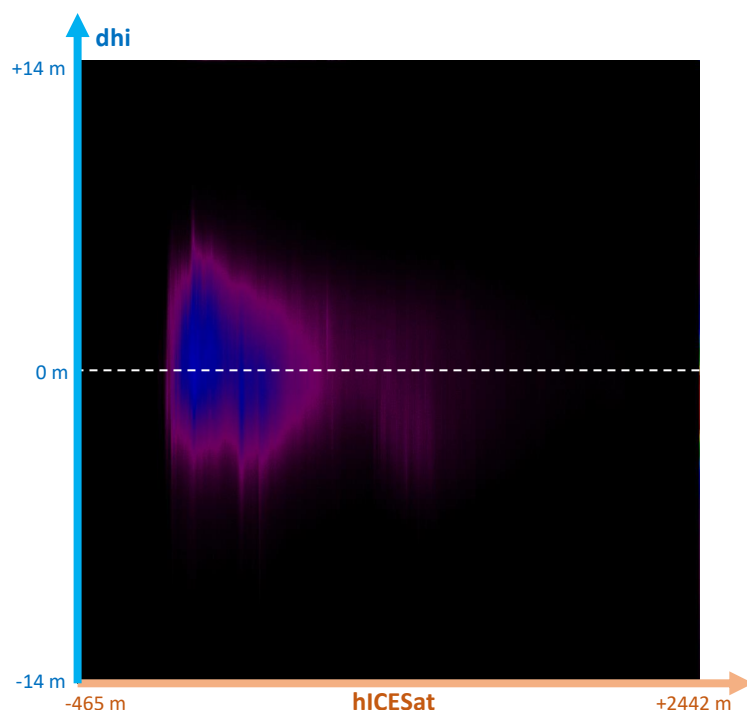


Figure 46 – Bidimensional histogram of ICESat heights (X-axis) and dhi (=ICESat-SRTM) height errors.



4.2.2.2.3 Correlation between height errors (dhi) and terrain roughness (local standard deviations)

The aim here is to detect a possible correlation between the roughness or variability of the relief (ground undulations, mountains or flat soils) and the amplitude of the height errors between the ICESat reference data and those of SRTM.

The variability of the relief is estimated by considering 9 points (the ICESat central point and its 8 neighbours) in a 3x3 window. This estimate is made at three scales: -11x11 (150 m between points), -101x101 (1500 m between points) or -501x501 (7500 m between points). The variability of the terrain is estimated by calculating the standard deviation of these 9 points.

Figure below shows the distribution of these local standard deviations. There is a strong predominance of the 0 values of the standard deviation indicating flat soils where the 9 DEM values are strictly identical. The saturation of the "r11" distribution (red curve) is simply due to the reduced interval of the input histogram values (computation limited by the number of data).

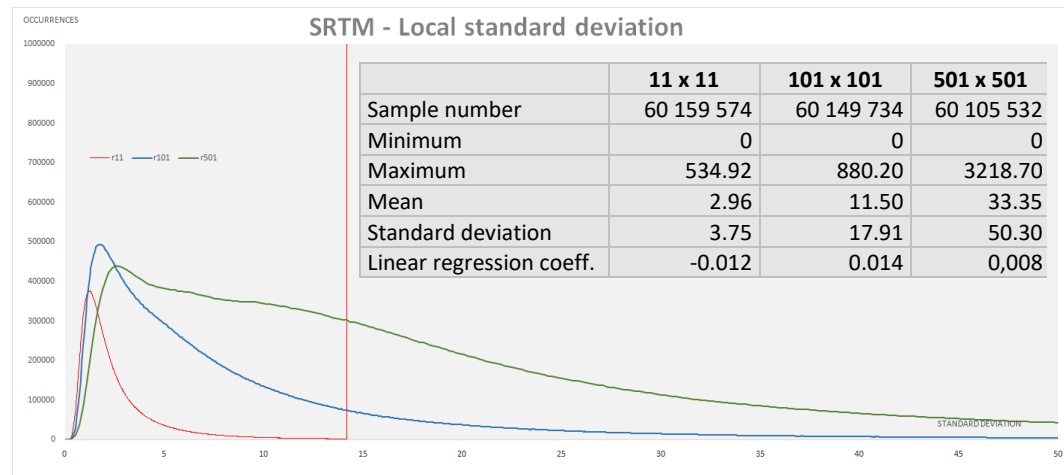


Figure 47 – Distributions of local standard deviations.

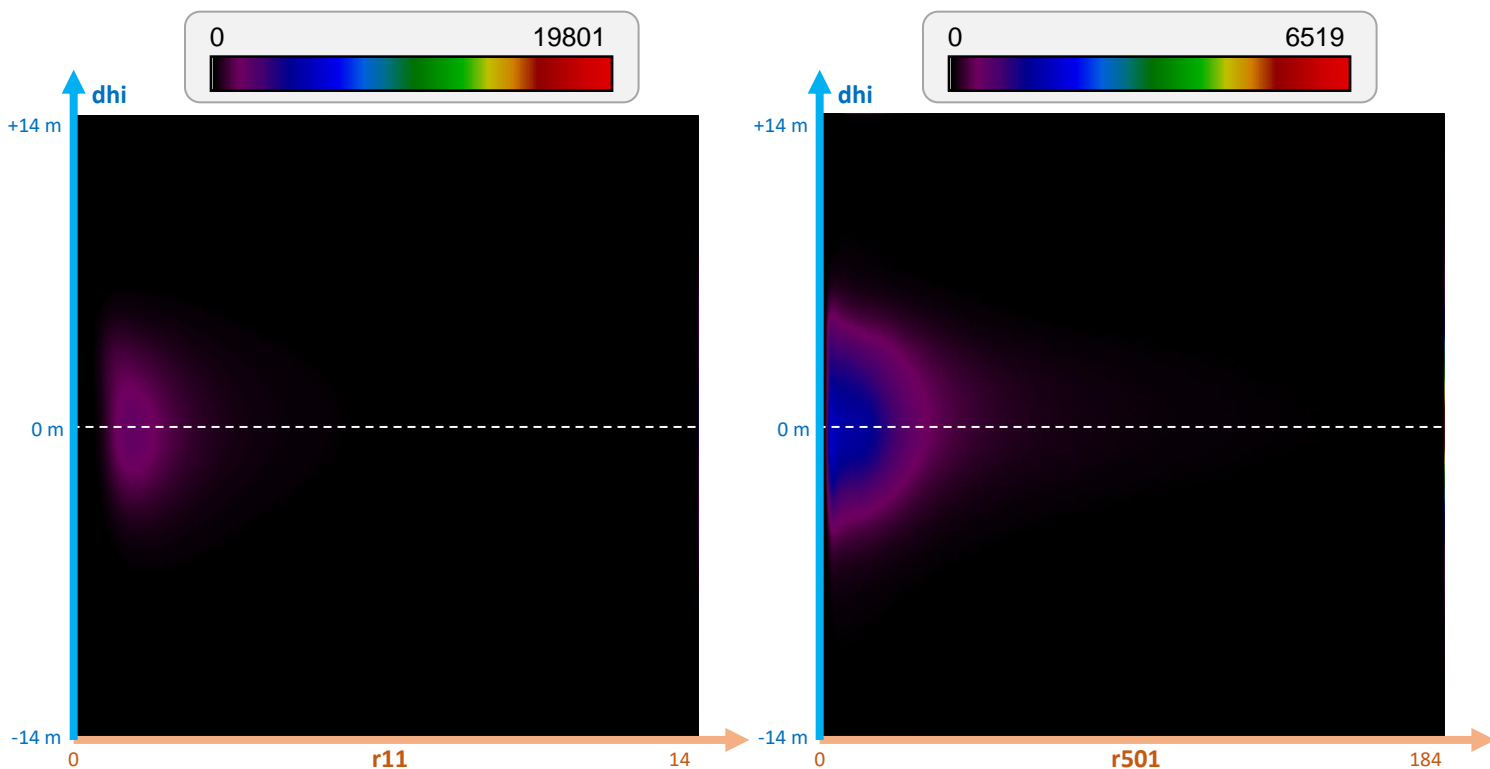


Figure 48 – Roughness (standard deviation) in a 11x11 square (left) and 501x501 square (right).

4.2.2.2.4 Correlation between height errors (dhi) and terrain curvatures

Another way of measuring the variation of the relief is to estimate the curvature of the valleys (concavity with positive second derivative) and ridges (convexity with negative 2nd derivative). It can be assumed that the sharper are the “characteristic lines” (narrow valleys or sharp ridges), the larger the height errors that match the difference dhi (ICESat - SRTM).

The figure below clearly shows that the larger the window, the smaller the curvature. It is therefore in the smallest area (11x11 matching a ground spacing between pixels of 150 metres) that we observe the largest curvatures (red curve).

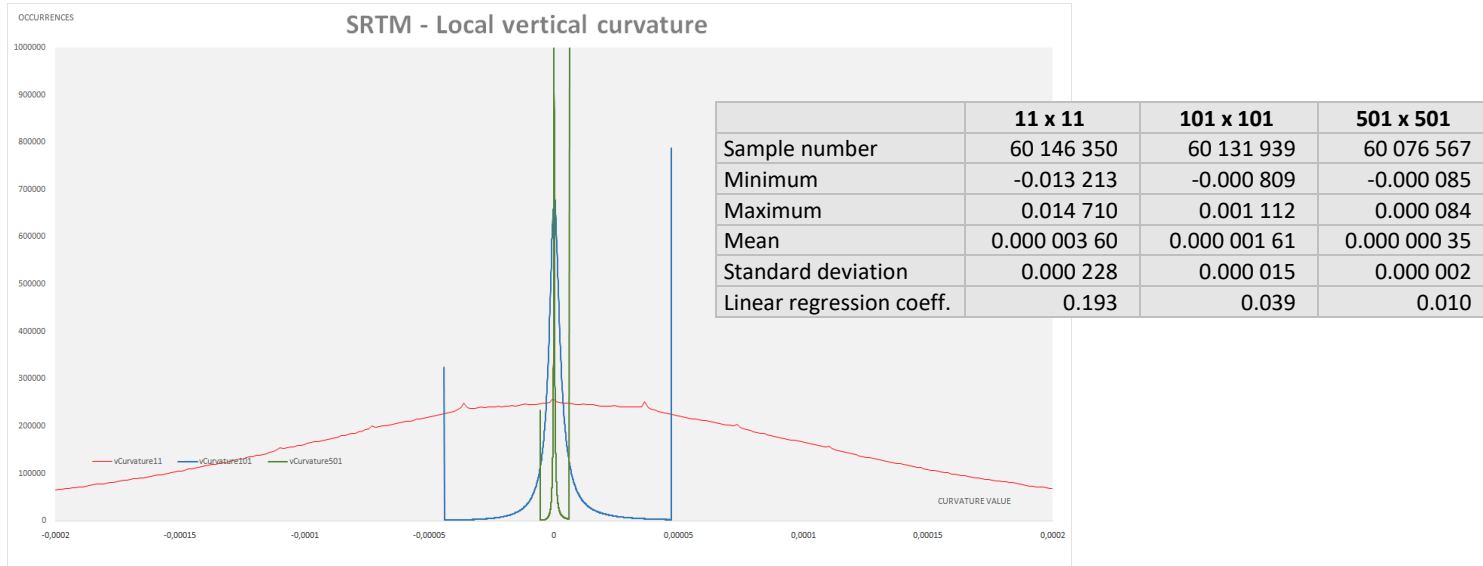


Figure 49 – Distributions of local vertical curvatures.

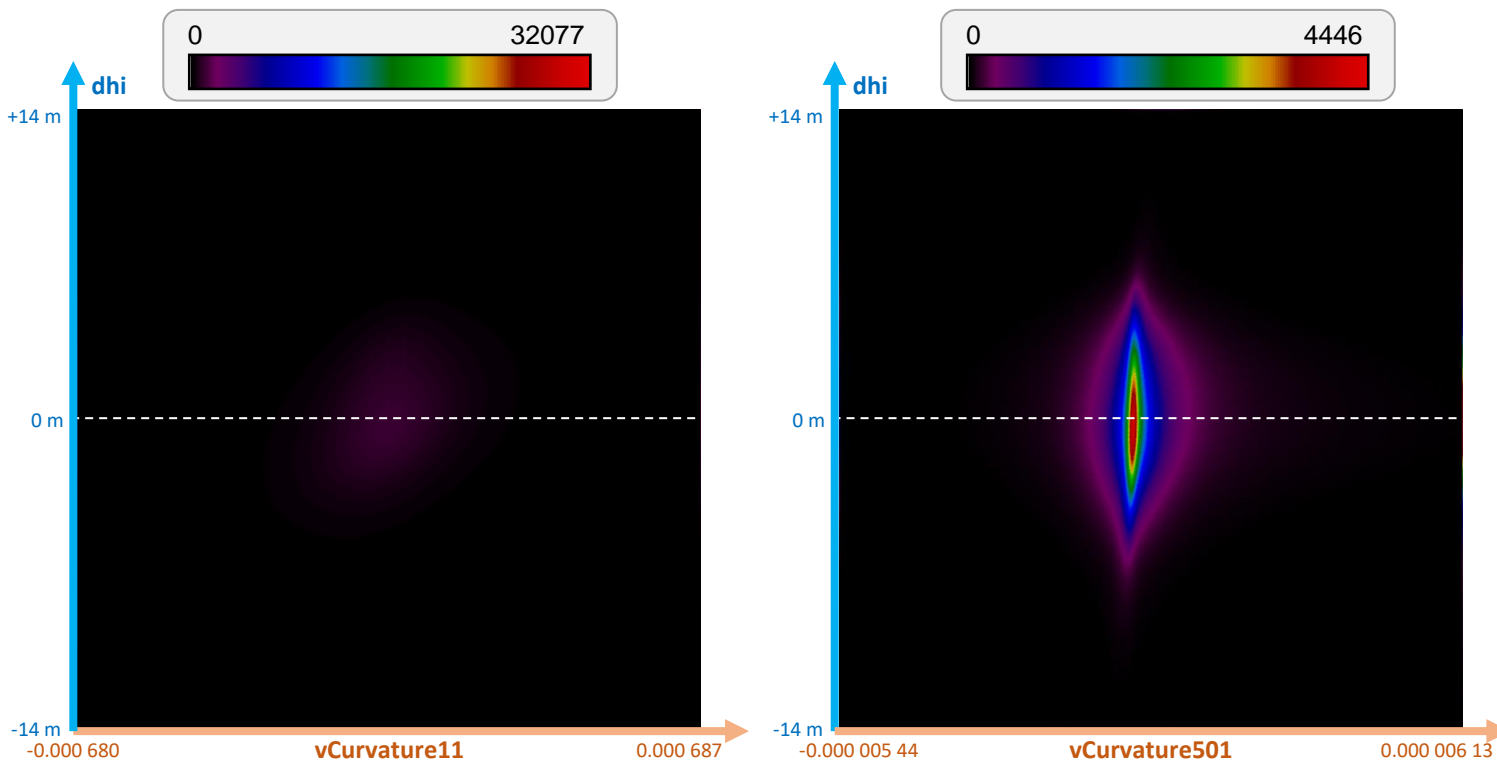


Figure 50 – Vertical curvature in a 11x11 square (left) and 501x501 square (right).

The appearance of the two figures confirms the very low linear correlation coefficients. Despite a 1000 times larger scale factor of the "vCurvature501" distribution compared to that of "vCurvature11", there is no correlation trend between the vertical curvature and the distribution of "dhi" height errors.

These observations were also made about the tangential and horizontal curvatures. No relevant results have been found.

4.2.2.2.5 Analysis of the geographical distributions of elevation errors

A KML file has been generated showing the geographical repartition of the height errors (see AD-1), based on the ones processed in the ICESat/DEM comparisons. This file is composed of a subsample of approximately 3000 points of comparison between ICESat and SRTM. The colour of each point represents the value of the noticed height error at its location. The label of each point corresponds to the value in metres of the height error (visible as label in the linked KML file).

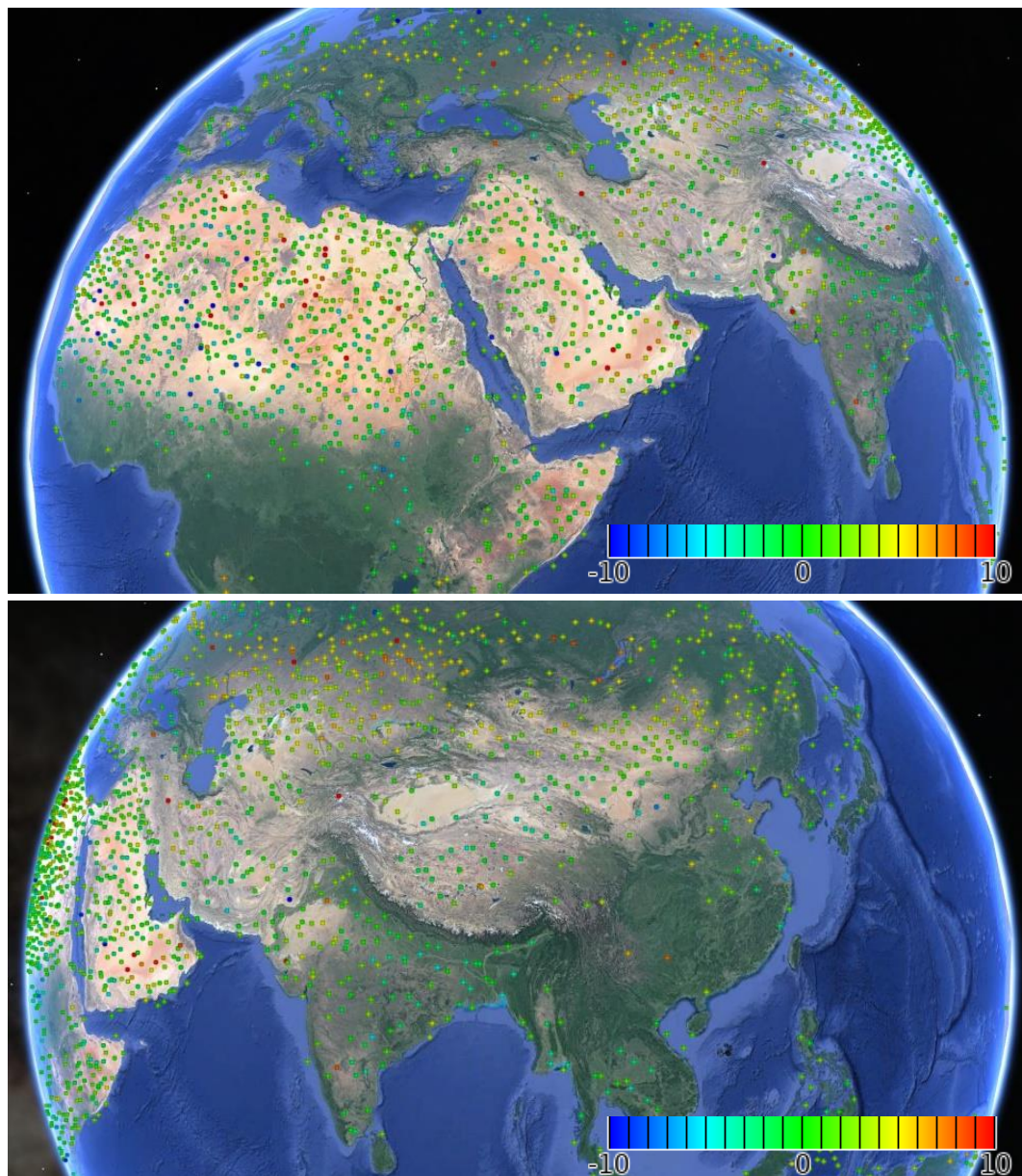


Figure 51 – Geographic distribution of SRTM height errors.

The generated KML shows that the SRTM-GL1 height error is low for most of the compared points. Clusters of green points show the constancy of the height error of SRTM-GL1, as well as the good accuracy of most of the heights of this DEM. A group of error points can be noticed over the Sahara. SRTM-GL1 visually tends to be more precise than ASTER GDEM, but less precise than ALOS World 3D most of the time.

The histogram shows a small percentage of outliers. These outliers can be explained by the following reasons:

- Events between the two missions - topography changed between the two missions, giving large errors near excavations, towns, canopy, and even lakes.
- Cloud contamination is a known issue on ICESat's data - filtering data with cloud related flags is efficient, but does not affect a small percentage of cloud contaminated elevation values.

The overall statistics of this study seem reliable taking into account SRTM's performances, which are assessed to have a vertical error from 5.6 metres to 9.0 metres depending on the continent (RD-3).

Negative and positive errors are not scattered, the visualization file (see AD-6) shows groups of error.

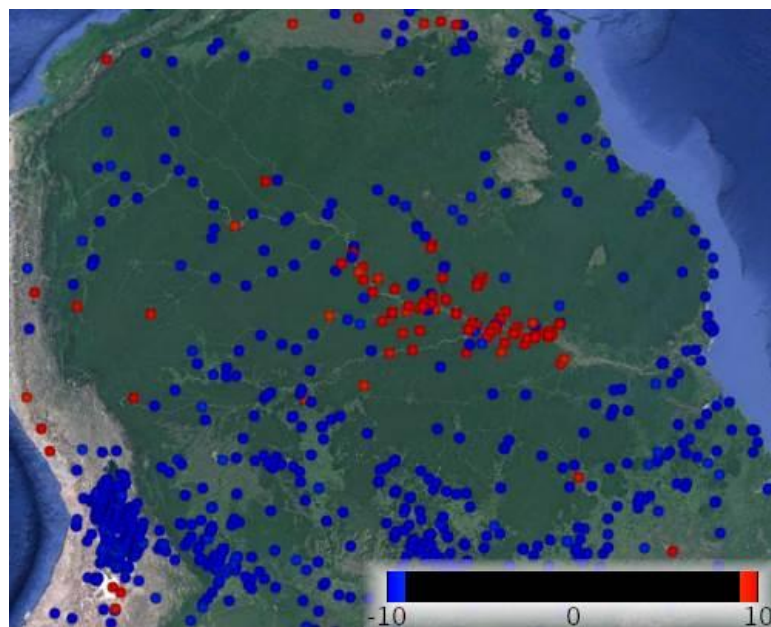


Figure 52 – Error repartition over the Amazon Forest.

The main negative differences in this area can be linked to the deforestation.



Figure 53 – Deforestation related height differences.

As SRTM's data includes canopy in areas of dense vegetation (RD-4), deforestation may have occurred between the two missions, resulting as an important negative error (as SRTM have higher elevations than ICESat, due to the presence of trees during SRTM's acquisitions period).

Other differences occurred near the Amazon River.

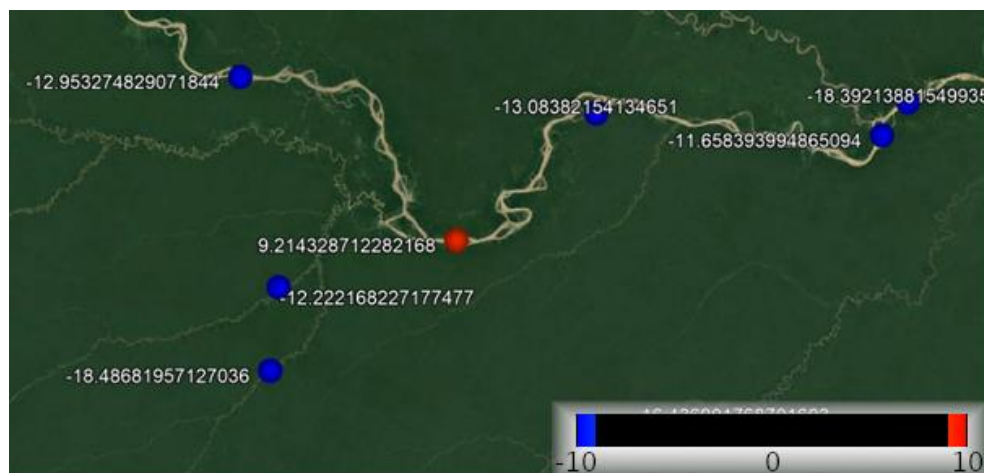


Figure 54 – River related height differences.

SRTM-GL1 is distributed as a grid of height values separated geographically by approximately 30 metres (near the equator). As big as this separation is, SRTM-GL1 cannot take into account drastic height changes, which ICESat can highlight by means of its accuracy and sampling frequency, resulting in a significant height difference.

Highly varying terrain roughness is causing big height differences.



Figure 55 – Relief related height differences.

SRTM and ICESat's horizontal accuracies have to be taken into account: a severe horizontal displacement can cause noticeable height differences in such highly varying topography.

Desert areas are the most common source of errors in this comparison.

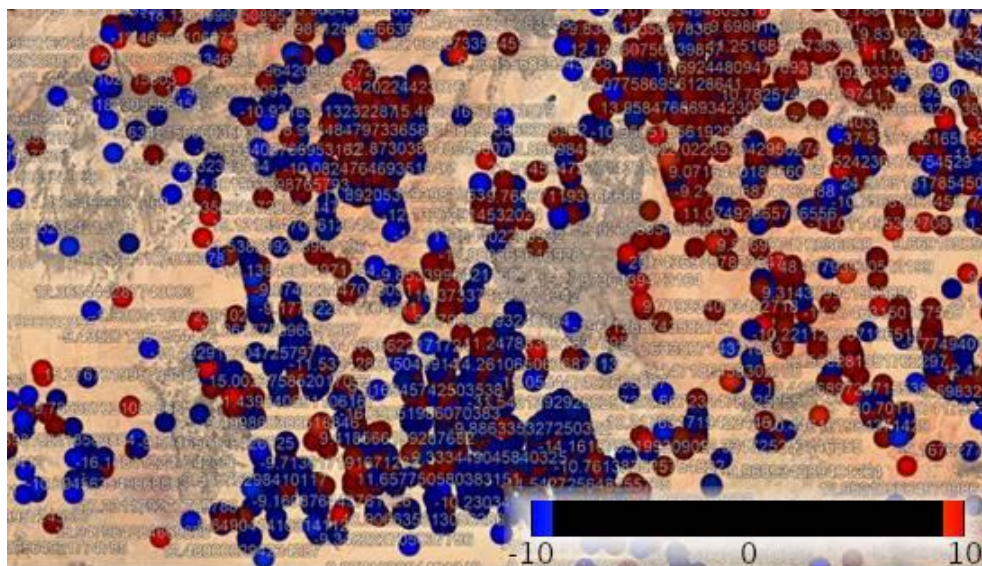


Figure 56 – Desert related height differences.

Moving sands is a factor that may explain such height differences between ICESat and SRTM-GL1.

4.2.3 Assessment of ASTER GDEM from ICESat / GLAS data

4.2.3.1 Method and notations

The methodology used is the same as the one for the assessment of SRTM GL1 from ICESat (see section 4.2.2).

ASTER GDEM is a global elevation model computed from photogrammetric methods (stereographic views). It can be verified that the more views we have, the more accurate is the elevation. The following chart shows the relation between the number of stereographic views and the average of elevation errors (dhi).

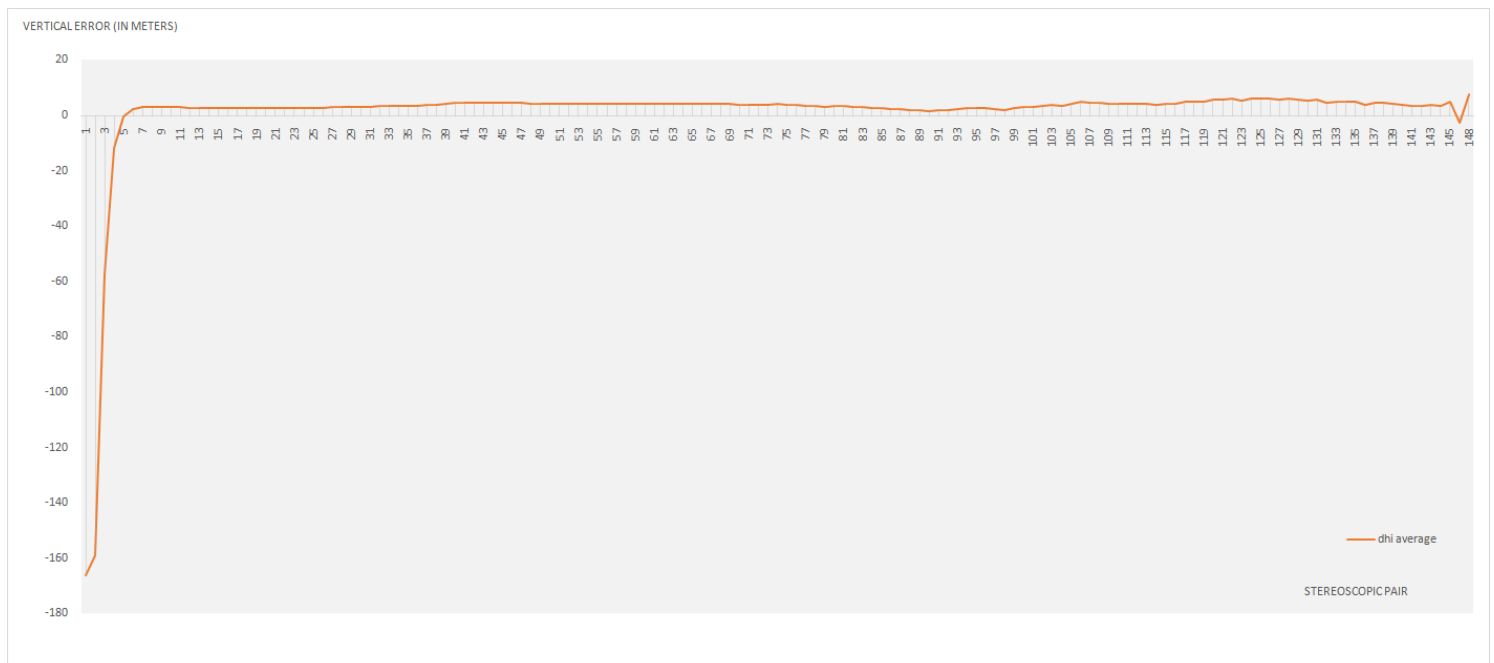


Figure 57 – Average of dhi value per number of stereographic views.

To avoid false statistics, the elevation values computed from a number of stereographic views lower than 5 have been ignored during the processing.

4.2.3.2 Results

4.2.3.2.1 Height differences

Here are the results of this study. All the statistics refer to the differences between ICESat's heights and ASTER GDEM's heights (ICESat – ASTER GDEM):

Number of ICESat products	642
Number of heights compared	92 913 348
Mean (metres)	2.315 m
RMSE (metres)	27.764 m
Standard deviation (metres)	27.667 m

Figure 58 – Statistics of the (ICESat – ASTER GDEM) comparison.

The following histogram shows the distribution of ASTER GDEM's error:

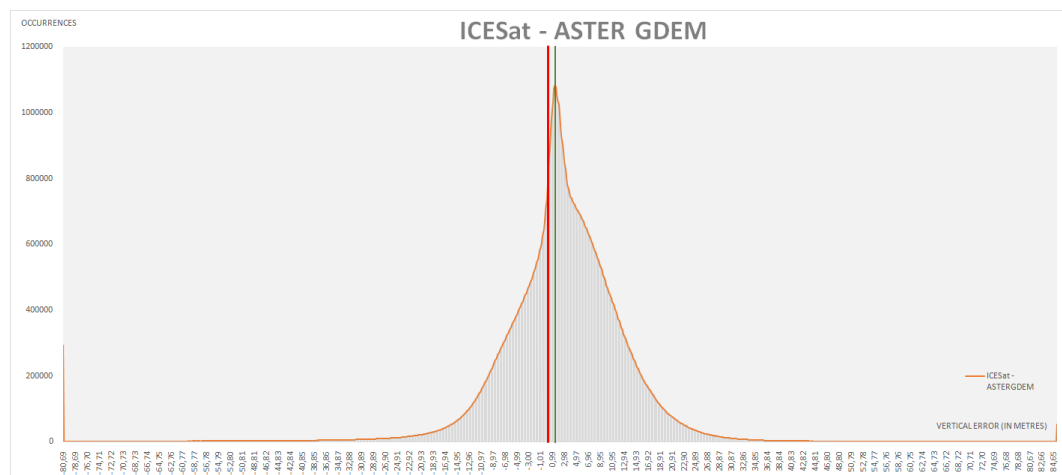


Figure 59 – Histogram of height difference between ICESat and ASTER GDEM.

One may note that the interval of value is much greater than SRTM (4.2.2.2.1).

4.2.3.2.2 Correlation between height errors (dhi) and height values (ICESat)

After conversion from TOPEX/Poseidon ellipsoid to WGS84 ellipsoid, the distribution of the ICESat heights is given by the statistics and histogram below:

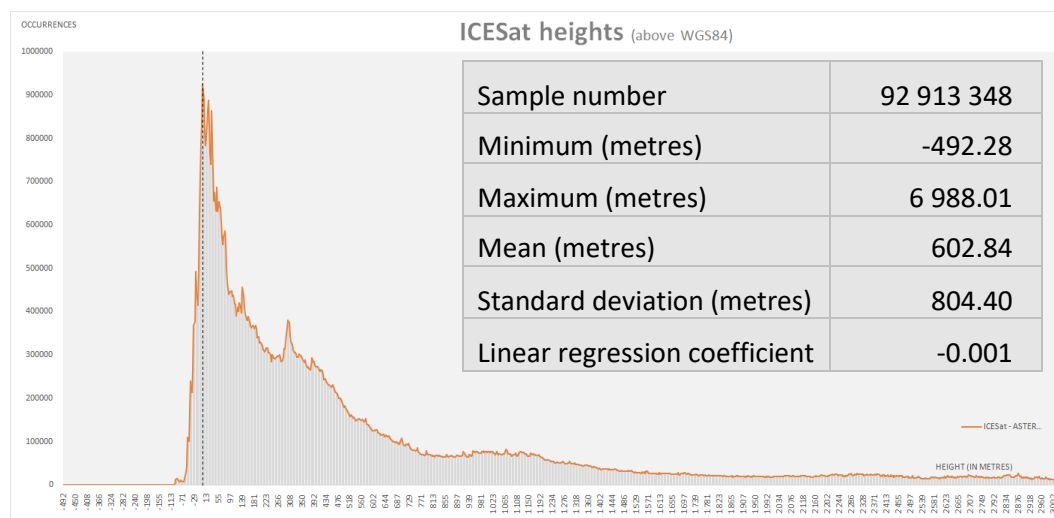


Figure 60 – Distribution of ICESat heights above WGS84.

Heights do not follow a Normal Distribution Law. This could explain the low value of the linear correlation coefficient ($r = -0.001$).

This low value is confirmed by computing the two-dimensional histogram with the heights ICESat (hICESat) on the ordinates axis and the observed errors (dhi) on the abscissa axis.

We observe a dispersion of the errors whatever the height and no straight line or even curve of regression appears in the attached figure.

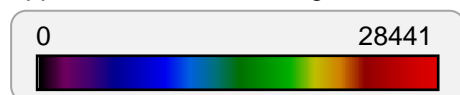
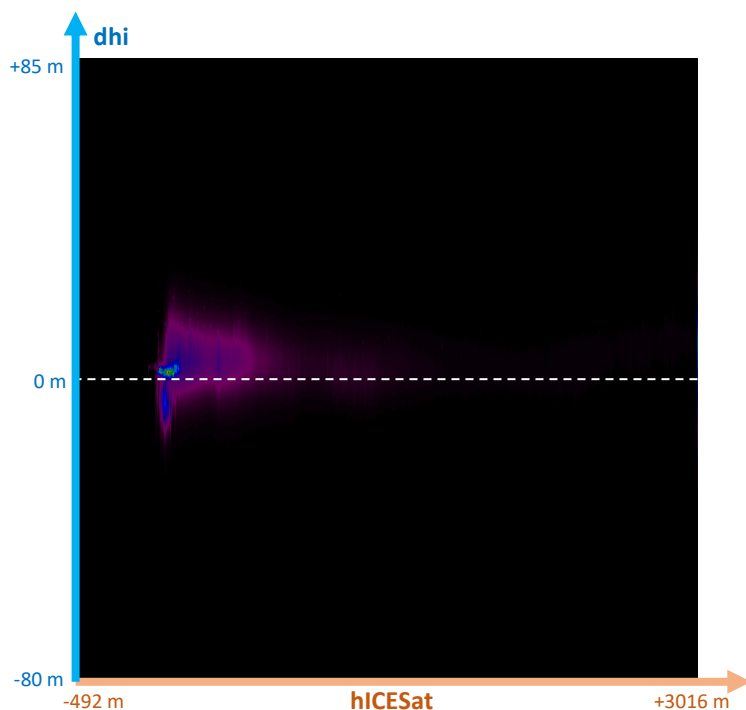


Figure 61 – Bidimensional histogram of ICESat heights (X-axis) and dhi (=ICESat-ASTER GDEM) height errors.



4.2.3.2.3 Correlation between height errors (dhi) and terrain roughness (local standard deviations)

Such as for SRTM-GL1, the aim here is to detect a possible correlation between the roughness or variability of the relief (ground undulations, mountains or flat soils) and the amplitude of the height errors between the ICESat reference data and those of ASTER GDEM.

Figure below shows the distribution of these local standard deviations. There is a strong predominance of the 0 values of the standard deviation indicating flat soils where the 9 DEM values are strictly identical. The saturation of the "r11" distribution (red curve) is simply due to the reduced interval of the input histogram values (computation limited by the number of data).

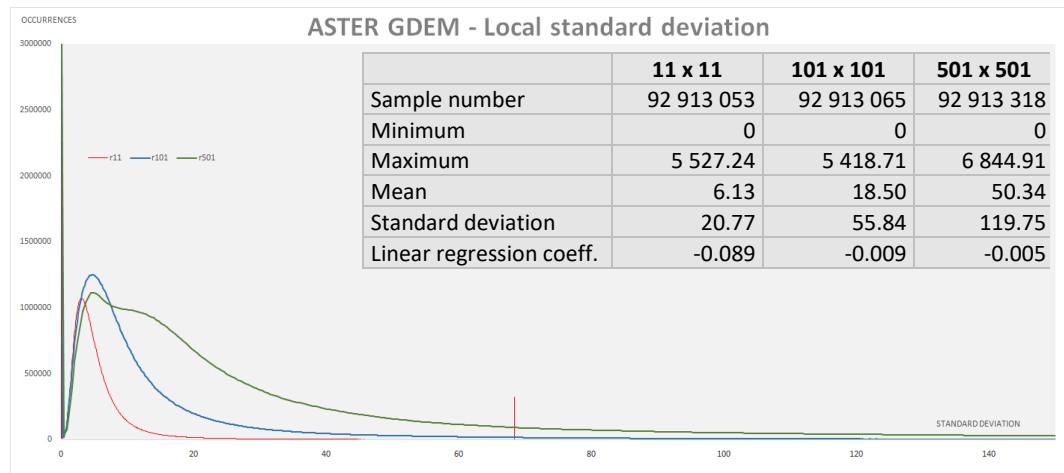


Figure 62 – Distributions of local standard deviations.

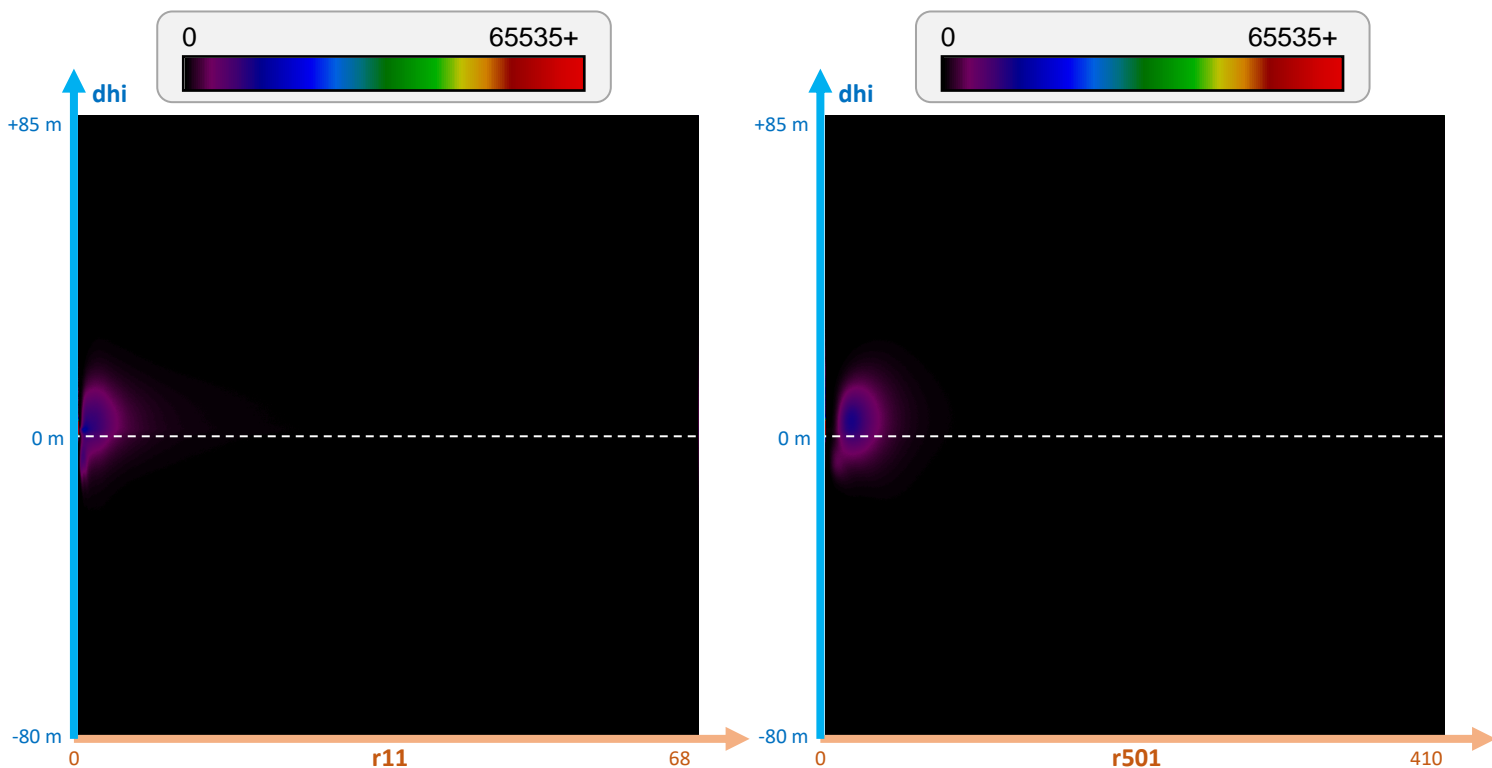


Figure 63 – Roughness (standard deviation) in a 11x11 square (left) and 501x501 square (right).

4.2.3.2.4 Correlation between height errors (dhi) and terrain curvatures

Another way of measuring the variation of the relief is to estimate the curvature of the valleys (concavity with positive second derivative) and ridges (convexity with negative second derivative). It can be assumed that the sharper the "characteristic lines" (narrow

valleys or sharp ridges), the larger the height errors that match the difference dhi (ICESat – ASTER GDEM).

The figure below clearly shows that the larger the window, the smaller the curvature. It is therefore in the smallest area (11x11 matching a ground spacing between pixels of 150 metres) that we observe the largest curvatures (red curve).

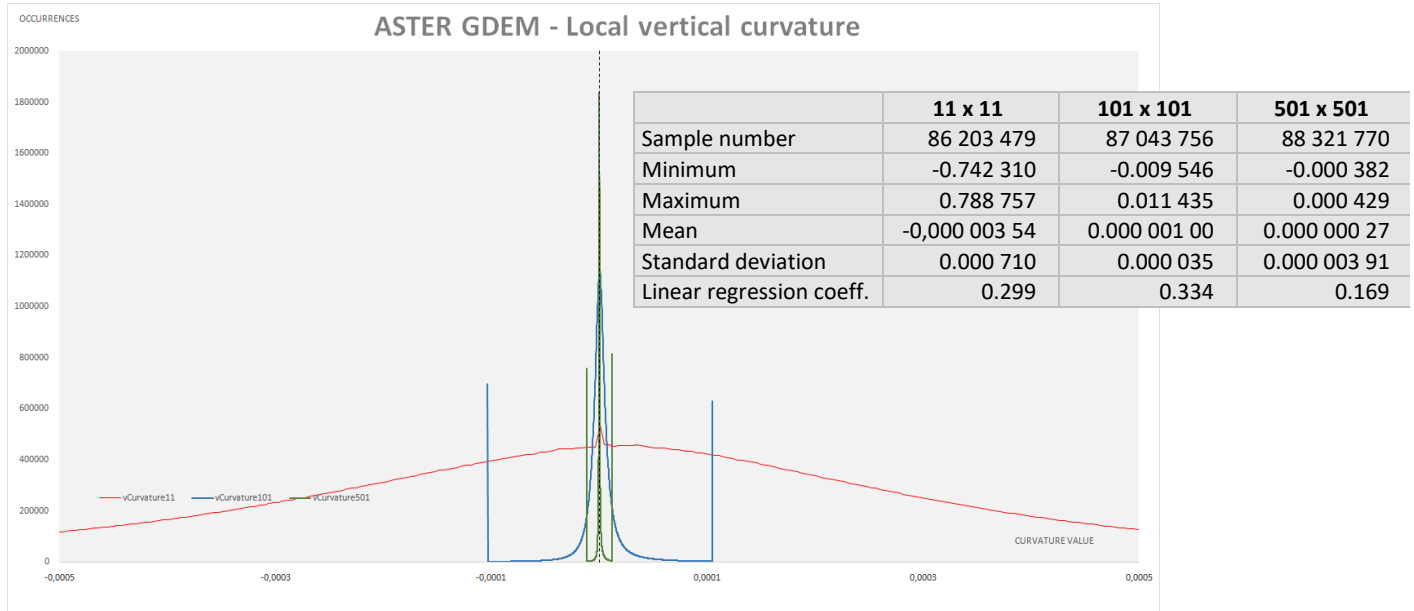


Figure 64 – Distributions of local vertical curvatures.

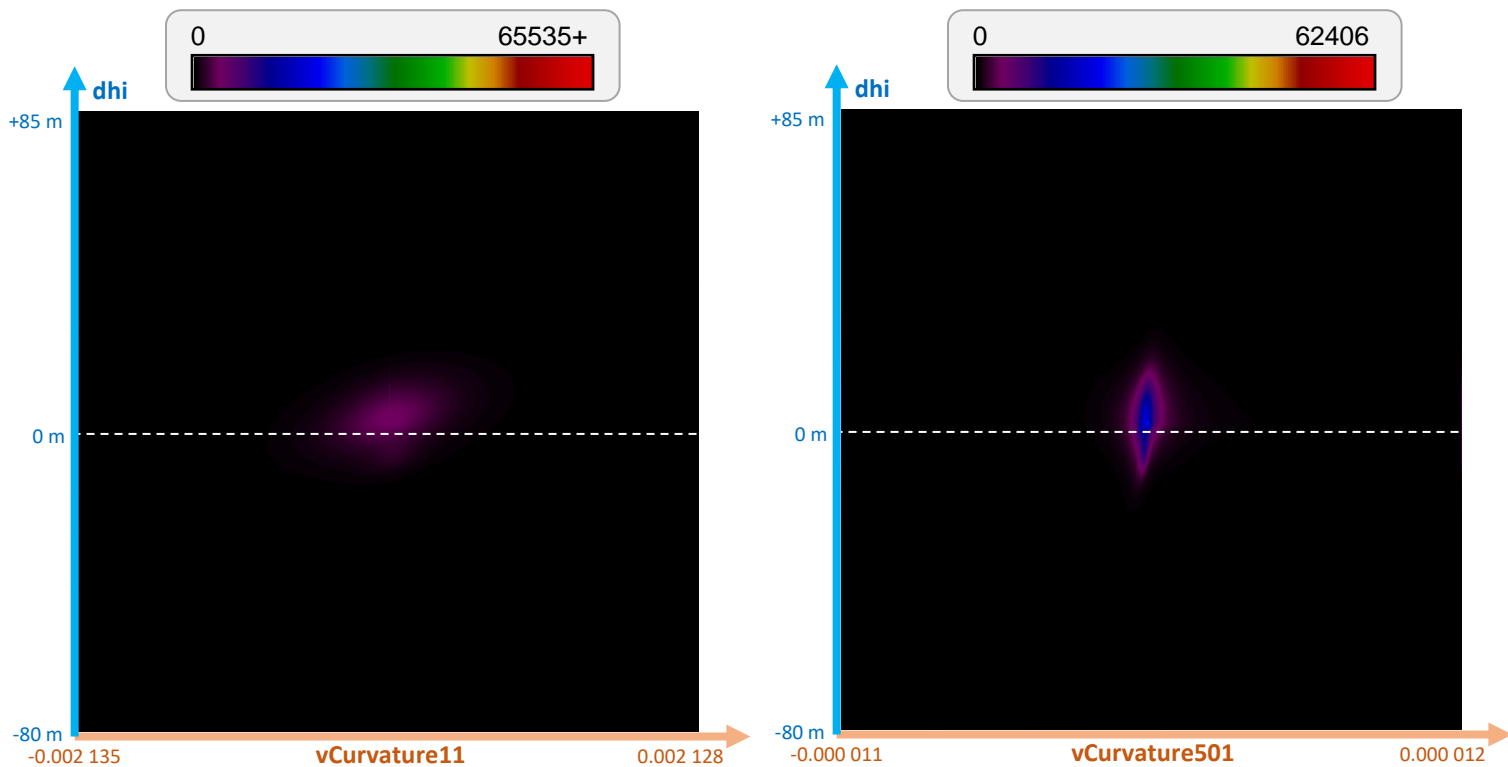


Figure 65 – Vertical curvature in a 11x11 square (left) and 501x501 square (right).

4.2.3.2.5 Analysis of the geographical distributions of elevation errors

In the same way as SRTM, a KML file has been generated showing the geographical repartition of the height errors (see AD-4), based on the ones processed in the ICESat/DEM comparisons. This file is composed of a subsample of approximately 3000 points of comparison between ICESat and SRTM. The colour of each point represents the value of the noticed height error at its location. The label of each point corresponds to the value in metres of the height error (visible as label in the linked KML file).

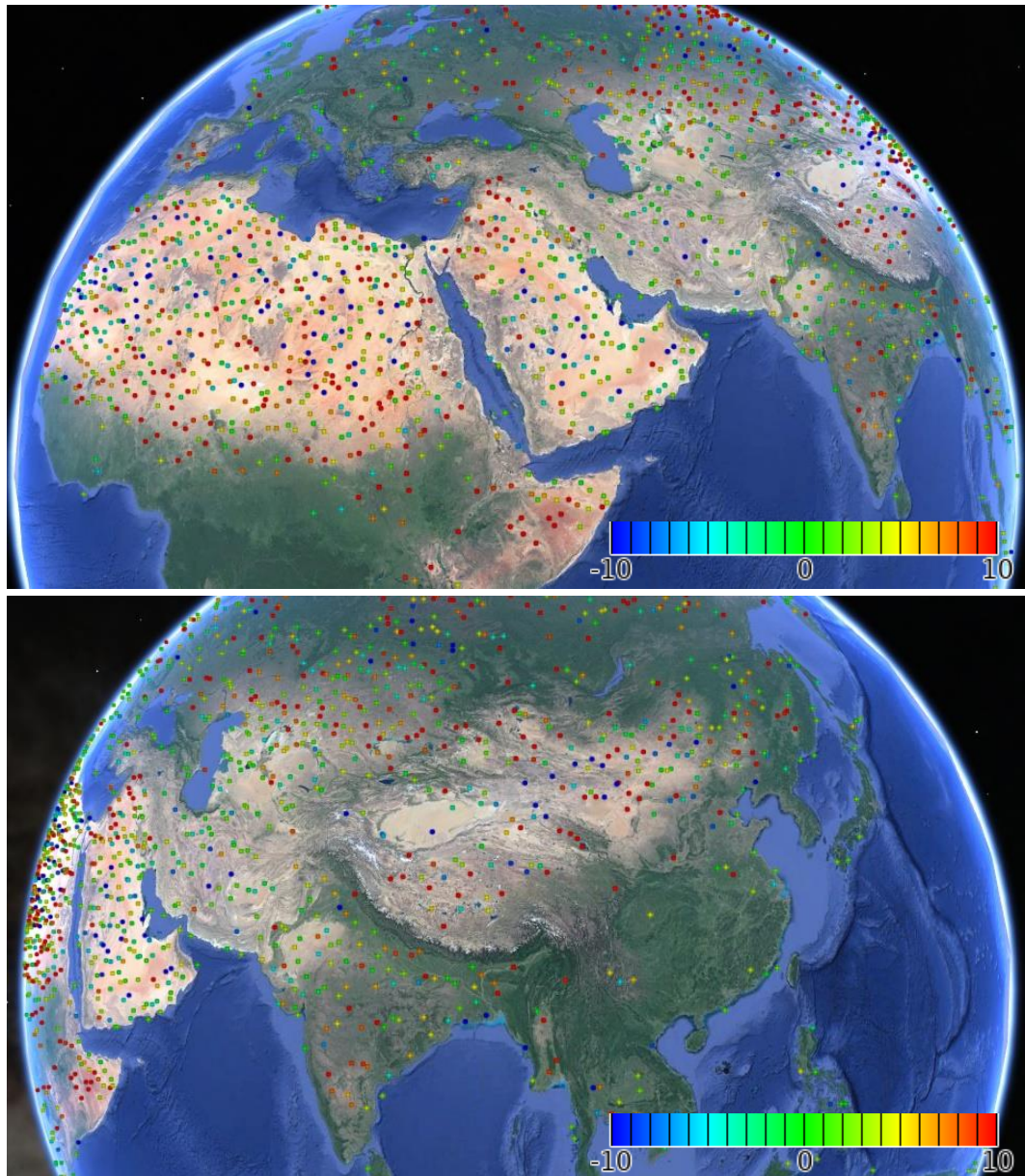


Figure 66 – Geographic distribution of ASTER GDEM height errors.

The generated KML shows that the height error of ASTER GDEM is randomly scattered, as no groups of identically coloured points could be visually established. High colour difference between two neighbour points can be noticed, highlighting the inconstancy of the ASTER GDEM heights. The high number of red and blue points indicates that the error of ASTER GDEM can often reach errors higher than 10 metres. ASTER GDEM visually tends to be less precise than SRTM and ALOS World 3D in most cases.

4.2.4 Assessment of ALOS World 3D from ICESat / GLAS data

4.2.4.1 Method and notations

The methodology used is the same as the one for the assessment of SRTM GL1 from ICESat (see section 4.2.2).

Like ASTER GDEM, ALOS World 3D is a global elevation model computed from stereoscopic pair. To filter the invalid elevation or the elevation coming from other DEM (like SRTM, ASTER etc), we have only used the information provided by flag value.

We have also filtered the elevation computed over the Arctic (above 60°N) and Antarctica (below 60°S) because invalid values over this region are poorly identified in the flag value.

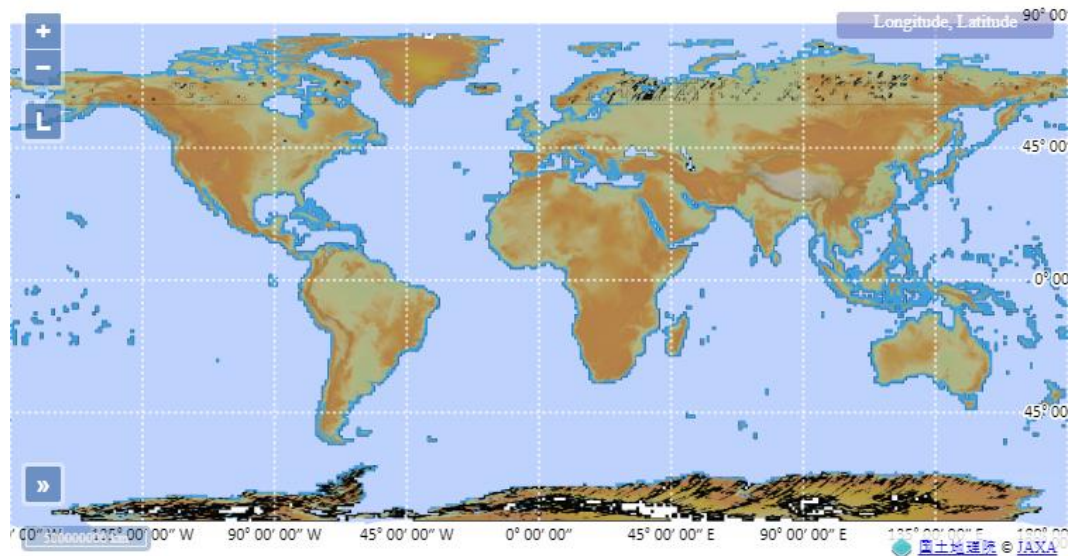


Figure 67 – Map of ALOS World 3D showing wrong values over poles.

4.2.4.2 Results

4.2.4.2.1 Height differences

Here are the results of this study. All the statistics refer to the differences between ICESat's heights and ALOS World 3D's heights (ICESat – ALOS World 3D):

Number of ICESat products	642
Number of heights compared	57 968 266
Mean (metres)	0.050 m
RMSE (metres)	4.516 m
Standard deviation (metres)	4.516 m

Figure 68 – Statistics of the (ICESat – ALOS World 3D) comparison.

The following histogram shows the distribution of ALOS World 3D's error:

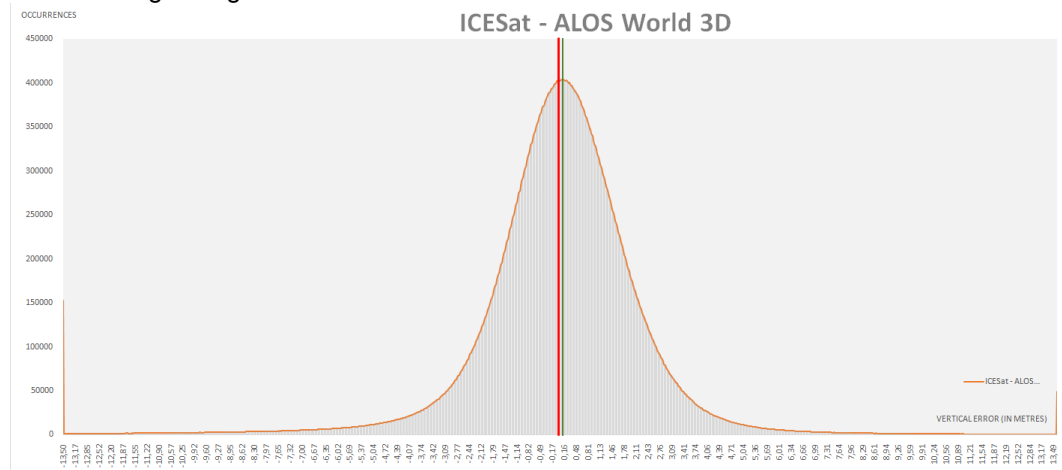


Figure 69 – Histogram of height difference between ICESat and ALOS World 3D.

4.2.4.2.2 Correlation between height errors (dhi) and height values (ICESat)

After conversion from TOPEX/Poseidon ellipsoid to WGS84 ellipsoid, the distribution of the ICESat heights is given by the statistics and histogram below:

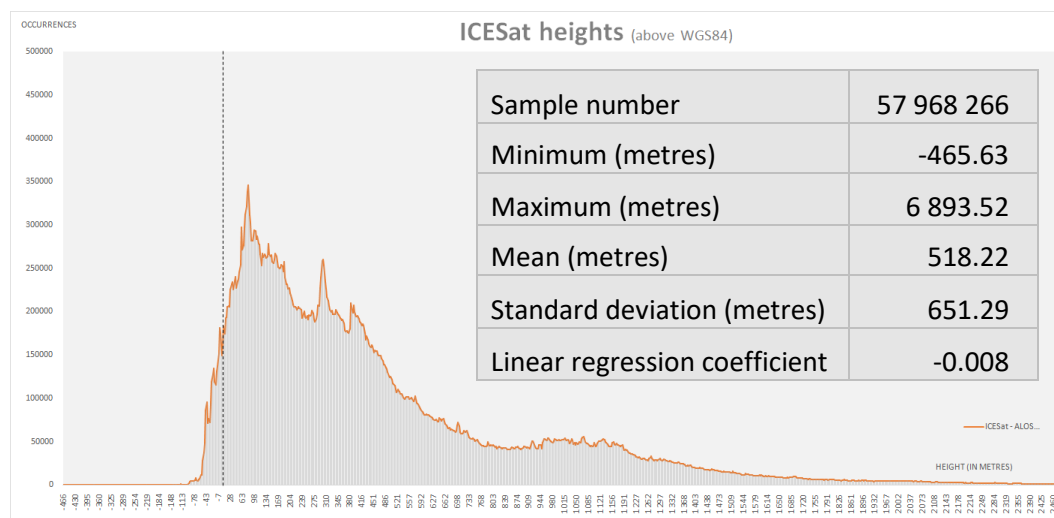


Figure 70 – Distribution of ICESat heights above WGS84.

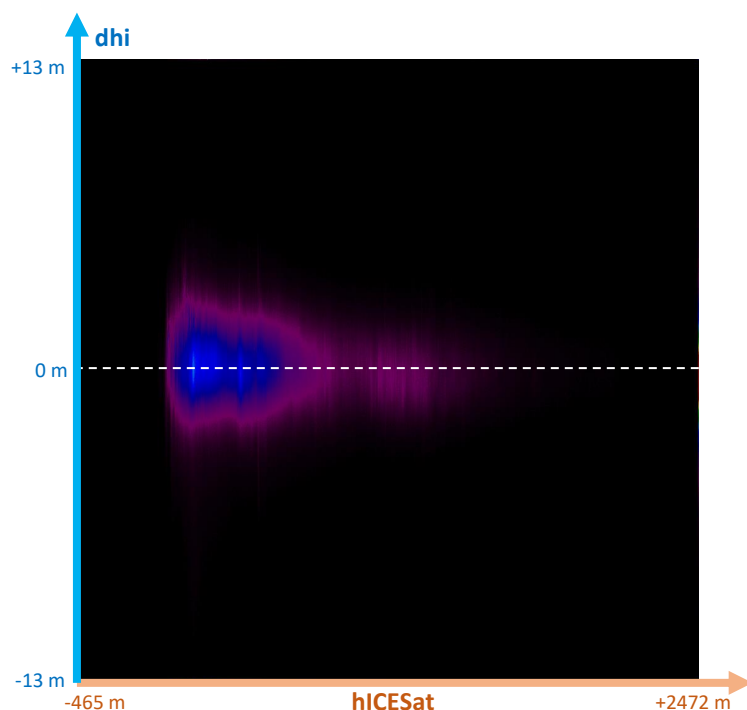
Heights do not follow a Normal Distribution Law. This could explain the low value of the linear correlation coefficient ($r = -0.008$).

This low value is confirmed by computing the two-dimensional histogram with the heights ICESat (hICESat) on the ordinates axis and the observed errors (dhi) on the abscissa axis.

We observe a dispersion of the errors whatever the height and no straight line or even curve of regression appears in the attached figure.



Figure 71 – Bidimensional histogram of ICESat heights (X-axis) and dhi (=ICESat-ALOS World 3D) height errors.



4.2.4.2.3 Correlation between height errors (dhi) and terrain roughness (local standard deviations)

Such as for SRTM-GL1, the aim here is to detect a possible correlation between the roughness or variability of the relief (ground undulations, mountains or flat soils) and the amplitude of the height errors between the ICESat reference data and those of ALOS World 3D.

Figure below shows the distribution of these local standard deviations. There is a strong predominance of the 0 values of the standard deviation indicating flat soils where the 9 DEM values are strictly identical. The saturation of the "r11" distribution (red curve) is simply due to the reduced interval of the input histogram values (computation limited by the number of data).

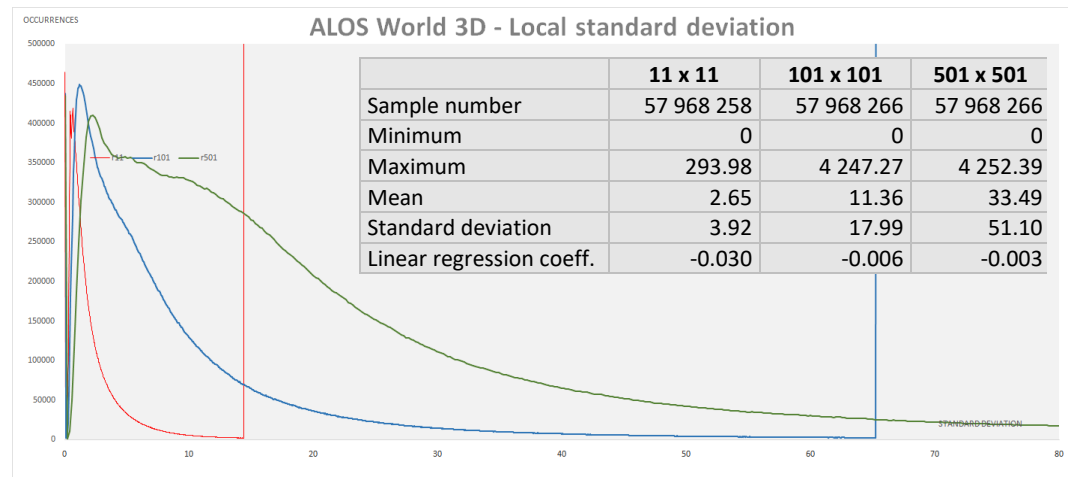


Figure 72 – Distributions of local standard deviations.

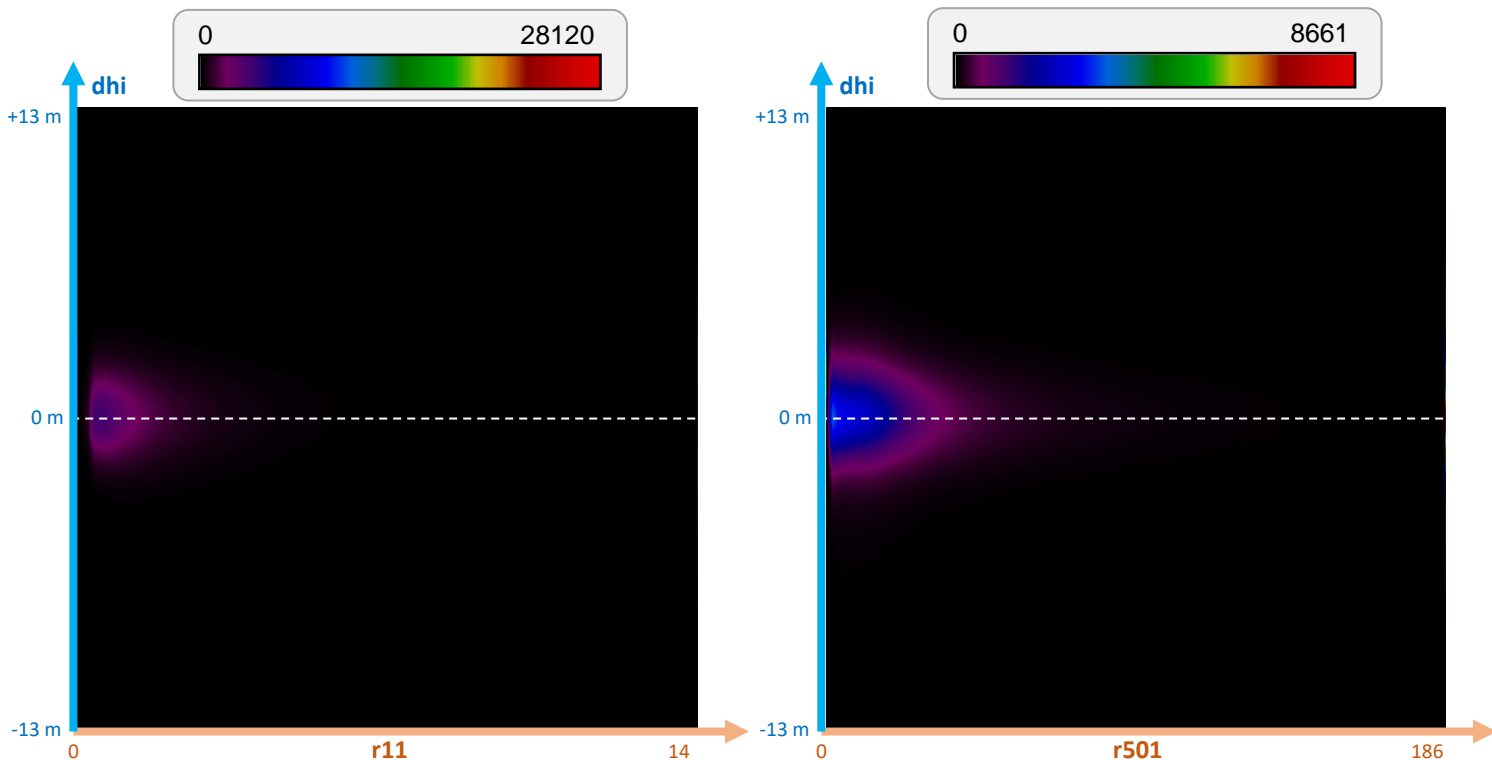


Figure 73 – Roughness (standard deviation) in a 11x11 square (left) and 501x501 square (right).

4.2.4.2.4 Correlation between height errors (dhi) and terrain curvatures

Another way of measuring the variation of the relief is to estimate the curvature of the valleys (concavity with positive second derivative) and ridges (convexity with negative second derivative). It can be assumed that the sharper the “characteristic lines” (narrow valleys or sharp ridges), the larger the height errors that match the difference dhi (ICESat – ALOS World 3D).

The figure below clearly shows that the larger the window, the smaller the curvature. It is therefore in the smallest area (11x11 matching a ground spacing between pixels of 150 metres) that we observe the largest curvatures (red curve).

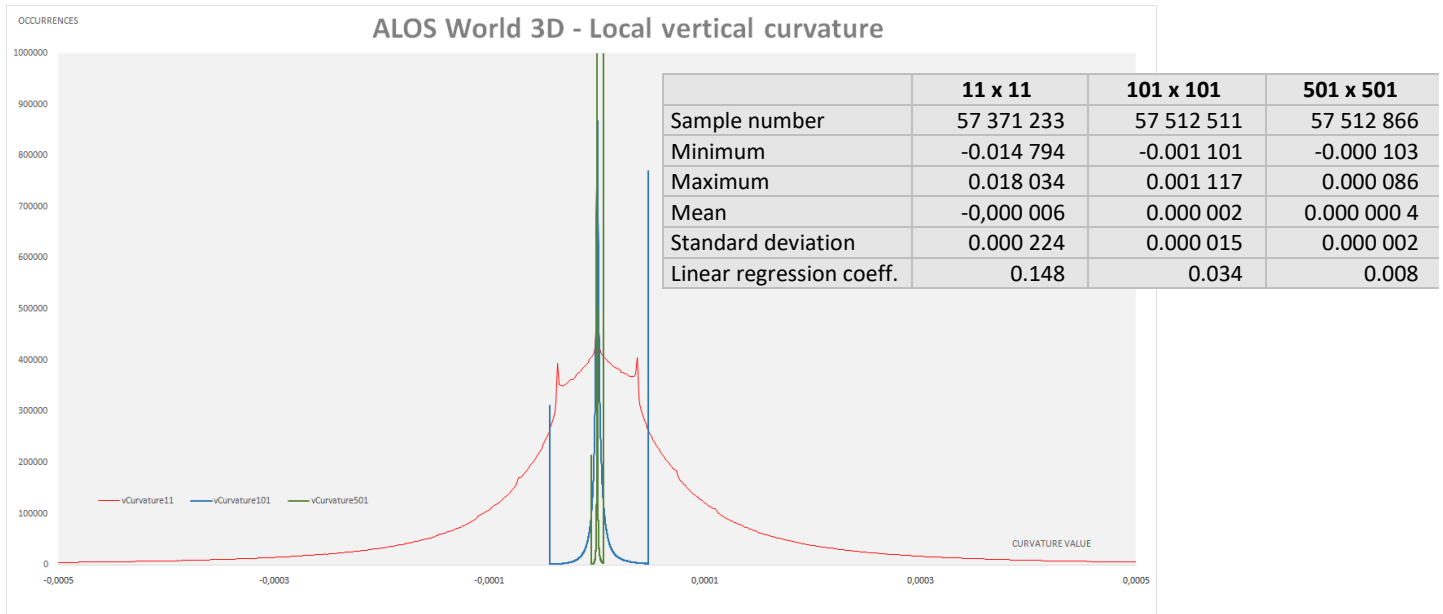


Figure 74 –Distributions of local vertical curvatures.

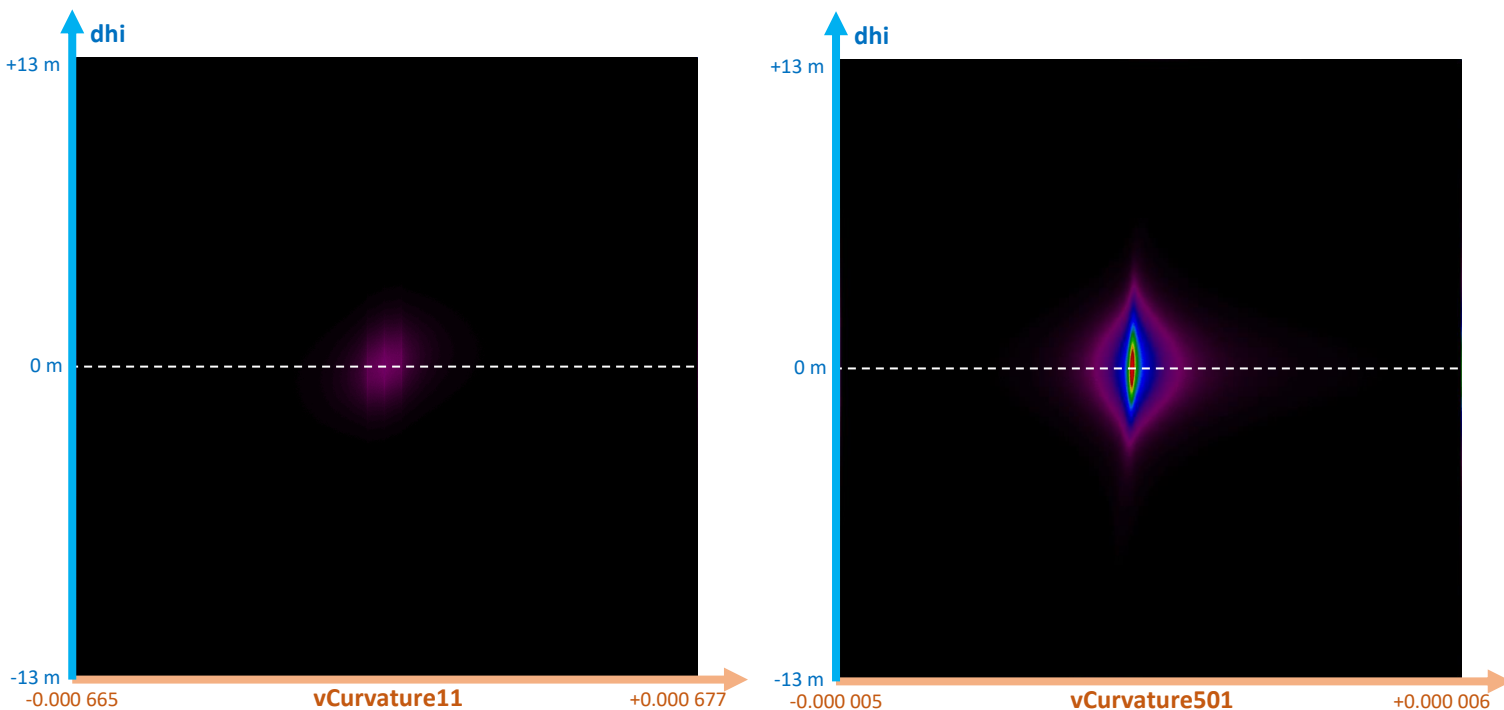


Figure 75 – Vertical curvature in a 11x11 square (left) and 501x501 square (right).

4.2.4.2.5 Analysis of the geographical distributions of elevation errors

In the same way as SRTM and ASTER GDEM, a KML file has been generated showing the geographical repartition of the height errors (see AD-5), based on the ones processed in the ICESat/DEM comparisons. This file is composed of a subsample of approximately 3000 points of comparison between ICESat and SRTM. The colour of each point represents the value of the noticed height error at its location. The label of each point corresponds to the value in metres of the height error (visible as label in the linked KML file).

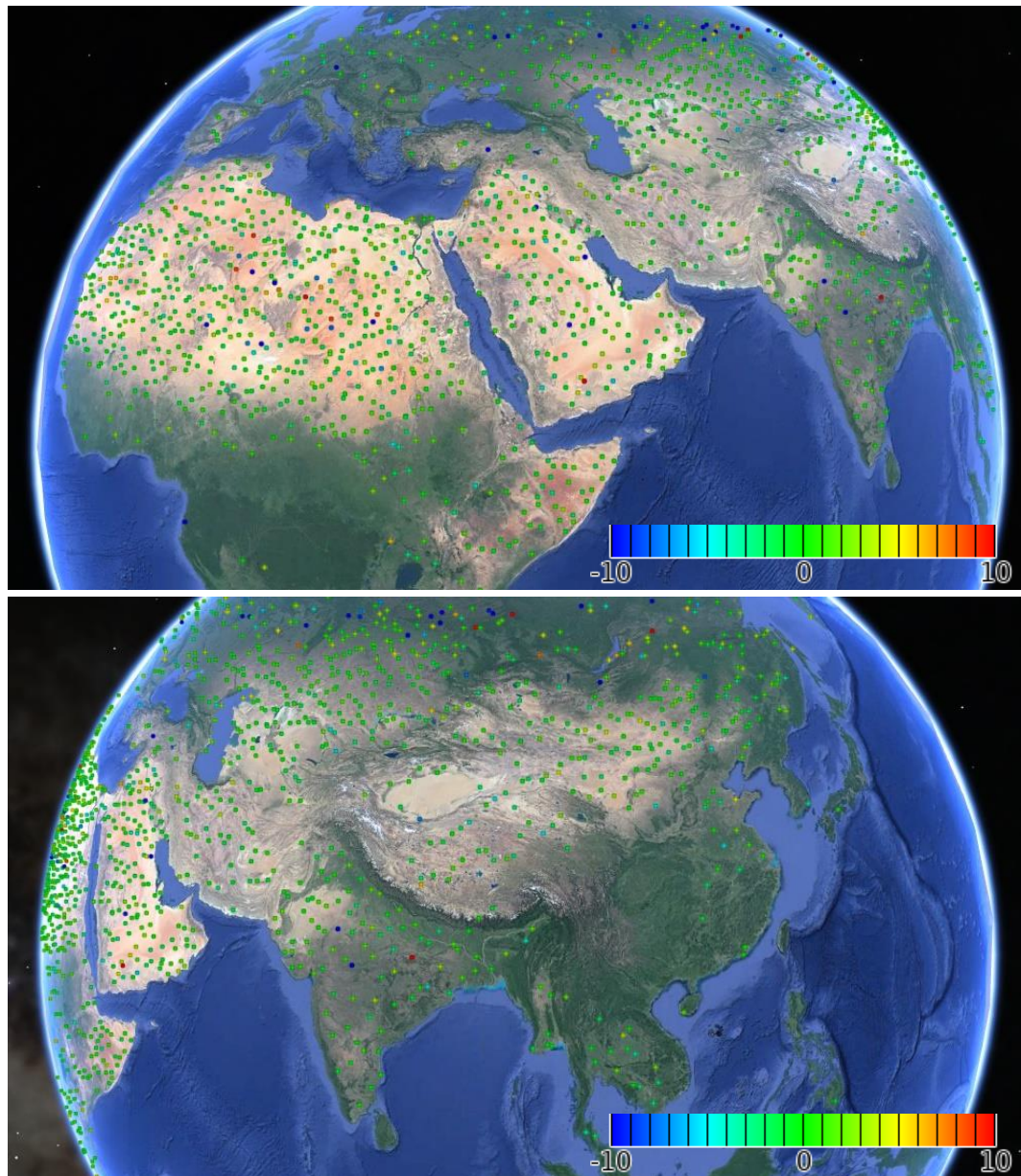


Figure 76 – Geographic distribution of ALOS World 3D height errors.

The generated KML file highlights the accuracy of ALOS World 3D, as the vast majority of the points are coloured in green. ALOS World 3D visually tends to be more precise than SRTM in most cases. The KML file highlights a small group of errors over the Sahara, as well as a loss of accuracy in Northern Russia. The points of latitude lower than -60 degrees, higher than 60 degrees could not be exploited, as most of the heights of these areas are considered as invalid (by the mask values).

4.3 Use-based assessment – DEMs to orthorectify satellite images

Among the many applications of digital terrain models, orthorectification of third-party data, i.e. the correction of geometric deformations due to relief, is one of the most used in geomatics.

One describes here after the deformations observed in the optical images (parallax), in the radar images (shortening, dilation, layover) then one demonstrates that the geometry of the deformations in optical imagery is a problem dual of that of the deformations in radar imagery. We conclude this introduction by describing the convergence algorithm of orthorectification processed on-the-fly in VtWeb to orthorectify the Sentinel-1 radar products.

Figures of this section are extracted from the courses of Serge RIAZANOFF at Paris Est University (see [Web site](#)).

4.3.1 Optical image – The parallax effect

As illustrated in **Figure 77**, the **parallax** error depends on two factors:

- the **local incidence β** of the viewing vector arriving at point P on the topographic surface and
- the **height h** of this point P above the reference surface (in the case of mathematical modelling, this surface is an ellipsoid such as WGS84).

The parallax error is the geodesic arc between point P_0 (vertical projection of point P on the ellipsoid) that corresponds to the exact geodesic position of point P, and point P_1 resulting from the perspective effect of point P according to the viewing vector from the satellite with elevation α . By neglecting the curvature (P_0, P_1), the parallax error e is equal to $h \times \tan(\beta)$.

The relationship between the viewing angle α and the local incidence β is given in the right part of **Figure 77**.

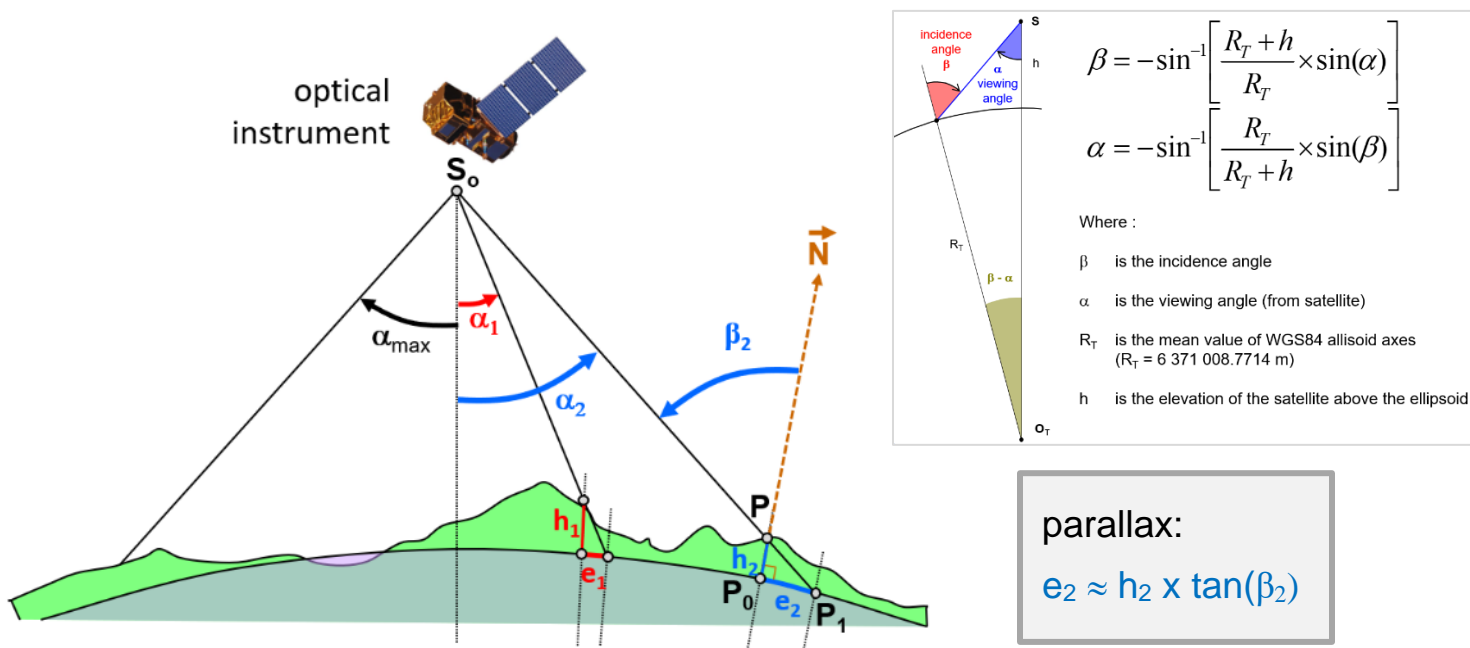
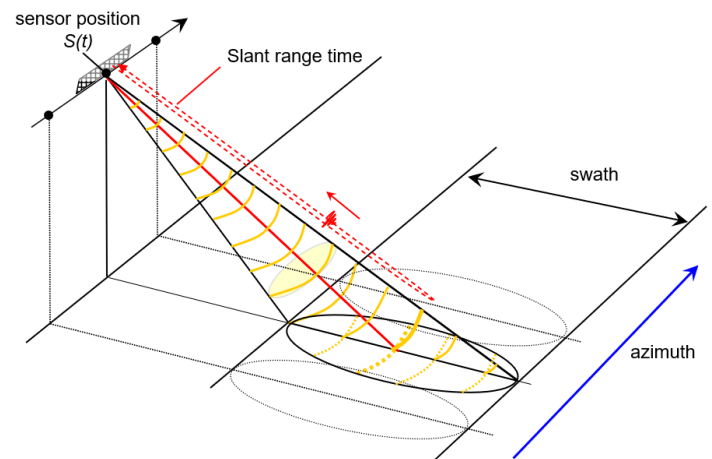


Figure 77 – Geometry of an optical instrument (left) and relation between the viewing angle α and the incidence angle β (right).

4.3.2 Radar image – The shortening / dilation / layover effects

As shown in the attached figure, the position of the target along an azimuth line depends on the go-return time of the electromagnetic signal. All the targets located at the same distance r from the satellite $S(t)$ are sampled on the same bin. The digital number of a pixel along the range axis is therefore the sum of the backscattered energies of all the targets located at a same distance r .



If we consider the altimetric profile of the terrain for a given azimuth line (see Figure 78), the restitution of the targets along the range axis (shown here in blue horizontally) depends on the distance between the target and the satellite S . Thus a hill (C,D,E) whose exposed slope (C,D) is as wide as the opposite slope (D,E) , i.e. whose geodesic distance $d(C'',D'')$ and $d(D'',E'')$ are roughly equal on the ellipsoid, will be restituted along the range axis with a distance $d(C',D')$ shortened for the exposed face and a distance $d(D',E')$ dilated for the opposite face. At low incidence (angle α low), this phenomenon can even produce the folding of the exposed slope leading to the topological inversion of points A' and B' (case of layover).

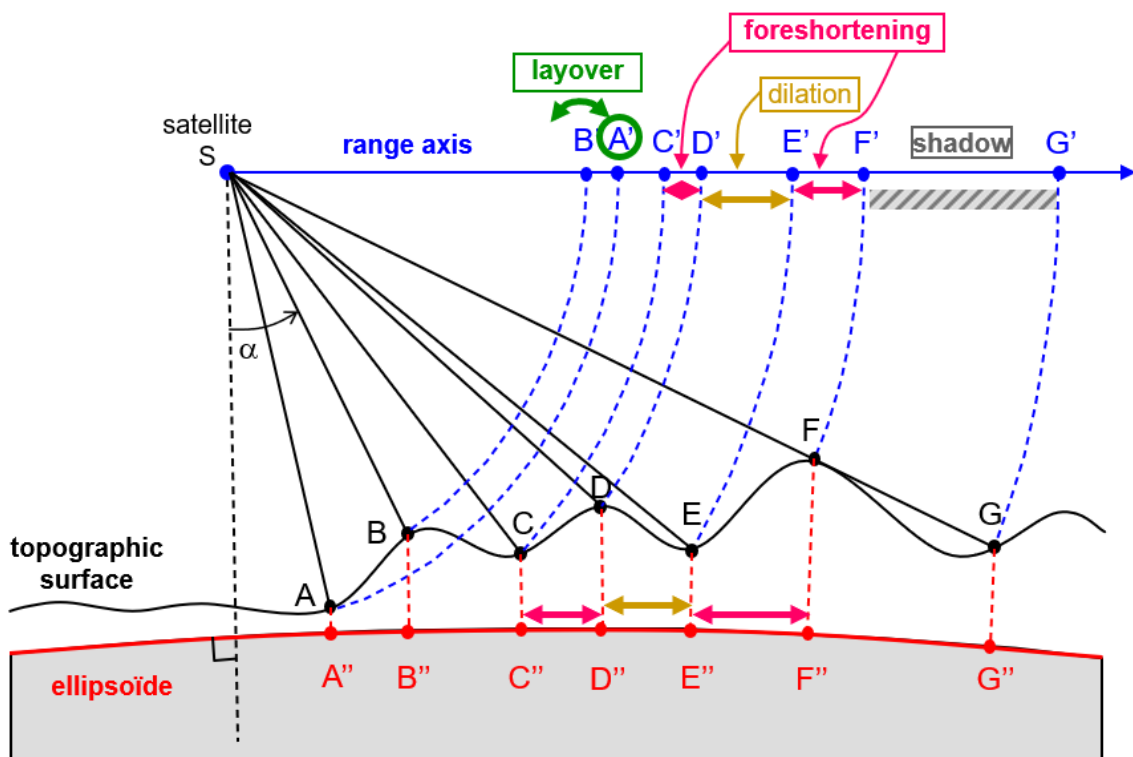


Figure 78 – Geometry defects of radar acquisition.

Animation <https://visioterra.org/VtWeb/hyperlook/8dafcada601748bb8717663c05b1e875> shows for example the Island of Malabo seen by Sentinel-1A on 20 April 2019 along an ascending orbit without orthorectification (left) and after orthorectification (right). The leftmost image illustrates the shortening of the exposed faces (illumination is coming from West in ascending orbit).

beam
illumination
→

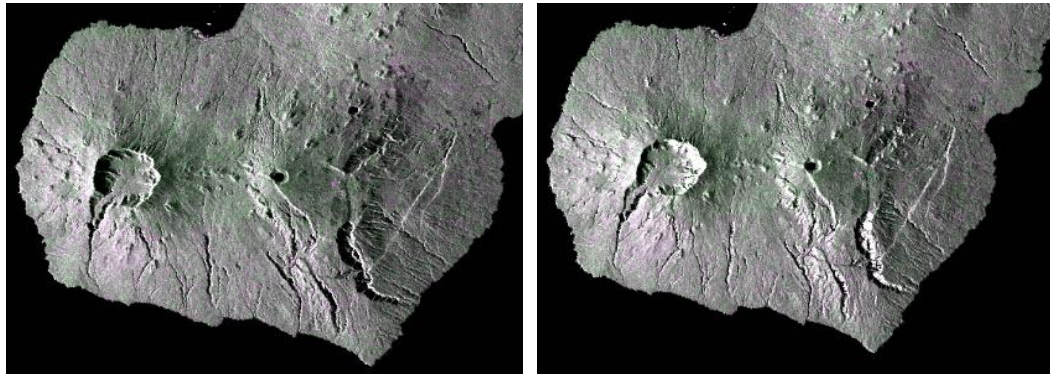


Figure 79 – Malabo Island geocoded over ellipsoid (left) and orthorectified (right).

4.3.3 Optical or radar orthorectification – A dual configuration

As illustrated in Figure 80, the geometric deformation observed in optical images that produces the parallax is the 90 ° conjugate of the deformations observed in radar images that produces shortening / dilation / layover.

parallax:

$$e_2 \approx h_2 \times \tan(i_0)$$

$$e_2 \approx h_2 \times \tan(\pi/2 - i_r)$$

$$e_2 \approx h_2 / \tan(i_r)$$

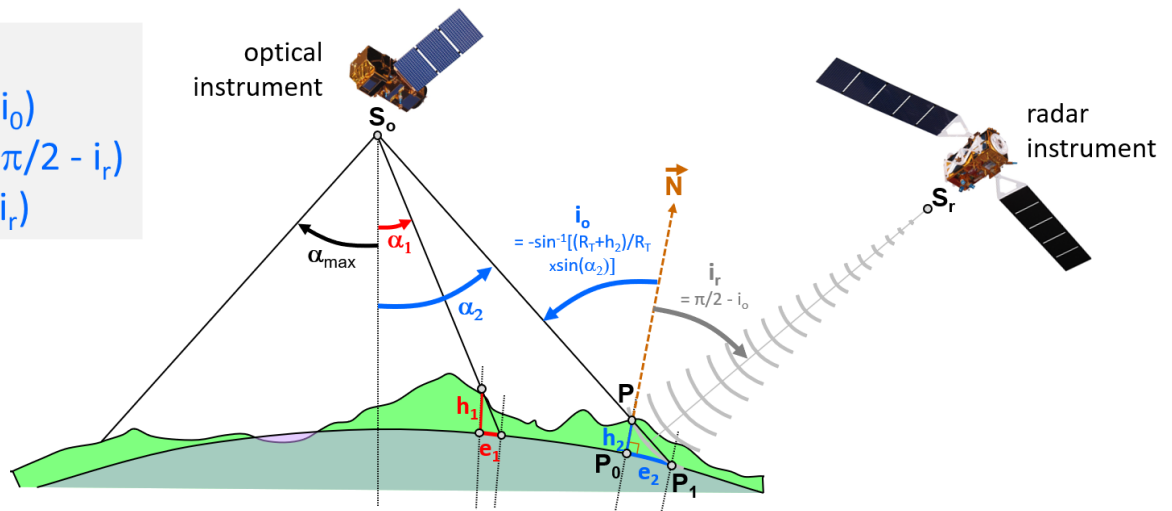


Figure 80 – Parallax effect of optical acquisition (left) and shortening / dilation / layover effects of radar acquisition (right) on a same target.

One may therefore transpose the classical algorithms of optical orthorectification (see for example RD-20) dealing with a “viewing vector” of optical instruments to the “line of sight” of a radar beam.

4.3.4 Algorithm of orthorectification

4.3.4.1 Principle and algorithm

When a DEM is available, the intersection with the topographic surface may be computed using the iterative algorithm detailed here below and illustrated by Figure 81 (see RD-19).

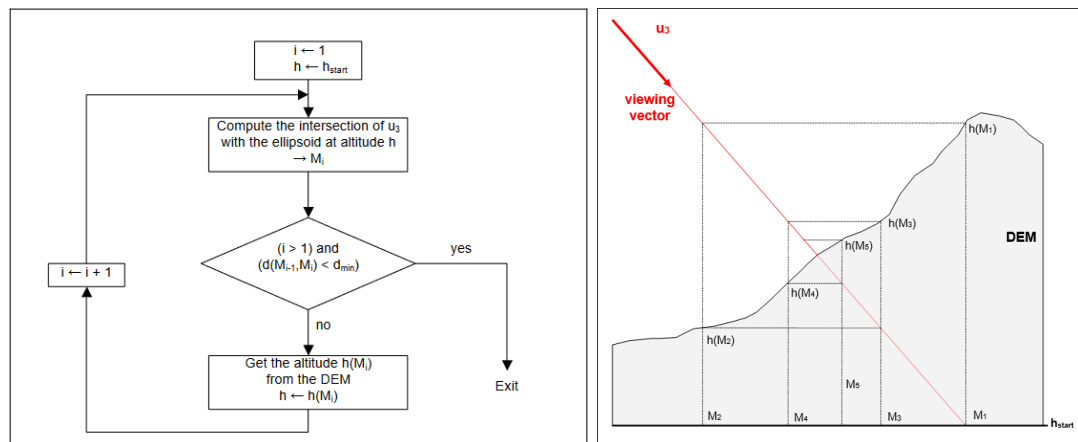


Figure 81 – Convergence algorithm to correct the parallax.

Algorithm stops when the geodetic distance between the computed intersection M_i and the one computed at the previous step becomes below a fixed threshold (d_{min}).

4.3.4.2 Speeding-up convergence

First altitude h_{start} shall be chosen as close as possible the final one. When pixels are processed sequentially, along the line, it is recommended to get the altitude of the previous pixel; or better, to estimate the local slope, setting the altitude in the continuity of this slope.

4.3.4.3 Algorithm convergence

When the DEM has a high resolution and when the look direction is very inclined, algorithm may diverge; in particular, within areas showing slopes with different orientations.


Various strategies may be adopted:

1. stop when $d(M_{i-1}, M_i)$ is not strictly decreasing,
2. process a DEM pyramid at various resolution ("coarse to fine" algorithm),
3. use DEM represented by facets (TIN)...

4.3.4.4 Implementation in VtWeb

The three DEMs SRTM, ASTER GDEM and ALOS World 3D were introduced in [VtWeb](#) to be able to use them to orthorectify on-the-fly Sentinel-1 radar scenes.

Figure 82 shows the different steps (see also the video "[Introduction to VtWeb](#)"):

- Define an area of interest in the "Services" panel of VtWeb (here a rectangle over part of the Alps).
- Select the Sentinel-1A and Sentinel-2B "Datasets".
- Optionally define a date range.
- Press on the "Search" button.
- Add a scene in the "Layer stack" by clicking on the right button of the mouse selecting an item from the list of search results.
- Display the "Layer stack" by clicking on the  icon located on the right of the display area.
- Select the "Style" option by right-clicking on the item to be processed.
- Choose a default style, create a new one or edit an existing style.
- Click on one of the buttons above the "Same preprocessing" label.
- Choose the "Geocoding" option by selecting the desired DEM.

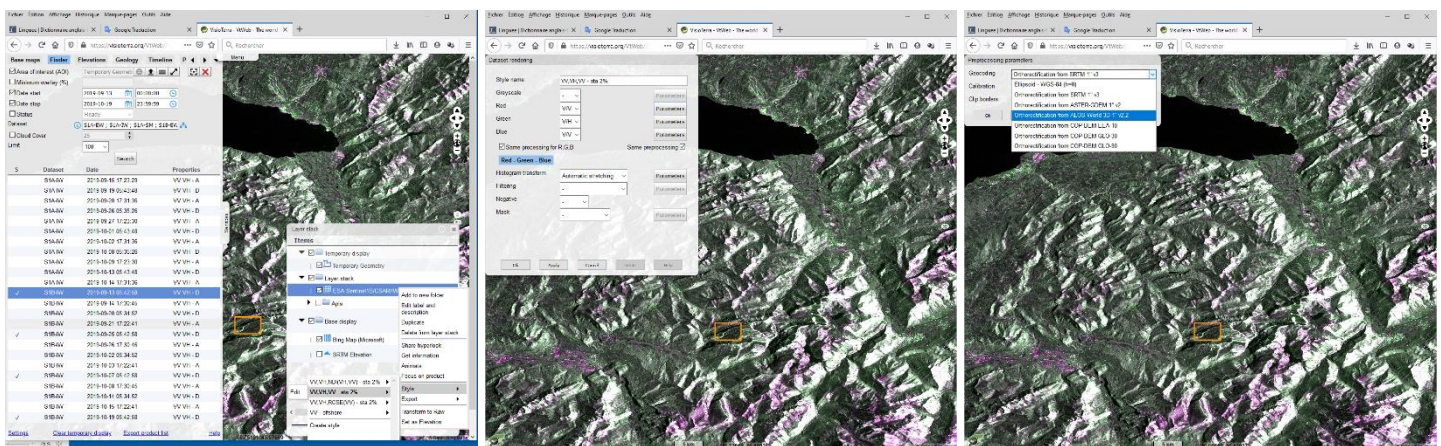


Figure 82 – Choosing the DEM to orthorectify a Sentinel-1 product.

4.3.5 Examples of radar orthorectification

In this section, we will compare the result of an orthorectification using two different DEMs: SRTM and ASTER GDEM. This orthorectification will be performed on Sentinel-1 Ground Range Detected (GRD) level 1 data. In order to reduce the speckle, we will use a temporal average based on four (4) homologues acquisitions.

4.3.5.1 Example in Alps

Here are three views of the Alps. The four data used in these views have been acquired between the 13 September 2019 and the 19 October 2019. These data have been calibrated in sigma0 (σ_0) between -20 and 0 dB.

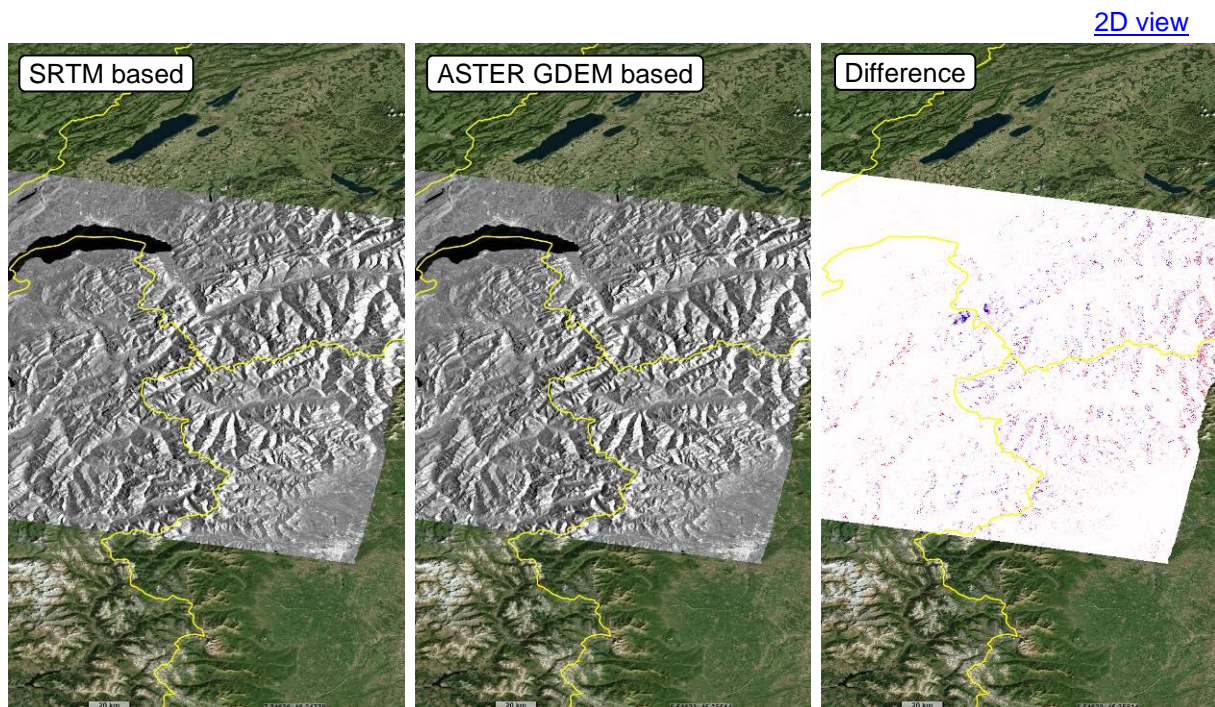


Figure 83 – Orthorectification based on SRTM (left) or ASTER GDEM (centre) and difference between the two orthorectified images (right) – Case of Alps (full scene).

From left to right, one may see the Sentinel-1 data orthorectified using SRTM, the same Sentinel-1 orthorectified using ASTER GEM and the normalised difference between the

two previous. At this scale, it is barely possible to see any difference expect for the difference image.

At a resolution of 10 metres (at the equator), the differences between SRTM (left) and ASTER GDEM (centre) based orthorectification is clearly visible. In this example, ASTER GDEM seems to give more consistent results.

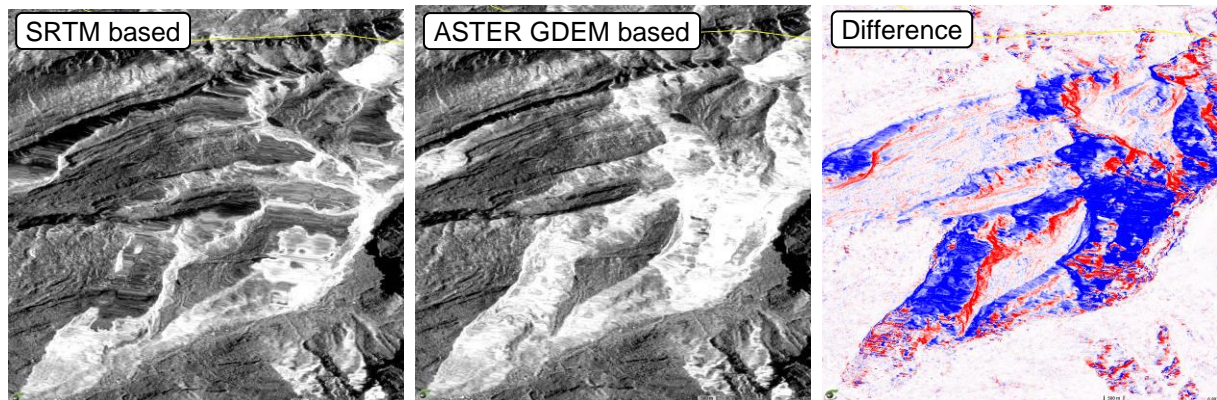
[2D animation](#)


Figure 84 – Orthorectification based on SRTM (left) or ASTER GDEM (centre) and difference between the two orthorectified images (right) – Case of Alps (full resolution).

4.3.5.2 Example in Himalayas

These three views have the same processing than the ones before. One may notice that the differences seem to be more marked at the near range than the far range (for similar elevation).

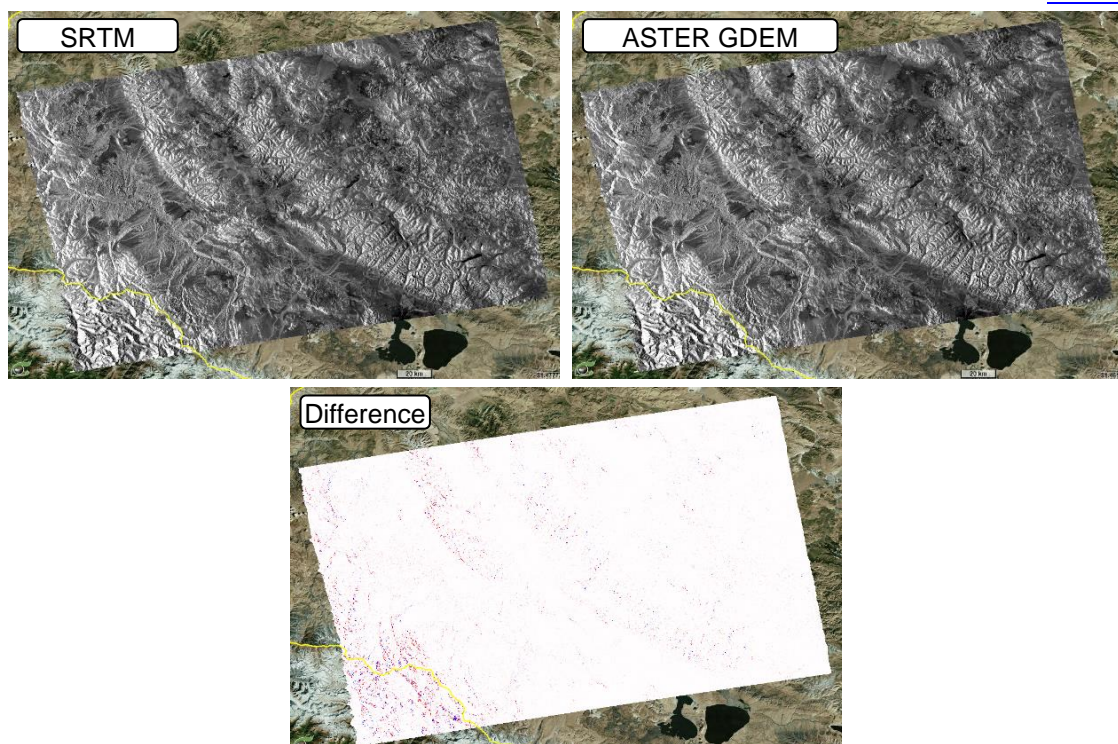
[2D view](#)


Figure 85 – Orthorectification based on SRTM (left) or ASTER GDEM (centre) and difference between the two orthorectified images (right) – Case of Himalayas (full scene).

Here after an example of defect in ASTER GDEM that introduces some incoherence in the orthorectification. This defect is mostly visible at the native resolution (10 metres) of the Sentinel-1 data.

[2D animation](#)

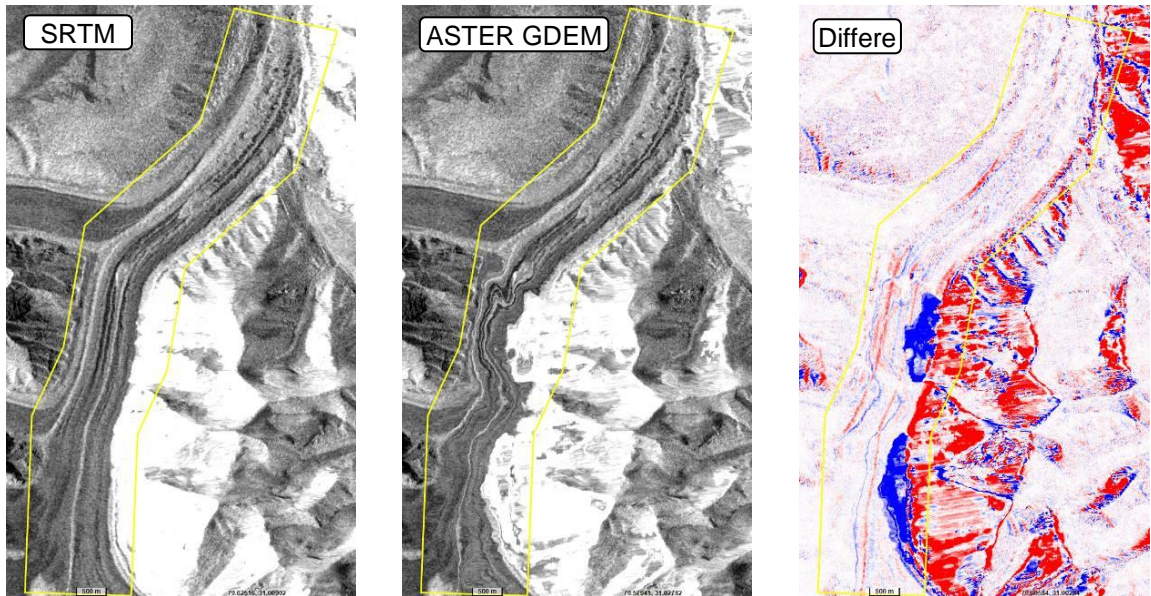


Figure 86 – Orthorectification based on SRTM (left) or ASTER GDEM (centre) and difference between the two orthorectified images (right) – Case of Himalayas (full resolution).

The SRTM based orthorectification (left) render the glacier reflects more the reality than the ASTER GDEM based orthorectification (middle).

4.3.5.3 Example in Democratic Republic of Congo (DRC)

The area covered by this example is an area with low elevations (lower than 700 metres). In this kind of area, the difference between SRTM and ASTER GDEM has a lower impact on the orthorectification.

[2D view](#)

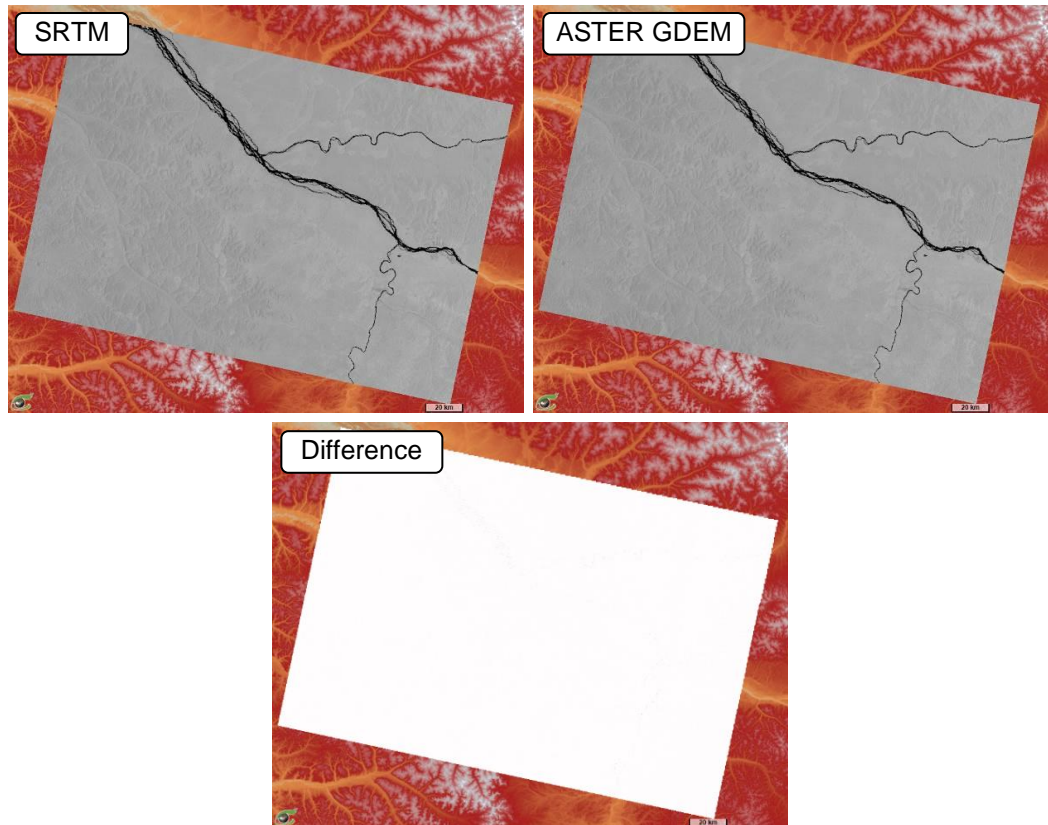


Figure 87 – Orthorectification based on SRTM (left) or ASTER GDEM (centre) and difference between the two orthorectified images (right) – Case of DRC (full scene).

One may have to zoom in this view to start seeing some differences especially near the rivers.

[2D animation](#)

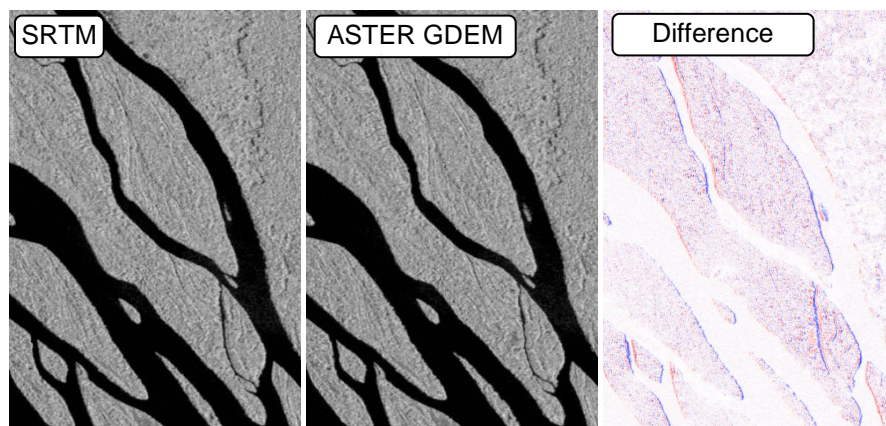


Figure 88 – Orthorectification based on SRTM (left) or ASTER GDEM (centre) and difference between the two orthorectified images (right) – Case of DRC (full resolution).

5. CONCLUSIONS

5.1 Mission / product assessment overview

As indicated several times in the document, the analysis framework described in “EDAP Quality Assessment Guideline” (RD-1) was designed for a mission operating over long time and not for a product. This is why the word “mission” has been replaced by the word “product” in several places and semantic adaptations have been made (see for example the introduction to section 2.1 “*Product Quality Assessment Matrices*”).

5.1.1 Clarifying the use of DTM, DSM and DEM

Acronyms DTM (Digital Terrain Model), DSM (Digital Surface model) and DEM (Digital Elevation Model) are used to describe a same object: a matrix containing elevation value above a specified vertical reference system (see section 1.4 “Definitions”).

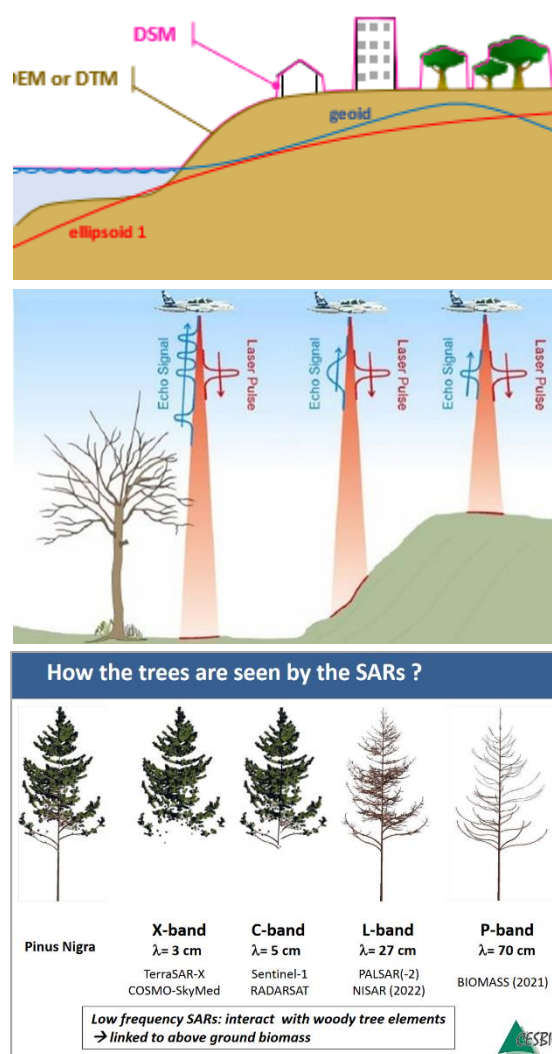
DTM (elevations above the ground) and DSM (elevations above the top of canopy, building roofs, top of man-made structures...) are the less ambiguous while DEM sometimes refer to the ground and sometimes to the top of structures.

This ambiguity has been resolved with LiDAR technology (see the attached figure) because the order of echoes; and sometimes their amplitude, refer to a specified surface. For example, the first echoes over a forest match the top of canopy, successive echoes are backscattered by the branches, the trunks, the ground surface...

For interferometric stereorestitution (case of SRTM), the surface responsible of the radar backscattering depends on the frequency of the signal: X, C, L, P are in the increasing order of penetration (see the attached figure).

For photogrammetric stereorestitution (cases of ASTER GDEM and ALOS World 3D), acquisition is performed in the visible domain leading to the detection of the upper surface (top of canopy, building roofs...).

In this study, the three DEMs have been restituted by techniques leading to the production of a “Digital Surface Model” (DSM). Filtering based on the minima and interpolations could lead to the suppression of buildings or sparse trees but basically, these three DEMs should be called DSMs.



5.1.2 Comparing the “FAIR”

As indicated in section 3.1.1, VisioTerra has introduced an individual notation of the four FAIR principles to assess a global notation more traceable. Table below summarizes these notations.

	Findable /4	Accessible /3	Interoperable /3	Reusable /4	FAIR /14
SRTM	3	3	1.5	3	10.5
ASTER GDEM	3	3	2	3	11
ALOS World 3D	4	3	1.5	4	12.5

Figure 89 – Comparison of the detailed FAIR notations.

One may notice that the “Interoperability” has a bad notation. This is probably due to the fact that the use of DEMs is still reserved to specialists. There is not for example OGC services enabling a wider public to “play” with the DEMS nor to produce on-the-fly products like slope / azimuth / curvature, nor to interactively analyse the pattern of the relief that is for example the purpose of geomorphometry.

ALOS World 3D achieves a better notation because more documentation is provided about it (see section RD-10) and certainly also, because this product is more recent and JAXA has gained benefit from the SRTM product and from its direct involvement in ASTER GDEM production.

5.1.3 Features of the three DEMs

The three DEMs have many common features:

- **CRS** - they are expressed in the same “Geographic CRS” that sacrifices the deformations at higher latitudes but is simple to describe.
- **GSD** – the ground sampling distance (size of pixels) is 1” (1 arc-second) matching approximately 30 metres along equator but tending to 0 metres of width when getting closer to the poles.
- **VRS** – the vertical reference system is a geoid model and not an ellipsoid. This is certainly due to the fact that sea-level altitudes have a value 0 above the geoid and this is that users are expecting. One may nevertheless deplore the fact that EGM96 has been chosen and not a more recent Earth gravity model like EGM2008 for the latest versions of the geoid.

DEM	version	mode ⁽¹⁾	observation interval	CRS ⁽²⁾	GSD ⁽³⁾	extents	VRS ⁽⁴⁾
SRTM GL1	3.0 (2015)	IF	11 Feb.2000 22 Feb.2000	Geo.	1”	56°S – 60°N	EGM96
ASTER GDEM	2.0 (2011)	PG	Dec.1999- Feb.2011	Geo.	1”	Global	EGM96
ALOS World 3D	2.2 (Apr.2019)	PG	2006 2011	Geo.	1”	Global	EGM96

(1) mode IF: interferometry – PG: photogrammetry

(2) CRS Coordinates Reference System – “Geo” for Geographic ([EPSG:4326](https://epsg.org/epsg/4326)).

(3) GSD Ground Sampling Distance (size of the pixel)

(4) VRS Vertical Reference System – EGM: Earth Gravity Model (or geoid).

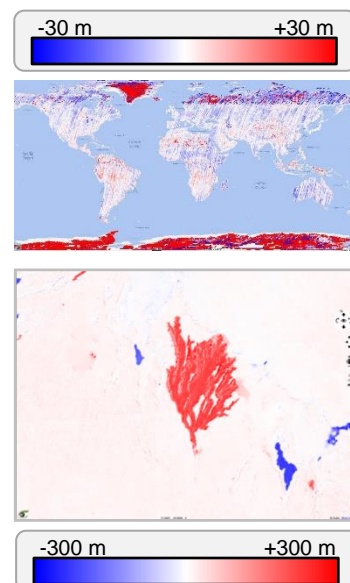
Figure 90 – DEM features.

5.2 Detailed assessment

5.2.1 Intercomparison of DEMS

By computing on-the-fly the difference between two DEMS, one may perform a qualitative assessment to very easily detect defects at global scale:

- **Footprints of Terra / ASTER** – leading to low-frequency variations between successive paths (see Figure 4 or Figure 5).
- **High differences at high latitudes** – that could be due to the difference of ice or snow heights been the acquisition dates, or due to the absence of SRTM data often used as reference (see the attached Figure 5).



By computing on-the-fly the difference between two DEMs at any scale, one may immediately detect artefacts in few views. The sign and magnitude of the difference often designate the DEM containing this artefact (see for example the attached extract of Figure 12 showing a part of the drainage network surprisingly majored of about 300 metres in SRTM).

The difference of magnitude between these two defects (+/-30 m versus +/-300 m) shows here again the advantage of dealing with these differences on the fly by simply adapting the rendering by traditional linear stretching techniques.

5.2.2 Elevation assessment from ICESat-1 / GLAS LiDAR

The table here after sum up the quantitative assessment of the three DEMs: SRTM, ASTER GDEM and ALOS World 3D with regard to the ICESat-1 reference data.

	SRTM	ASTER GDEM	ALOS World 3D
Number of ICESat products	642		
Number of heights compared (% of valid samples)	60 160 803 (84.63 %)	92 913 348 (41.99 %)	57 968 266 (26.20 %)
Arithmetic mean (metres)	0.590 m	2.315 m	<u>0.050 m</u>
RMSE (metres)	4.741 m	27.764 m	4.516 m
Standard deviation (metres)	4.704 m	27.667 m	4.516 m
Median (metres)	0.618 m	2.647 m	<u>0.104 m</u>

Figure 91 – Quantitative assessment of the heights of three DEMs.

We observe here the very mediocre values obtained by ASTER GDEM in the:

- *arithmetic mean* (2.315 m) which assesses the accuracy (or bias) of the heights compared to the ICESat-1 reference data,
- *root mean square error* (27.764 m) essentially due to the large spreading of errors measured by the
- *standard deviation* (27,667 m) which assesses the precision of the distribution.

Conversely, the best accuracy is obtained by ALOS World 3D with an arithmetic average of 0.050 m and a median value of only 0.104 m. The mean square errors of ALOS World 3D and SRTM are however very close to each other (4.516 m vs. 4.741 m).

The following histogram shows the distribution of the three DEMs in percentage of occurrence. One can see the distribution of: -ICESat-SRTM in orange, -ICESat-ASTER GDEM in blue and -ICESat-ALOS World 3D in green.

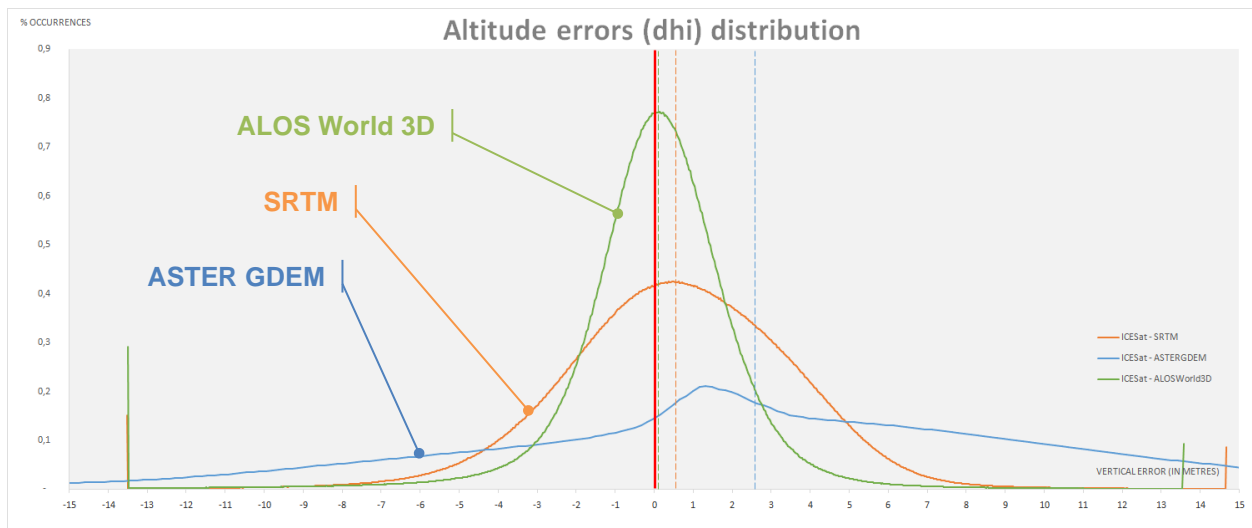
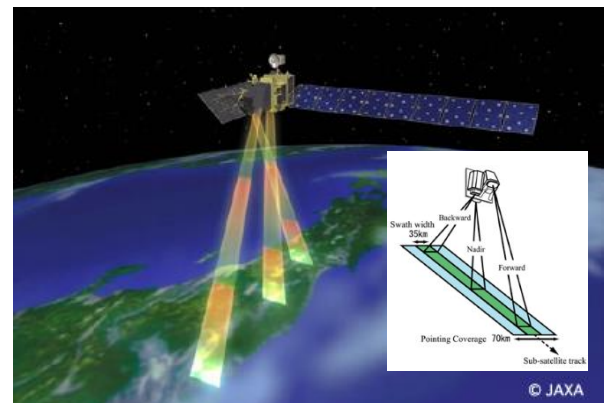


Figure 92 – Histogram of height difference between ICESat and DEMs.

According to this study, **ALOS World 3D** seems to be the best DEM with the lowest median value (0.104 m) but these statistics have been computed only between -60° and $+60^{\circ}$ of latitude.

These good results are certainly due to the tri-stereo (forward, nadir and backward) acquisition technique of the PRISM instrument on board the “DAICHI” satellite (ALOS), more stringent quality assurance procedures (see bibliography in section RD-10) and the experience gained through the production of ASTER GDEM.

For more information about ALOS World 3D, please refer to <https://www.aw3d.jp/en/technology/> from which the attached figure has been extracted.



5.2.3 Use-based assessment - Impact on radar orthorectification

5.2.3.1 Example of Sentinel-1 IW products orthorectification

As we could observe in section 4.1.1 and as summarized in Figure 92 above, we observe very significant altimetric errors in the three DEMs and in particular in ASTER GDEM.

Section 4.3 shows the observable effect when comparing geocoded scenes of the same Sentinel-1 orthorectified scene using two different DEMs. This section 4.3 shows the relative location accuracy errors between the two geocoding without ruling on which one of the two DEMs produces the altimetric errors. In some cases, coarse DEM aberrations such as those noted when calculating the 3 differences between the 3 DEMs suggest that 2 of the 3 DEMs probably have better altimetric values than the third one. These ambiguities can obviously only be resolved if external references (VHR geocoded image, geodetic points, maps...) are used to assess the absolute location accuracy.

As illustrated in **Figure 93**, a difference in altitude Δh even small between two DEMs can produce very distant rendering in the corresponding orthorectified images. Difference of location error Δe is $1/\tan(\beta)$ time the altitude error Δh , i.e. for example a **factor x1.80** as shown in near range of IW mode (see table in Figure 94).

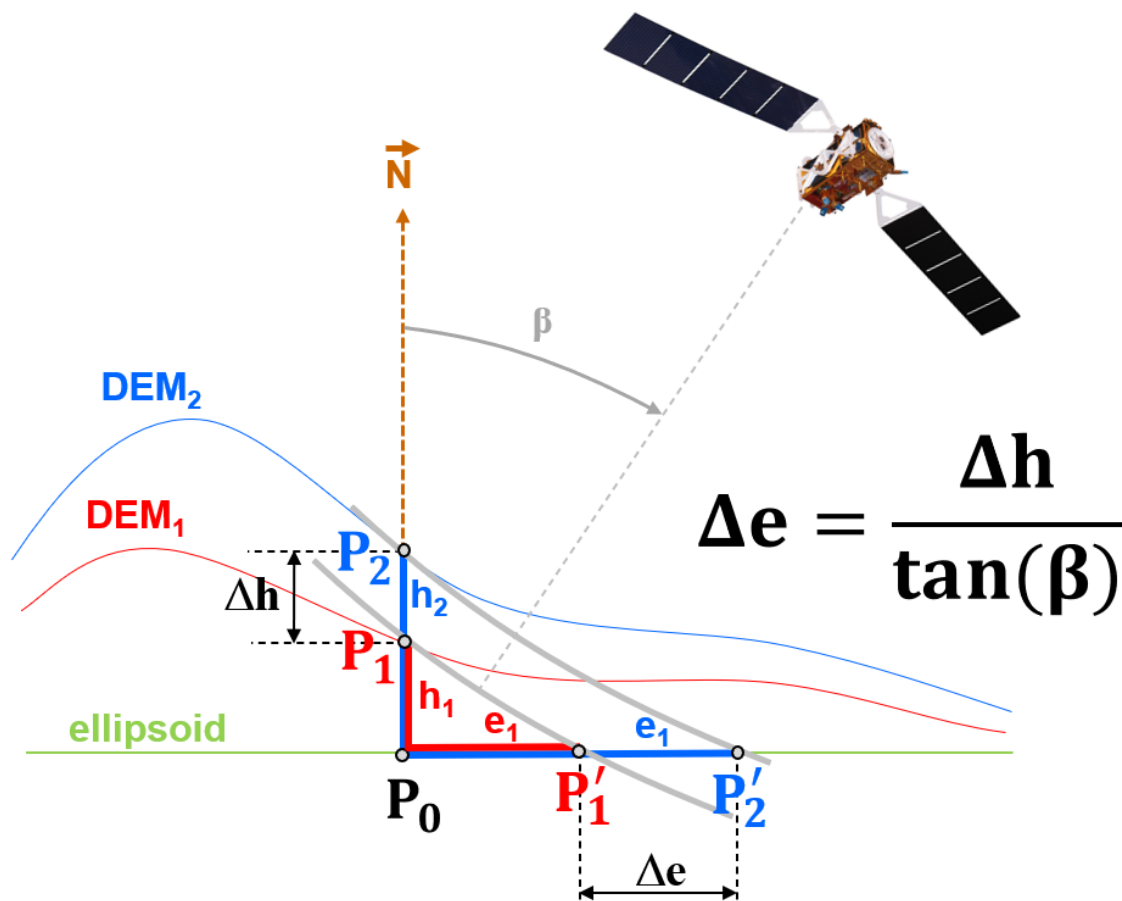


Figure 93 – Planimetric error Δe of orthorectification due to an altimetric error Δh .

As shown in the table in Figure 94 – Examples of altimetric errors Δh depending on the incidence extrema for the different observation modes of Sentinel-1., this positioning error is particularly sensitive to low incidences angles (near range) whereas it is the opposite for the parallax error of an optical instrument (see **Figure 80**).

Mode incidence (degrees)	IW		EW		SM	
	near range minimum (°)	far range maximum (°)	near range minimum (°)	far range maximum (°)	near range minimum (°)	far range maximum (°)
	29.1°	46°	18.9°	47°	18.3°	46.8°
$\Delta h = 1\text{m}$	1.80	0.97	2.92	0.93	15.12	0.94
$\Delta h = 5\text{m}$	8.98	4.83	14.60	4.66	30.24	4.70
$\Delta h = 10\text{m}$	17.97	9.66	29.21	9.33	30.24	9.39
$\Delta h = 30\text{m}$	53.90	28.97	87.62	27.98	90.71	28.17

Figure 94 – Examples of altimetric errors Δh depending on the incidence extrema for the different observation modes of Sentinel-1.

5.2.3.2 Other orthorectifications

To demonstrate the impact of the quality of DEMs on the quality of orthorectified images, it is suggested to extend this study to the orthorectification of Earth observation products in the optical domain at medium resolution (for example the Envisat MERIS FRS products at 300 meters GSD) or even at very high resolution (for example SuperDove products from PlanetScope or BlackSky products).

5.2.3.3 Other use-based assessments of DEMs

DEMs are not only used for auxiliary use such as orthorectification; they constitute an instructive representation of the relief and therefore of the landscapes by providing morpho-structural information.

In the context of a more extensive study, it is suggested to compare different DEMs in their ability to render watersheds, hydrographic networks and characteristic lines such as the ridges and saddle points that constitute the “arch stones” of the relief.